JOHNSON GRANT
IN-18 -CR
103481
P.108

INVESTIGATION OF PLASMA CONTACTORS
FOR USE WITH ORBITING WIRES

Grant NAG9-126

Final Report

For the period 1 January 1986 through 30 June 1987

Principal Investigator

Dr. Robert D. Estes

September 1987

Prepared for
National Aeronautics and Space Administration
Lyndon B. Johnson Space Center
Houston, Texas 77058

Smithsonian Institution
Astrophysical Observatory
Cambridge, Massachusetts 02138

The Smithsonian Astrophysical Observatory
is a member of the
Harvard-Smithsonian Center for Astrophysics

The NASA Technical Officer for this Grant is
Dr. James M. McCoy, Code SN3, Lyndon B.
Johnson Space Center, Houston, Texas 77058

INVESTIGATION OF PLASMA CONTACTORS

FOR USE WITH ORBITING WIRES

Grant NAG9-126

Final Report

For the period 1 January 1986 through 30 June 1987

Principal Investigator

Dr. Robert D. Estes

Co-Investigators

Dr. Mario D. Grossi
Prof. Robert Hohlfeld

September 1987

The Smithsonian Astrophysical Observatory
is a member of the
Harvard-Smithsonian Center for Astrophysics

CONTENTS

1.0 INTRODUCTION

The use of electrodynamic tethered satellite systems for space applications such as electrical power generation for space system use, tether-current-generated thrust, and electromagnetic wave generation depends critically on the ability of these systems to exchange charge efficiently with the ionosphere. Whether the source of the electromotive force that drives the current in the tether is a spaceborne power supply or the motion of the system across the geomagnetic field-lines, the amount of current that can flow through the tether depends upon the rate at which the system can exchange charge with the ionospheric plasma at the ends of the system.

The original electrodynamic tethered satellite system concept envisaged a large metallic surface to collect electrons at one end of the system and an electron gun to expel them at the other end. Such a system might be adequate for a demonstration experiment, but it has a number of drawbacks from the standpoint of practicality. First there is the problem of carrying into orbit, deploying, and maintaining the large electron-collecting satellite. If calculations based on ordinary plasma probe theory can be trusted, a satellite radius of tens of meters would be required to collect currents of several Amperes. Electron guns require their own power supply, as well as pointing mechanisms. They are notoriously unreliable in space applications, since their operation is susceptible to disruption by arcing brought on by local contaminants among other things.

It has been proposed that hollow cathode devices could be utilized to effect charge-exchange at each end of the tethered system, eliminating the need for both the large metallic surface and the electron gun. Furthermore, it is hoped that

they will provide a low-impedance path between the system and the ionosphere, thus nullifying high charge buildups at either end and substantially increasing efficiency. There is reason for optimism based on plasma chamber experiment results and the successful utilization of hollow cathode devices to prevent charge buildup on satellites in geosynchronous orbit and in sounding rocket experiments.

Nonetheless, hollow cathode devices have not yet been tested extensively in orbit in the part of the ionosphere where electrodynamic tethered satellite systems would likely be utilized. Even more importantly, they have not been demonstrated to work within a tethered system drawing substantial currents. The peculiarities of the environment — the combination of a motional electric field, a streaming background plasma and neutral gas, and the geomagnetic field — are practically impossible to duplicate in a plasma chamber (without mentioning the difficulties of eliminating wall effects). Experiments on hollow cathodes in orbiting systems at altitudes corresponding to high velocities with respect to the Earth's rotational velocity will provide interesting new physics results as well as information on how well the technology performs under these conditions. One of the purposes of this report is to elucidate some of the important questions that electrodynamic experiments on orbiting short tethered systems equipped with hollow cathode systems might answer.

While much of the analysis could be applied to any experiment on hollow cathodes in space, and some of it deals with general problems of electrodynamic tethered satellite systems, the main focus is on a specific set of proposed experiments. These are to be conducted from the Space Shuttle and utilize a spin-casting reel to store and unreel the tether. The small satellite, which is basically just a hollow cathode system, is connected (both mechanically and electrically) to one end of the tether. The satellite is propelled away from the Shuttle by means

of a spring mechanism. The tether is also connected by a switching device to a hollow cathode at the end that is fastened to the reel. As the the tether reels off, it experiences an increasing motion-induced emf due to the orbital motion through the Earth's magnetic field. The experimental apparatus also includes a 50V battery that may be placed in series with the tether and hollow cathodes with either choice of polarity, so as to add to the motional emf or to act in the opposite sense. Once the tether is fully extended, it disconnects itself from the orbiter by the tension in the tether. Thus the experiment is limited to the time it takes the tether to unwind from the reel, or around five minutes for the 200m tether case. The current through the tether is measured at intervals of 0.1 sec in the present design of the experiment. This is the basic outline of the experiments we have been considering with the aim of maximizing their scientific return and their usefulness for future experiments and hollow cathode design.

The Challenger disaster and subsequent grounding of the Shuttle for redesign of the Shuttle engines have placed these specific experiments on hold. In the meantime, other hollow cathode space experiments to be carried out on sounding rockets have been proposed. Although the future of the originally proposed experiments is a bit cloudy at present, we have focused our analysis on them because it was our original task and because they offer significant advantages over sounding rocket experiments in approximating the operation of a real tethered satellite system.

The fundamental difference between the Shuttle-based experiments and any sounding rocket experiments is the relative motion between the experimental system and the background ionospheric plasma and geomagnetic field found in the orbiting case. This is what makes the orbiting experiments much more valuable as predictors of hollow cathode performance in electrodynamic tether experiments

such as TSS-1, which will almost certainly include hollow cathode devices on the orbiter, though not on the subsatellite. The orbiting system will experience the motional electric field that will drive an electrodynamic tether. The plasma cloud emitted by the hollow cathode will be subject to ExB drift to the extent that the geomagnetic field is not canceled by fields generated by plasma cloud currents. The ionosphere will be streaming by with the orbital velocity of around 8 km/sec, experiencing the local disturbance caused by the electrodynamic tether's operation as a time-varying phenomenon, due to this relative motion. This time-varying disturbance will give rise to electromagnetic plasma waves in the ionosphere. It is within this complex of interactions that the hollow cathodes must perform if they are to function as plasma contactors suitable for electrodynamic tethered satellite systems. The short-tether Shuttle-based experiments still promise to give the first answers to many questions about hollow cathode behavior in this environment.

The short tether experiments we have studied offer another important advantage over experiments involving space-borne hollow cathode devices that are mounted on rockets. They allow for much greater separation between the hollow cathodes, greatly increasing the probability that a separation will be reached for which the devices are magnetically insulated from each other, as would be the case in a long tethered system. Hollow cathode plasma cloud overlap could essentially rule out electrical contact between the tether and ionospheric plasma by providing an alternative circuit closure path. Perhaps the greatest strength of the variable length tether experiments is their potential for allowing us to observe the distance at which this cloud overlap ends. This matter is discussed in detail within the context of planning the experiments in Section 2.

Several aspects of the physics of hollow cathodes in low earth orbit are addressed in the analysis presented in Section 3, which is due to Prof. R.G.

Hohlfeld. In particular we have tried to obtain a better picture of the size and shape of the hollow cathode plasma cloud, taking into account the dynamical interaction with the ionosphere. Results from both a fluid theory and kinetic theory approach are presented in Section 3. The distance to which the hollow cathode cloud expands against the ionospheric stream exhibits the expected dependence on the mass flow rate and the atmospheric density.

The effect of the Earth's magnetic field in limiting the hollow cathode cloud expansion is considered in Section 4. This is the one part of our analysis that may be more applicable to a sounding rocket experiment than to the short tether experiments, since orbital motion effects are not included. The results in this section are from a computer code originally written by Prof. Hohlfeld to describe a chemical release cloud in its "diamagnetic cavity" phase. The analogy with a hollow cathode cloud is not perfect, but may be a good model for the higher density clouds with a high ratio of dynamic to magnetic pressure (high β). The observed elongation of the cloud along the field lines is a reasonable result.

The hollow cathode systems are looked at from the perspective of the ionospheric plasma waves they excite in their passage through this medium in Section 5, where we deal with a challenge raised to the operation of electrodynamic tethers in the form of supposed very high ionospheric wave impedances which would effectively shut off tether currents. The experiments of Stenzel and Urrutia, which have been advanced as evidence that electrodynamic tethers will not work, are also examined in this Section.

The importance of choosing the location of the experiments is emphasized in Section 6, which considers how the two most important environmental parameters, the ionospheric plasma density and the $v \times B$ force, vary along the

orbital path for a low inclination (28 degree) orbit at 300 km altitude. We make some suggestions for planning and experimental procedure from the standpoint of timing the experiments to coincide with optimal conditions in this section.

The concluding section summarizes some of our results and highlights our proposals for future work and for the conduct of the experiments.

2.0   ANALYSIS OF THE EXPERIMENTS

The proposed short tether experiments that are the subject of this study will have some obvious limitations. We are specifically referring to the "fishing reel" experiments to be conducted from the Space Shuttle, which will not be equipped to make measurements of electromagnetic fields and plasma cloud properties. Simple though the electrodynamic component of the experiments will be, however, they have the potential for yielding considerable information about the functioning of the plasma contactors in low earth orbit, including information that will not be obtained during the first full-scale deployment of a long electrodynamic tether in the TSS-1 mission. This is because the short tether experiment will be running continually during the wire's extension, allowing measurements of tether current to be made in the various operating modes of the system for tether lengths that range from very short on out to respectable lengths.

It is still undetermined when the electrodynamic part of the TSS-1 experiments will commence during the tether deployment phase, but it is unlikely that there will be any results for orbiter-satellite separations as small as the fully extended wires that will be used in these earlier experiments. Furthermore, since the TSS-1 experiment makes no provision for producing an emf by use of an on-board power supply, the experiment will be limited to low values of motion-induced voltages for short tether extensions, while the full resistance of the tether (some 2000 ohms) will be in the circuit at all times, not to mention the large inductance of the tether wound on the reel. Thus any "short tether" measurements made during TSS-1 will necessarily be very low current results.

Though the boom-mounted probes on the TSS-1 satellite will provide information about the local plasma and fields at that end of the system, measurements of the environment at the orbiter end, where the hollow cathodes will be operating, will be limited. Their interpretation will be complicated by the simultaneous operation of one to three electron guns pointed at varying angles with respect to the magnetic field and operating for various durations. At present there is not even a way to operate the proposed orbiter-mounted hollow cathodes without the electron guns, while the switch connecting the ends of the tether is closed.

Thus, while it is to be hoped that the TSS-1 experiments will provide new data that is interesting from both the scientific and technological standpoints, they are not likely to give much detailed information on the physics of hollow cathodes in space, beyond an answer to the question of how well they work in maintaining low potential differences between the Shuttle and the ambient plasma in conjunction with electron guns. This is a key question, but at some point an understanding of the basic physics will be needed to guide the design of hollow cathode systems for use with electrodynamic tethered satellite systems, since trial and error is not really practical, given that plasma chamber experiments cannot completely simulate the necessary conditions. The precursor experiments now under study will provide results that may prove helpful in the design of the TSS-1 hollow cathode system.

What extra information will the short tether experiments provide? They should answer the question of how far the plasma clouds of the hollow cathodes can effectively transport charge across the geomagnetic field lines, which is a critical property in their ability to collect current from the ionosphere. The two clouds may be said to overlap, in an electrical sense, while they can conduct a

substantial current across the magnetic field between the two electrodes of the system. The combination of operational modes planned for the experiments should allow us to see where the plasma clouds emitted by the hollow cathode devices at the opposite ends of the system stop overlapping. By repeating a series of measurements in the different modes of operation while the tether reels out, as indicated below, we should obtain enough information to observe how the "leakage" current across the hollow cathodes varies with tether length.

Let us consider the physics of the system in the three basic modes of operation planned for the experiment (six modes if hollow cathodes on and off are included and twelve if different combinations of on and off are considered). First there is the mode that we might call the motion-driven mode: the current through the tether is strictly a result of the emf induced by the system's motion with respect to the Earth's magnetic field. For a long electrodynamic tethered satellite system (Figure 2.1) this mode should not be fundamentally different from the battery-driven modes, since the hollow cathodes at the ends of the systems are separated far enough to be considered insulated from each other by the magnetic field. In the following discussion when we say plasma cloud dimensions we mean the size of the plasma cloud that can effectively conduct current across the magnetic field lines. When the tether length is much greater than the hollow cathode plasma cloud dimensions, the potential difference between the two ends of the system is much greater than the motion-induced potential difference between the upper and lower parts of a single hollow cathode cloud.

However, when the tether is short enough so that the plasma clouds emitted by the hollow cathodes at each end of the tether overlap, the motion-induced potential drop across the ends of the system and the combined plasma clouds are the same. In this case, the plasma clouds not only provide a path of contact
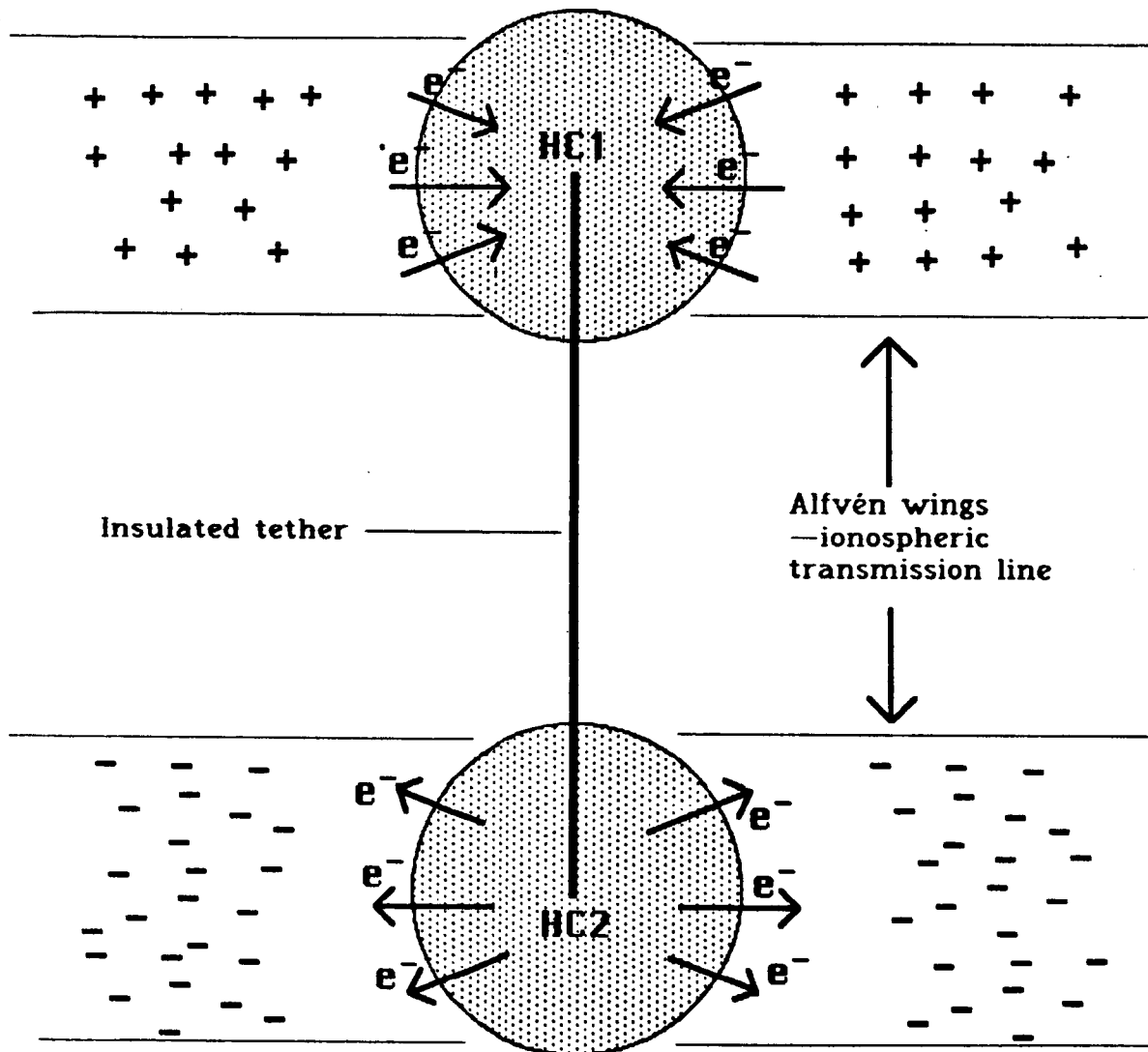
Figure 2.1: Long electrodynamic tether viewed head-on. Plasma clouds from upper and lower hollow cathodes (HC1 and HC2) are magnetically insulated from each other.

between the ends of the tether and the ionospheric transmission line, they also provide an alternative electrical path between the two layers of the ionospheric plasma at the ends of the tethered system. In effect, the overlapping plasma clouds form a column of plasma that acts as a fat conducting tether, with the insulated wire of the real tether being the core of this "plasma tether." This plasma column is in contact with the ionosphere all along its length, so it is analogous to an uninsulated wire. Since the cross-section of this alternative electrical path would be so much greater than that of the tether wire, it could in fact end up carrying most of the current. Thus, while the current in the overall system (the current traveling in the ionospheric transmission line) might be substantially increased by turning on the hollow cathodes in a short tether configuration, the tether flowing through the wire might decrease. This effect depends on the plasma clouds' experiencing the same motional electric field that the rest of the orbiting system does. This is a real electric field, and it will not be eliminated by diamagnetic currents within the plasma clouds, which could cancel out the geomagnetic field.

The situation is quite different when a battery is inserted into the circuit. If the polarity of the battery is such that it adds to the motion-induced emf, then it will act to increase the current flowing in the system, especially through the tether wire. The overlapping hollow cathode plasma clouds now act as an alternative path for circuit closure in competition with the ionospheric transmission line, since the hollow cathode clouds experience this applied potential only through their contact with the ends of the tether. Depending on the relative magnitudes of the battery potential and the motion-induced emf, the current in the plasma column will either be reduced or reversed in direction.
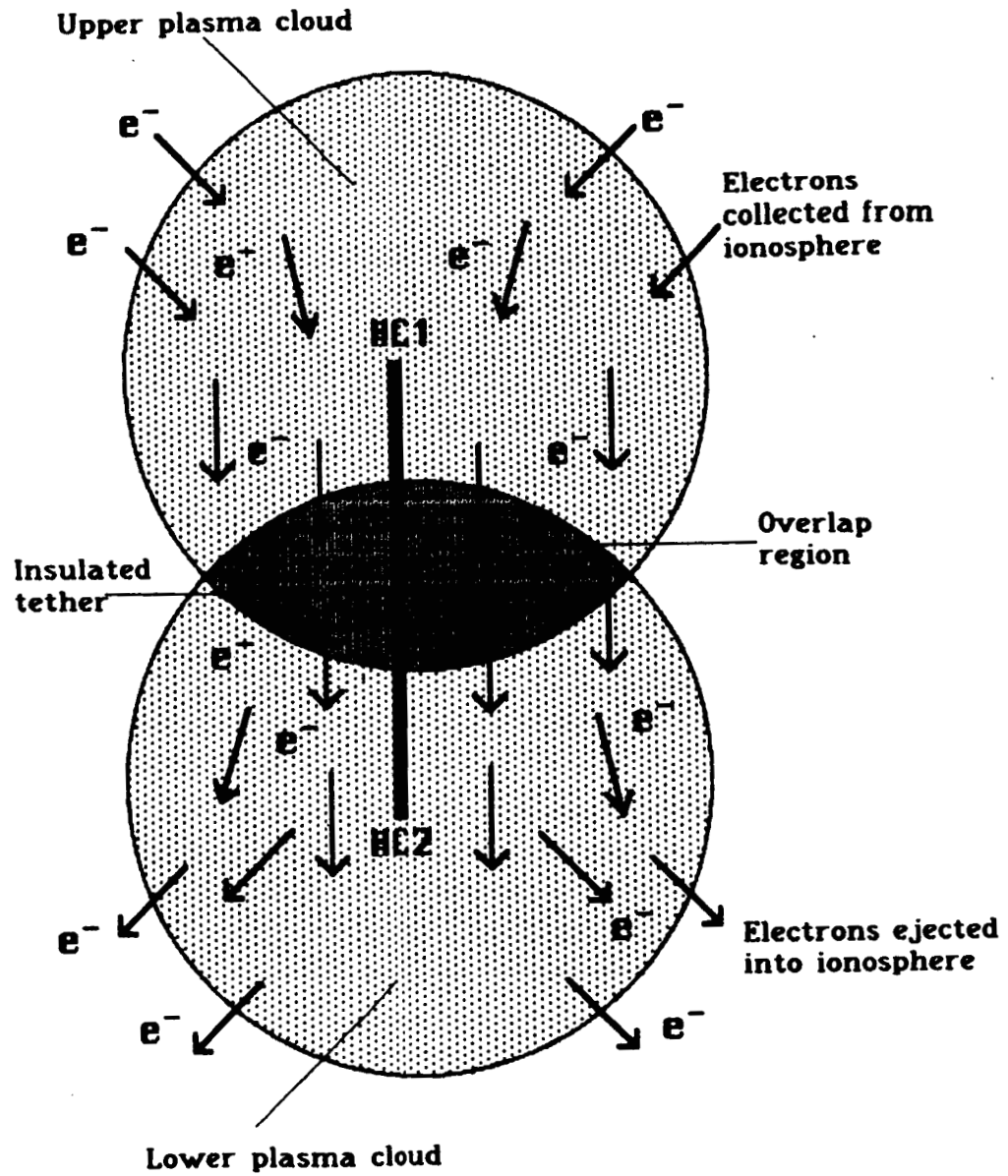
Figure 2.2: Short electrodynamic tether with plasma cloud overlap in motion-driven mode. Hollow cathode clouds compete with tether as conducting path between upper and lower ionospheric levels.

Upper plasma cloud

e⁻

e⁻

Electrons
collected from
ionosphere

HC1

e⁻

e⁻

e⁻

e⁻

e⁻

Insulated
tether

Overlap
region

HC2

e⁻

e⁻

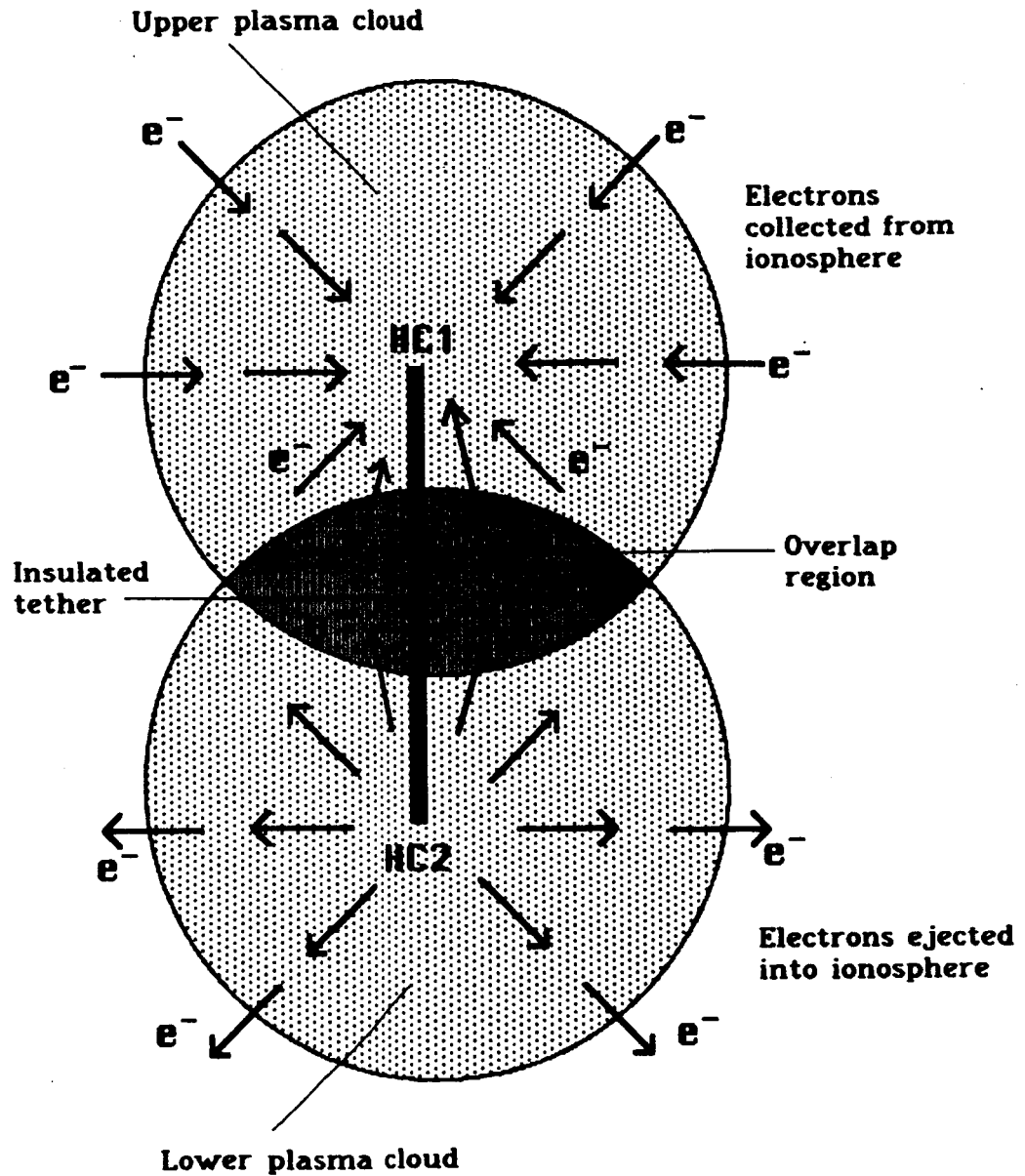Electrons ejected
into ionosphere

e⁻

e⁻

Lower plasma cloud

Figure 2.3: Short electrodynamic tether with plasma cloud overlap in battery-driven mode. Hollow cathode clouds compete with ionospheric transmission line as circuit closure path.

This is all made clearer by the use of simplified circuit diagrams to represent the experiment in its several modes of operation. First, let us consider the long tether case, for which there is no question of hollow cathode cloud overlap. A circuit diagram representation of a long tether electrodynamic system is shown in Figure 2.4. Here the tether resistance is represented by R_t and the impedance across the hollow cathode cloud by Z_{hc}, where the upper and lower hollow cathode impedances are taken as equal to simplify the discussion. We represent Z_{hc} by a resistor symbol, while keeping in mind that this is shorthand for what is more likely to be a nonlinear function of the satellite potential and the hollow cathode and ambient plasma parameters. The ionosphere is represented by an infinite bifilar transmission line with impedance Z_A. The applicability of the transmission line model of the ionosphere is discussed in a later section of this report. The motion-induced voltage is represented by $V_B = vB\ell/c$. The simple circuit equation is then $V_B = i\ (R_t + 2\ Z_{hc} + Z_A)$. Since Z_{hc} and Z_A always occur in this combination, and since we expect that Z_{hc} will be much greater than Z_A, we represent $(2\ Z_{hc} + Z_A)$ by Z_P in the rest of the discussion.

The short tether experiments allow for the introduction of a battery (with the choice of polarization). In Figure 2.5 this is represented by V_A. The three modes of operation during the experiment are then $V_A = \pm\ |V|$, $V_A = 0$. The diagram also explicitly allows for current to flow from one hollow cathode plasma to the other. The induced voltage across the combined clouds is also given by V_B. The effects of plasma cloud polarization, which would reduce the electric field within the cloud, are included in Z_X, the impedance to current flow across the cloud overlap region. The current in the ionospheric transmission line is now the sum of the currents through the tether and the plasma cloud overlap. The tether current I_t and the cloud overlap current I_p may be in the same or opposite
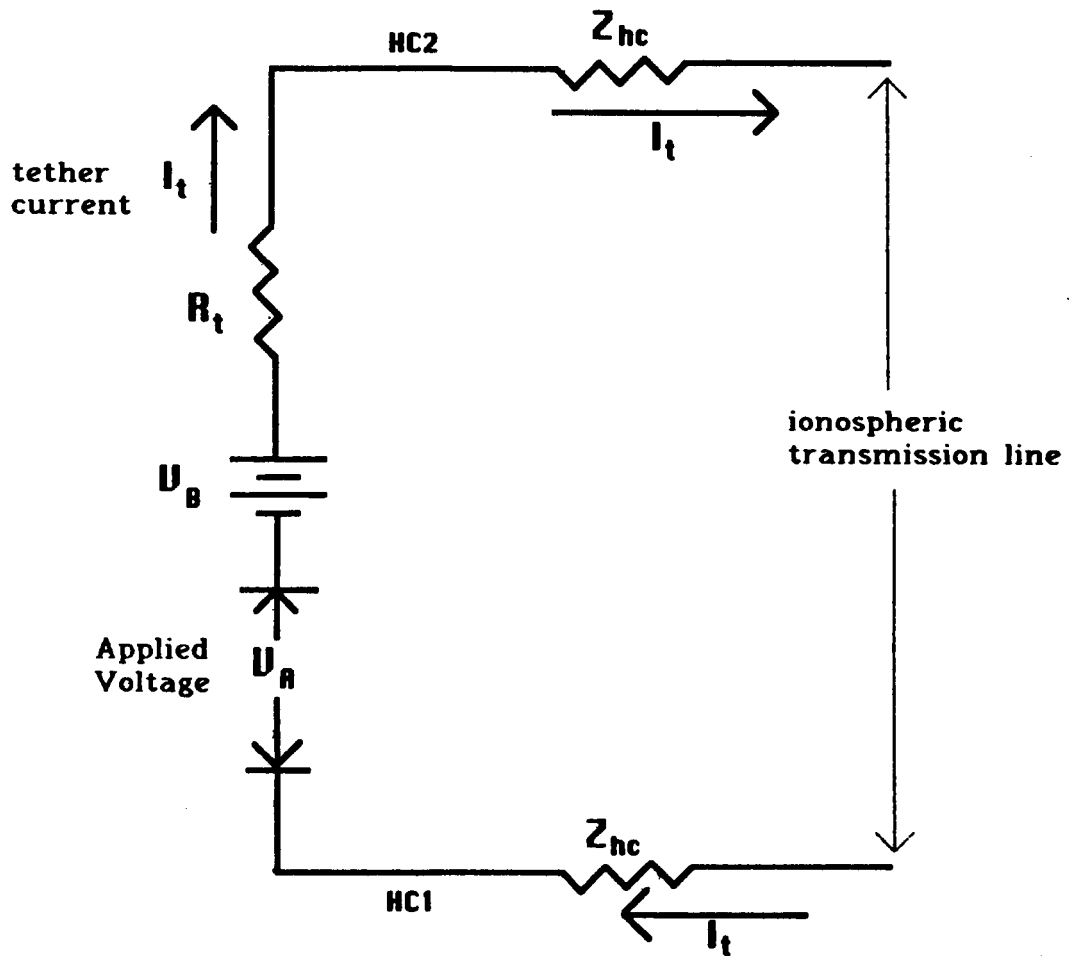
Figure 2.4: Simplified circuit diagram for long electrodynamic tether (hollow cathode clouds from HC1 and HC2 separate). V_B is the motion induced emf $\left(V_B = vB\ell/c\right)$. R_t is the tether resistance and Z_{hc} the impedance across the hollow cathode cloud between the system and the ionosphere.
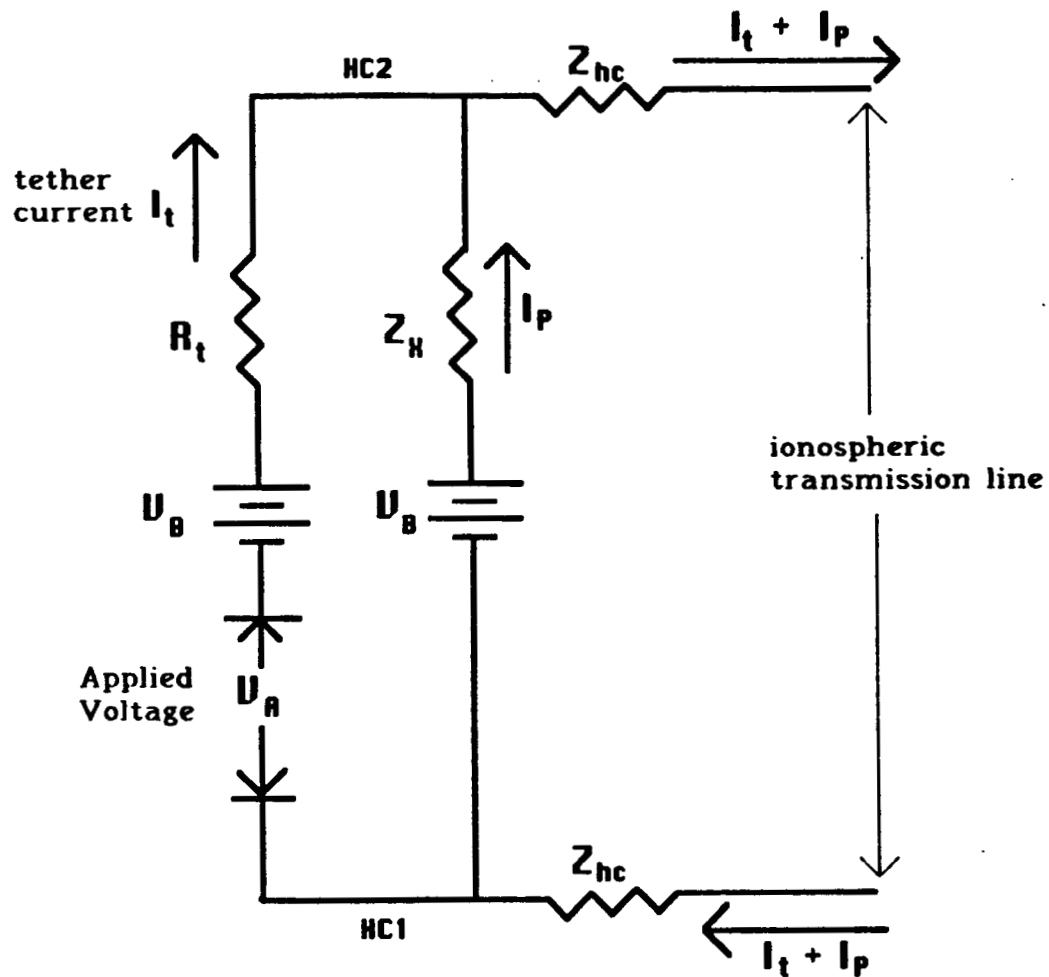
Figure 2.5: Simplified circuit diagram for short tether with overlapping hollow cathode clouds. I_p is the plasma current between the hollow cathode clouds. The impedance to current flow across the cloud overlap is symbolized by Z_X. Relative sign of I_t and I_p depends on magnitude and polarity of the applied voltage V_A.

direction depending on the relative magnitudes of V and V_B and the sign of V.

We emphasize again that Z_X will be a function of tether length and voltage. The clean separation between Z_X and Z_{hc} is another obvious oversimplification. The circuit diagrams are meant to be suggestive, nothing more. Nonetheless, the circuit diagrams demonstrate the basic difference between the effect of plasma cloud overlap in the cases where the battery is in or out of the circuit.

If we make the assumption that the circuit diagrams approximate reality, i.e., that breaking up the physics of hollow cathode current flow into the effects of Z_X and Z_{hc} makes sense, we can proceed to use the corresponding circuit equations to derive a method for analyzing the experimental results. Z_X and Z_{hc} need remain approximately constant only long enough for a series of measurements to be made in the different operational modes of the experiment. The circuit equations provide consistency criteria that will enable us to determine whether the approach makes sense for any given series of tether current measurements.

The equations corresponding to Figure 2.5 are

$$V_B - Z_P\left(I_t + I_P\right) = I_t R_t - V \qquad (2.1a)$$

$$V_B - Z_P\left(I_t + I_p\right) - Z_X I_p = 0 \qquad (2.1b)$$

where I_t is the measured tether current and I_p is the unknown plasma current drawn across the overlapping hollow cathode clouds.

First, let us consider the case for $V = 0$. Then I_t and I_p have the same sign, and their ratio is determined by the ratio of the tether resistance to Z_X.

$$I_t/I_p = Z_X/R_t \tag{2.2}$$

This just expresses what has already been pointed out: in the motion-driven case, the tether plus plasma cloud system acts as a single (composite) electrical path (in parallel) between the ionospheric layers at the ends of the tethered system.

Each tether current measurement gives us two equations. Our unknowns are Z_X, Z_P, V_B, and the plasma current at the given applied voltage. So, for the first measurement we have two equations and four unknowns. Another measurement leaves us with four equations and five unknowns with the additional unknown plasma current. Analysis reveals that additional measurements yield no more information (assuming that our "constants" are really constant). Thus we are left with one unknown, in terms of which we can solve for the other unknowns. Although V_B will not be a well-known quantity, we should be able to estimate it at least to within a factor of two, which would give us estimates of the other quantities with the same level of precision.

First we can eliminate I_p^i from the equations since

$$I_p^i = \frac{C^i}{Z_X} \tag{2.3}$$

where

$$C^i = I^i R_t - V^i$$

From two separate measurements with voltages V^1 and V^2 we then obtain

$$Z_P = \frac{\left(C^1 - C^2\right)}{\left(C^1 I_t^2 - C^2 I_t^1\right)} \; V_B = A \; V_B \tag{2.4}$$

If our analysis based on constant Z_P, V_B, and Z_X (over a given short range of tether length) makes sense, then

$$A = \frac{\left(I^1 - I^2\right)R_t + \left(V^2 - V^1\right)}{V^2 I^1 - V^1 I^2} \tag{2.5}$$

must be a constant for any pair of measurements. We thus have a criterion by which to judge whether or not the circuit analysis approach is valid in a particular range of measurements.

Having eliminated I_p^i and Z_P from the equations, we can now solve for Z_X in terms of V_B. The result is

$$Z_X = \frac{A \; V_B C^i}{V_B - A I_t^i - C^i} \tag{2.6}$$

In the interest of concreteness, let us postulate a set of system parameters and see what the consequences are for the measured tether current in the three voltage modes of the experiment as the tether length increases. For simplicity we assume a constant Z_p of 20Ω, which is consistent with estimates based on laboratory results. The big assumption here is that Z_p does not change as the voltage varies over the range of -50 to 90 volts. The tether resistance is chosen to be 5Ω and the motional electric field to be 0.2 V/m, which corresponds to a

maximum of 40V at the 200 m full extension of the wire. The cross-cloud impedance Z_X is taken to be 1Ω at 5m and to increase as $(L/5m)^2$ for larger tether length L. This "law" is not based on any physical model and is merely chosen to give a fairly steep drop off in the cross-cloud current I_p, so that effects of cloud overlap are apparent. For reference, the motional emf and Z_X are displayed as functions of the tether length in Figures 2.6 and 2.7.

First let us consider the motion-driven mode. As previously discussed, I_p and I_t have the same sign in this case. This is illustrated in Figures 2.8(a) and 2.8(b). For the parameters chosen, this mode is not very useful for observing cloud overlap, since the only measured quantity is I_t. Only a slight deviation from linearity is observed in I_t at small tether lengths. This is because cloud overlap is significant only for smaller separations and, hence, lower motion-induced voltages. The rise in I_p for lower separations occurs as the voltage increases while Z_X is still smaller than R_t.

The currents for the positive 50V mode are shown in Figures 2.9(a) and 2.9(b). The high ($>$8A) tether currents at the smallest separations are due to the local circuit closure across the cloud overlap region. As the overlap impedance Z_X increases with separation, I_t falls off, since circuit closure is now across the hollow cathode/ionosphere system. The rise in I_t seen after it reaches a minimum around 60 meters is due to the increasing motional emf as the tether length increases. I_p is seen to have the opposite sign from I_t and to be of about the same absolute value for small separations, where circuit closure is local.
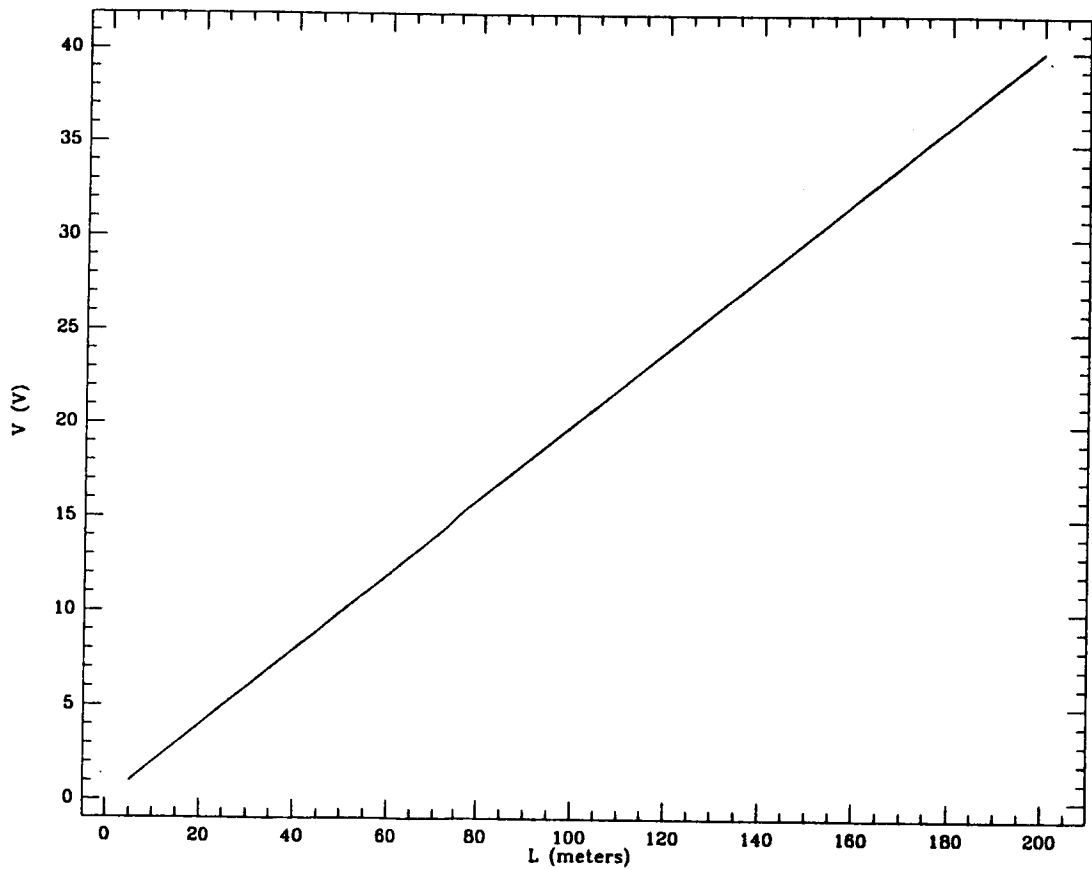
Figure 2.6.   Motion-induced voltage as a function of tether length for the example considered (E = .2 V/m).
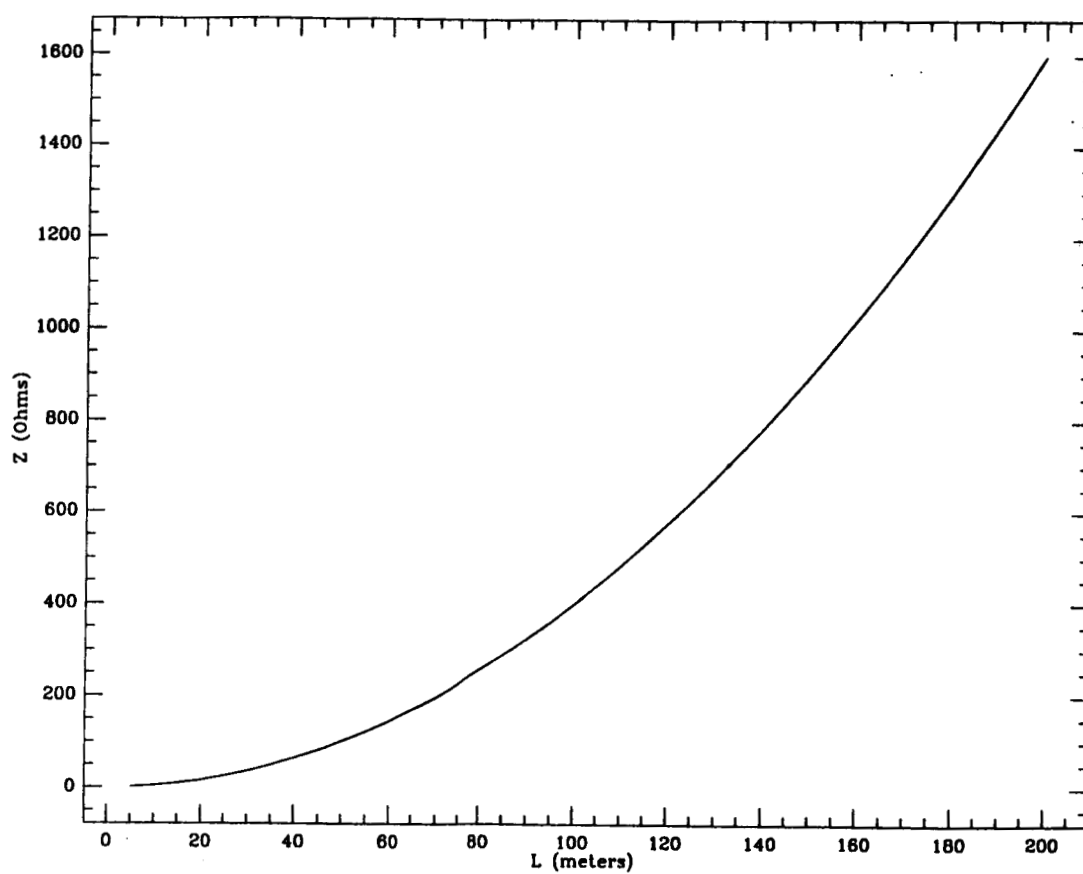
Figure 2.7. Z_X, the cross-cloud impedance, plotted versus tether length for the example described in the text. This is simply for illustration and not based on a physical calculation.
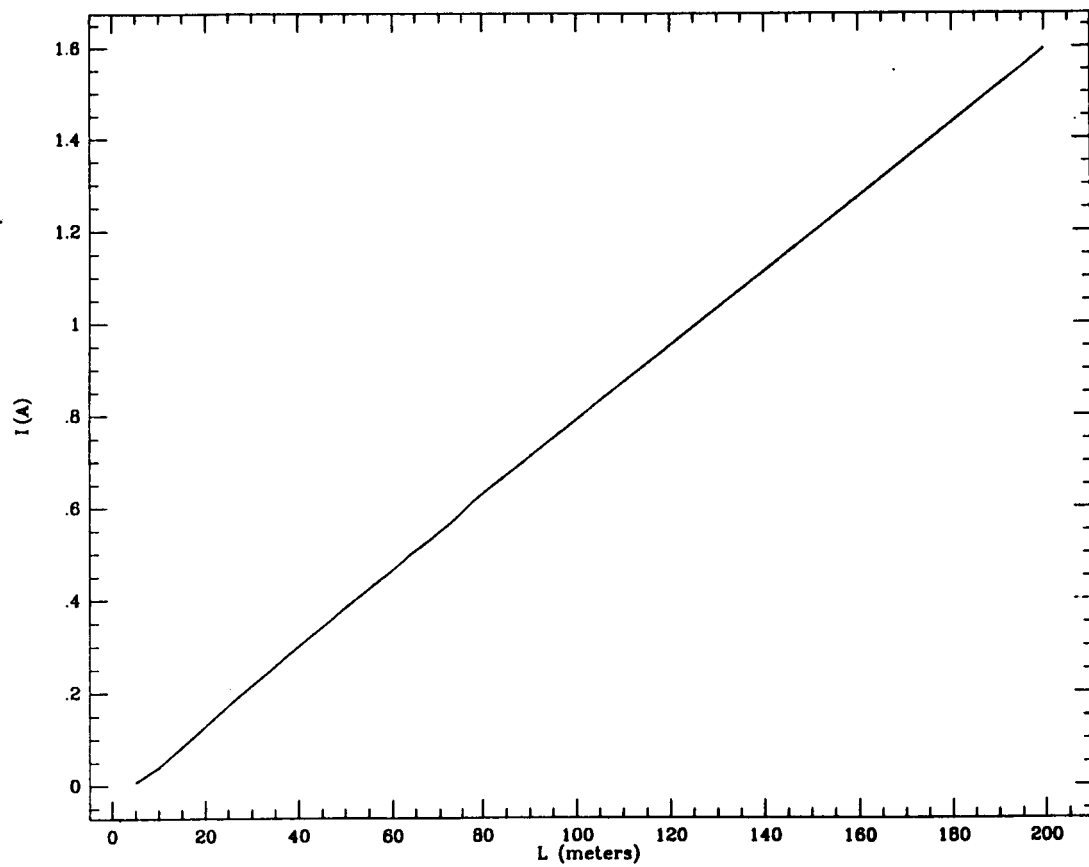
Figure 2.8(a). Tether current I_t in the motion-drived mode as a function of tether length for the example described in the text.
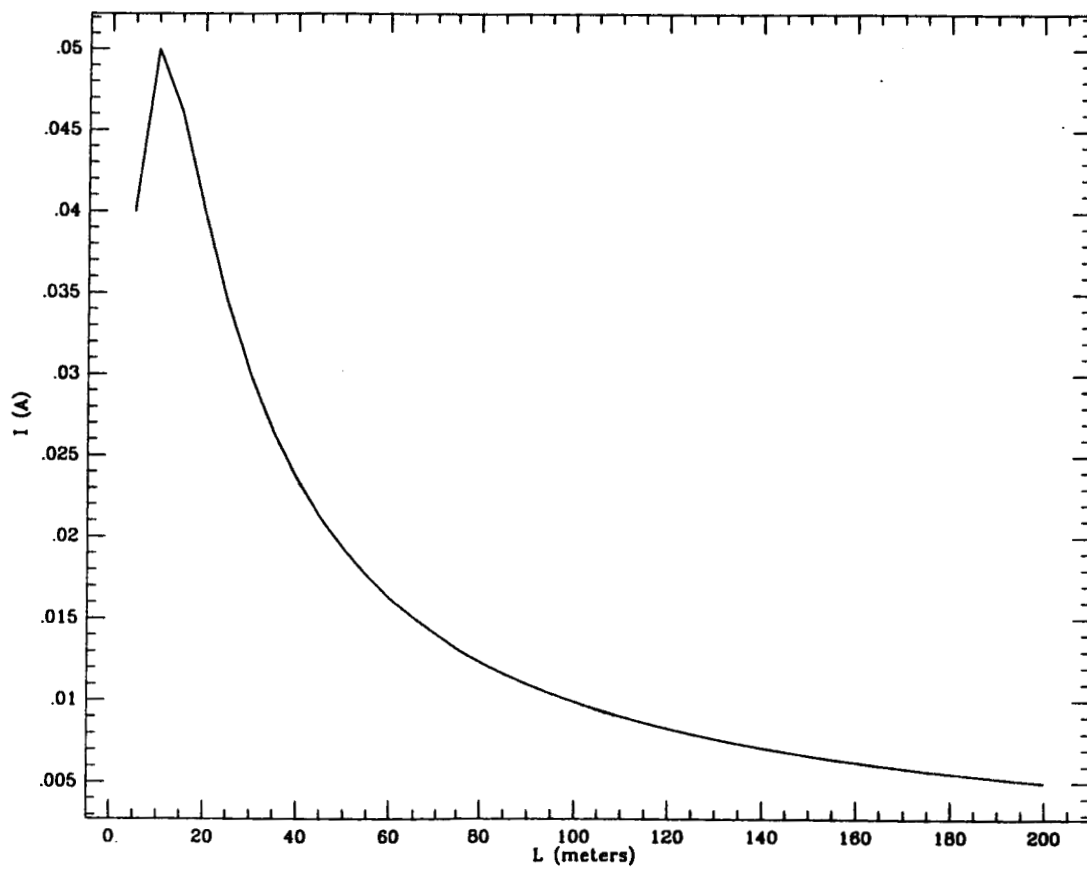
Figure 2.8(b).   Cross-cloud current, I_p, in the motion-driven mode as a function of tether length for the example described in the text. Note current has same sign as corresponding I_t in Figure 2.8(a).
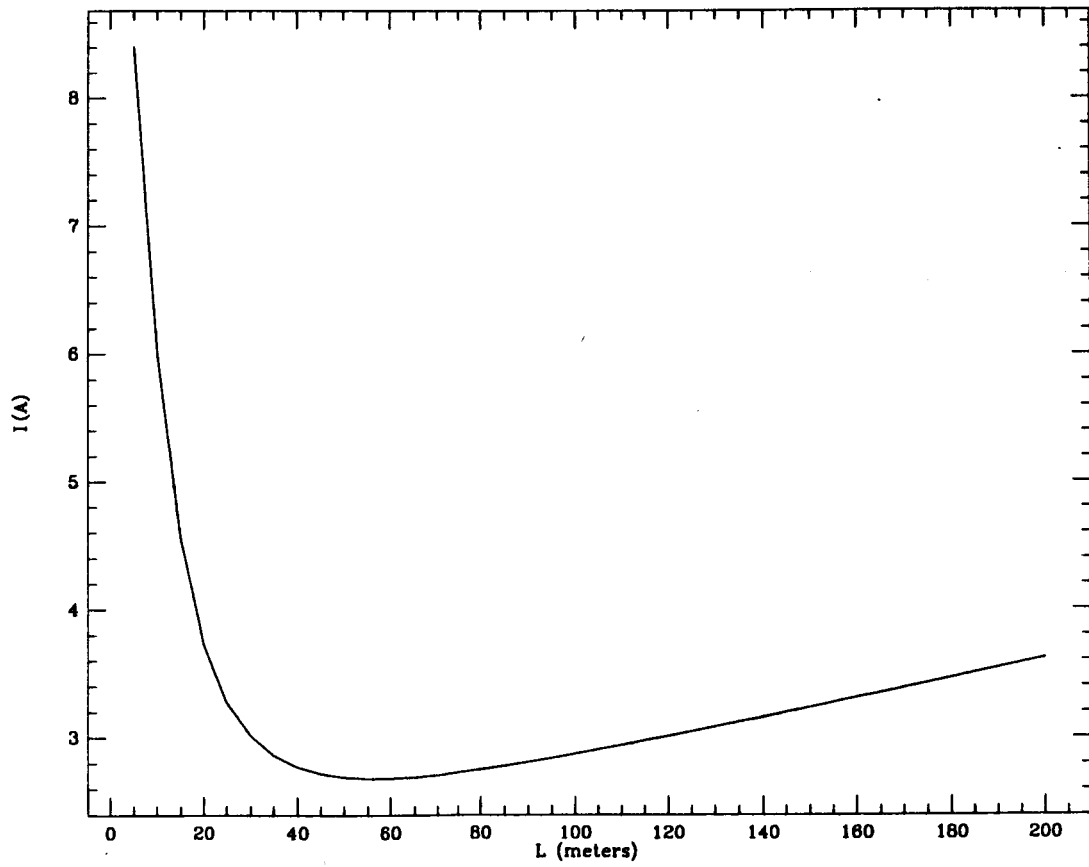
Figure 2.9(a). Tether current I_t for a positive voltage (same sign as motional emf) of 50V as a function of tether length for the example described in the text.
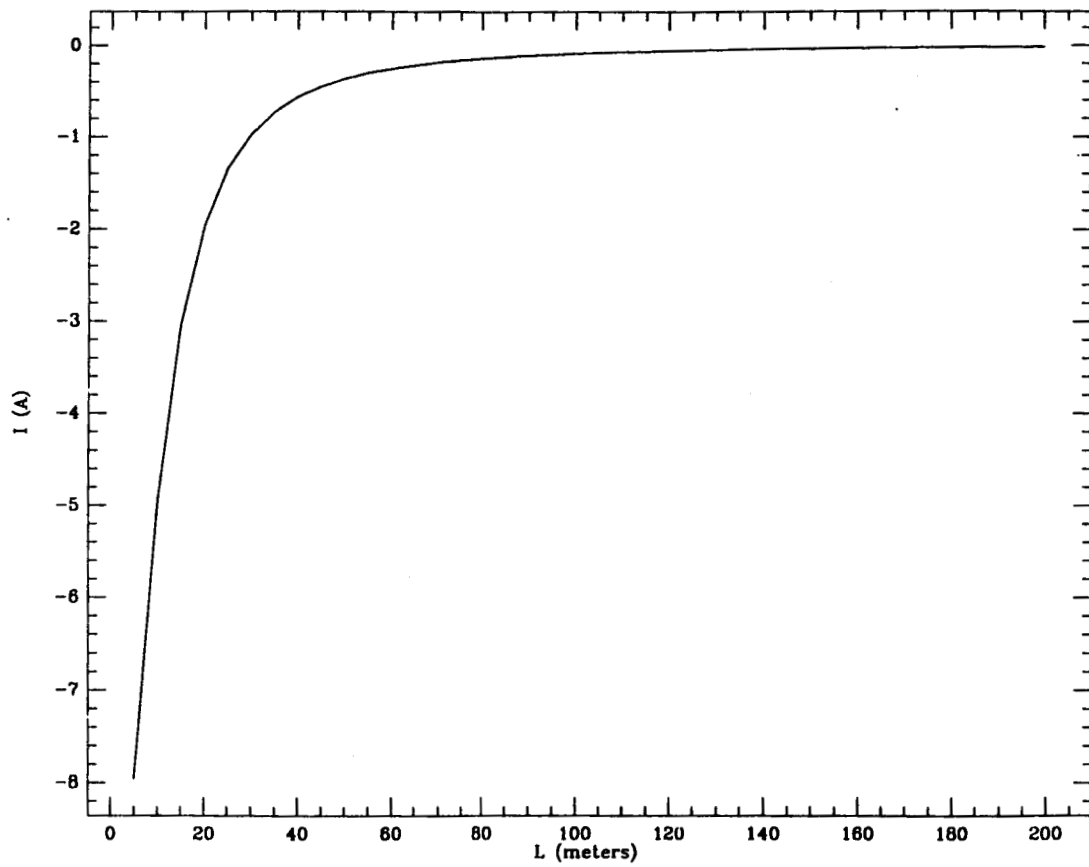
Figure 2.9(b).   Cross-cloud current I_p for a positive voltage of 50V as a function of tether length for the example described in the text.   Note current has opposite sign from corresponding I_t in Figure 2.9(b).

Figure 2.10(a). Tether current I_t for a negative applied voltage (opposite sign from motional emf) of 50V as a function of tether length for the example described in the text.

Figure 2.10(b).   Cross-cloud current I_p for a negative voltage of 50V as a function of tether length for the example described in the text. Note current has opposite sign from corresponding I_t in Figure 2.10(a).
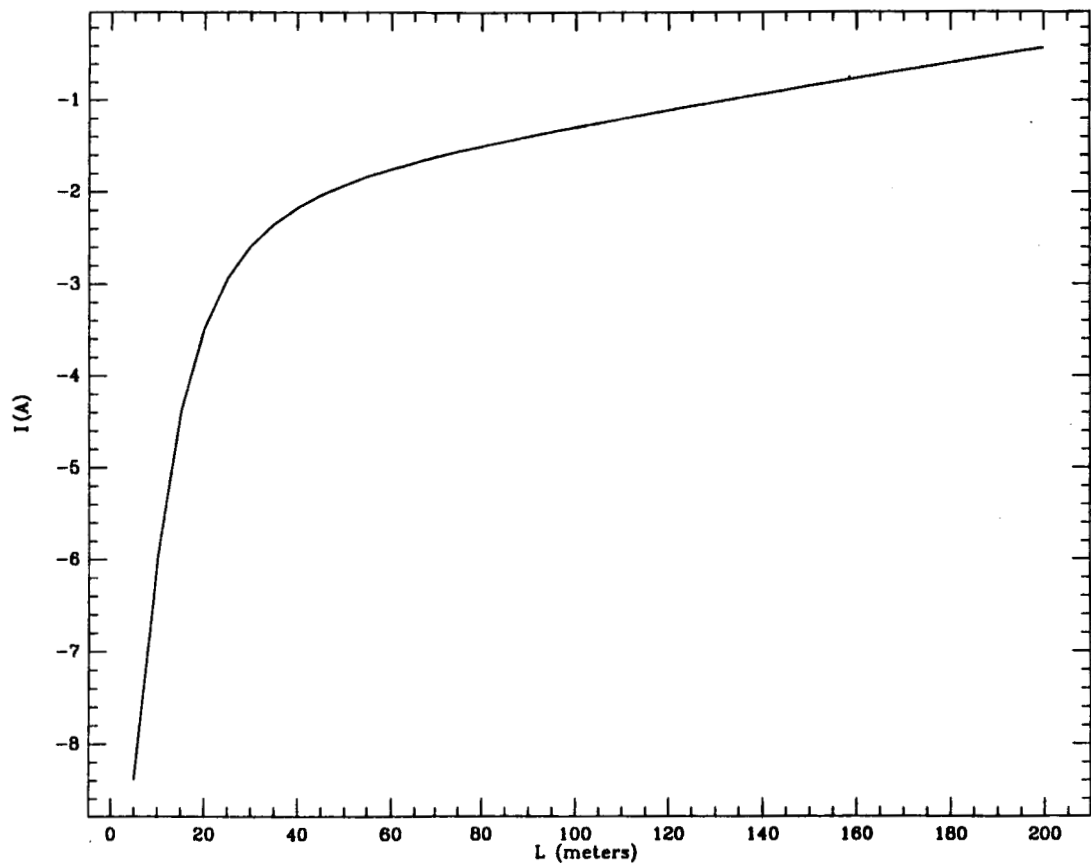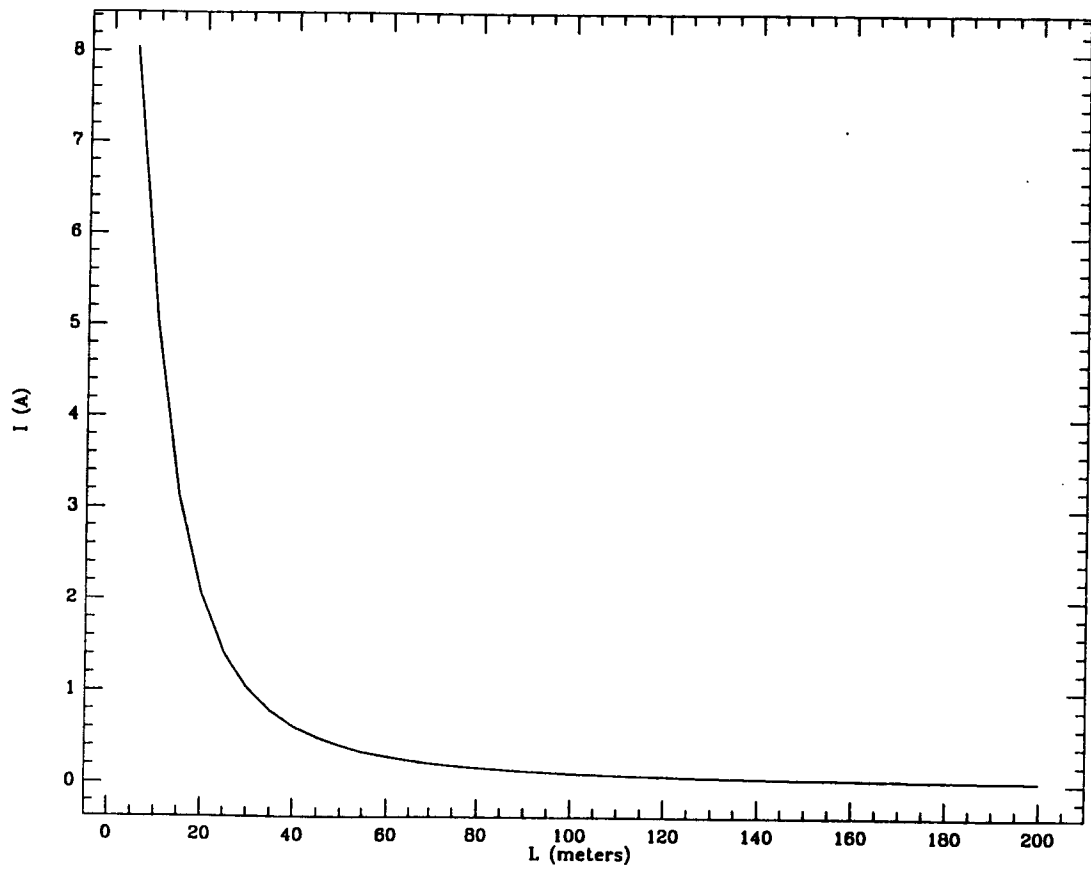
The general features of the negative voltage battery-driven case shown in Figures 2.10(a) and 2.10(b) are almost the reverse of the positive voltage case, except that the increasing motional emf now works against the applied voltage, thus reducing the tether current further after the decrease due to the increase in Z_X.

Although the model used in this example is oversimplified, the simulated results are useful as illustrations of the effect the cross-cloud current can have on the measured quantity I_t. A more complicated version of the circuit diagrams could provide useful in the data analysis.

An obvious conclusion from the line of reasoning presented here is that measurements in all three voltage modes should be made in sequence repeatedly with both hollow cathodes operating throughout the early (smaller separation) part of the experiment in order to obtain the maximum amount of information on cross-cloud current flow and, hence, plasma cloud size.

3.0   HOLLOW CATHODES IN LOW EARTH ORBIT

3.1   General Introduction

Several problems of great significance for understanding plasma contactors and the physics of plasma contactor clouds have been identified in this research. Work done on these problems will be of immediate utility for determining the efficacy of plasma contactors for maintaining spacecraft electrical neutrality during experiments involving electrodynamic tethers, and for the design of experiments relating to understanding the operations of plasma contactors in the lower ionosphere.   We consider the plasma contactor cloud as a conducting object embedded in an ionospheric medium flowing past the Shuttle at orbital velocity. This viewpoint is consistent with the qualitative picture of the mechanism by which a plasma contactor operates as being due to its larger collecting area available for collection of charge from the ambient plasma.   It also allows us to make a direct connection with the body of literature pertaining to the charging of spacecraft in general.   This qualitative mechanism of the plasma contactor operation suggests the crucial importance of determining the characteristic size and the detailed geometry of the boundary of the plasma contactor cloud.   These questions have an immediate bearing on the value of the current drawn through the plasma contactor as a function of applied voltage, and on the possible overlap of the two plasma contactor clouds in the upcoming Shuttle experiment.

To the best of our knowledge, up until the present, plasma contactors have been operated either from sounding rockets or from satellites in geosynchronous orbit.   In these situations the relative motion of the plasma contactor and the ambient plasma (and terrestrial magnetic field) is comparatively slow.   The

proposed Shuttle experiments introduce the novel feature of significant motion of the ambient plasma with respect to the plasma contactor. This changes the basic physics describing the plasma contactor cloud in several significant ways.

Motivated by the requirement of collecting charge to maintain spacecraft neutrality during electrodynamic experiments or to enhance tethered satellite currents, we have considered the trajectories of charged particles in the neighborhood of a charged satellite (such as the plasma contactor when gas flow is turned off) and in the neighborhood of the conducting plasma contactor cloud. We have determined that even under very modest applied voltages, the guiding center approximation, as applied to the trajectories of particles in the ionosphere outside the plasma contactor cloud, breaks down. This has the effect of increasing the effective cross section of the plasma contactor cloud for collecting charge from the ionosphere. Experiments are suggested to be performed in plasma chambers which could illuminate this question.

We have attempted to obtain physically meaningful bounds on the dimensions of the plasma contactor cloud and on its characteristic shape. We have computed a fluid dynamic estimate of the size of the plasma contactor cloud using a technique analogous to those used by workers investigating the interactions of comets with the solar wind. If it is assumed that the mean free path for plasma contactor cloud particles and ionospheric particles is sufficiently small that a fluid dynamic description is valid, the growth of the plasma contactor cloud is limited by the ram pressure due to the motion of the ionosphere with respect to the Shuttle. Given the assumptions made in this calculation, it is apparent that this calculation yields a lower bound on the characteristic size of the plasma contactor cloud.

The analogy we have made with comets and the plasma contactor cloud suggests the possibility of the existence of a standing shock wave in the ionosphere and shock-heated plasma surrounding the plasma contactor cloud, which would be bounded by a tangential discontinuity. There would also be expected to be a substantial elongation of the plasma contactor cloud along the direction of the line of flight (though not a dramatic as a comet tail).

Plasma kinetic calculations have been carried out to provide an upper bound on the plasma contactor cloud size. The intention was using calculations with differing physical assumptions, to bound the plasma contactor cloud dimensions above and below.

An immediate result of the theoretical calculations described here is a set of estimates of relevant time scales for the evolution of plasma contactor clouds. We have found that almost all relevant physical time scales are of the order of tens of milliseconds. If it is desired to sample the rise times of the current trace when voltage is applied, faster data acquisition rates will be required. In view of the information contained in the transient response, such data is highly desirable. Experiments in plasma chambers are suggested which will provide insight into possible breakdown of the guiding center approximation in the neighborhood of the plasma contactor cloud. Geometric considerations of the plasma contactor cloud suggest experiments which can be tried in the Shuttle experiment in which two plasma contactors with separately definable bias voltages will be deployed.

3.2   Magnetically Limited Flow In A Plasma Contactor Experiment -- Breakdown Of Guiding Center Motion

Typical electron gyroradii in the ionosphere are of the order of 1 centimeter. This is much smaller than other relevant scale lengths for the collection of current by a plasma contactor cloud, or by a metallic collecting surface. Consequently, we may consider electrons as being effectively "tied" to magnetic field lines and will treat their motion in a guiding center approximation. Current will only be collected from magnetic field lines which intersect with the collection surface, and so the magnetic field will act to limit the total current which may be collected by such devices. We shall begin with a treatment of the limits of validity of a guiding center approximation treatment of electron trajectories.

The mathematical treatment here will be based on the results of Parker and Murphy [1967], who attempted to calculate the current collected by a conductor biased positive with respect to the ambient plasma. Since electrons may be collected only if the magnetic field lines which determine their gyro-orbits intersect the current collector, the relevant scale for current collection is the cross-sectional area of the current collector projected normal to the magnetic field. The current collecting surface for this experiment is a cylinder 14 3/4 inches in diameter and 10 inches long. Since the ratio of diameter to length of this cylinder is near unity, we can approximate it as a sphere with a diameter the geometric mean of these two dimensions, i.e. 30.8 centimeters. (The principal motivation for considering a spherical collector is to eliminate the orientation of the collector with respect to the direction of the magnetic field vector as a relevant physical parameter.)

We shall work in a cylindrical (r, θ, z) coordinate system centered on the current collector. Electrons being collected by the system will be tightly bound to geomagnetic field lines, but will experience a radial drift velocity due to the potential, Φ. This radial drift velocity is given by

$$v_r = - \left(v_z/m\omega^2 \right) \frac{\partial^2 \Phi}{\partial r \, \partial z} \qquad (3.1)$$

with $\omega = eB/mc$, the gyrofrequency. If a form for the potential is adopted of a strictly Coulombic field,

$$\Phi = - \Phi_o a / \sqrt{r^2 + z^2} \qquad (3.2)$$

where a is the radius of the current collector, then from equation (3.1)

$$\frac{dr}{dx} = - \frac{1}{m\omega^2} \frac{\partial^2 \Phi}{\partial r \, \partial z} = \alpha a^3 rz/(r^2 + a^2)^{5/2} \qquad (3.3)$$

where

$$\alpha \equiv 3\Phi_o/(m\omega^2 a^2) = -1.71 \times 10^{-3} \frac{V[volts]}{\left(a[meters]B[gauss] \right)^2} \qquad (3.4)$$

Taking $a = 0.154$ meter and $B = 0.45$ gauss, we find that $\alpha = (0.356)$ V[volts]. This would give $\alpha = 17.8$, even for a bias voltage of only 50 volts, as currently contemplated for the plasma contactor experiment. The value we have chosen for a would be appropriate for a description of current collection when the gas flow

through the plasma contactor is turned off and current collection occurs only due to the bias voltage applied to the contactor. A larger value of a would be appropriate if the gas flow is on, generating a conducting plasma cloud around the contactor.

Parker and Murphy have derived that values of $\alpha < 7.2$ are required for the validity of the drift approximation of electron motion in the vicinity of the current collector. On the basis of the calculation given above, we can see that the regime of conditions in which the guiding center approximation breaks down is easily accessible in this experiment when plasma is not being generated by the plasma contactor.

We may adopt a simple model to describe current collection in the case when the guiding center approximation breaks down. We shall assume that all electrons whose trajectories depart from guiding center motion will eventually impinge on the collector. This is probably not a bad approximation, since these electrons are not well confined to magnetic field lines, although not all such trajectories can be expected necessarily to intersect the collector surface. On this basis we can define an effective current collection radius, a_{eff}, by

$$7.2 = 3\Phi_0/\left(m\omega^2 a_{eff}^2\right)$$

$$\rightarrow \quad a_{eff} = \frac{0.0154\sqrt{V(volts)}}{B[gauss} \tag{3.5}$$

where a_{eff} in equation (4) is measured in meters. When $B = 0.45$ gauss, we have that $a_{eff} = 0.34$ meters for a bias voltage of 100 volts.

It is apparent that current collection with an applied bias, and with gas flow through the plasma contactor turned off, will almost certainly be in a regime in which electron trajectories deviate significantly from the guiding center approximation in the neighborhood of the current collector. However, for laboratory experiments in which we can control B, we may recover a regime of guiding center electron trajectories, for the purposes of comparison with theoretical limits on current collection. For example, if we take $B = 10$ gauss and $V = 100$ volts, we find that $\alpha = 0.072$ which is still definitely in the guiding center regime.

3.3 Magnetic Diffusion, Magnetic Reynolds Numbers, And Access Of Electrons To A Plasma Contactor

As electrons in the earth's ionosphere are effectively tied to geomagnetic field lines (since typical gyroradii are on the order of 1 centimeter), in order for current collection to occur by a conductor orbiting through the ionosphere, it is necessary for magnetic field lines to diffuse through some conducting surface. This is true whether the conductor in question is a metallic conductor, or the plasma cloud generated by a plasma contactor. The time available for diffusion of magnetic field lines through conducting surfaces will be limited by the orbital motion of the spacecraft, amounting to approximately 8 kilometers per second in low earth orbit.

Note that this simple picture of accessibility of electrons along magnetic field lines is applicable as long as the guiding center approximation holds. The previous calculation demonstrated that that this breakdown may occur at comparatively modest potential differences with respect to the local plasma potential, if the collector is of a sufficiently small size.

A further requirement for the general validity of this treatment is that the conductivity of the medium external to the moving conductor have a sufficiently high conductivity that we may speak of magnetic field lines being "frozen in" the plasma. This condition allows us to treat the evolution of magnetic fields as physical objects. This high conductivity situation commonly exists in astrophysical and magnetospheric plasmas where the conductivities as high and/or scale lengths are long (Alfvén 1950; Parker, 1979; Rossi and Olbert, 1970).

The diffusion time for magnetic field to fully penetrate a conductor of scale length ℓ, and conductivity σ is (in Gaussian cgs units),

$$\tau = 4\pi\sigma\ell^2/c^2 \tag{3.5}$$

and the magnetic Reynolds number if that conductor is moving at a velocity, v is,

$$R_M = v\tau/L \tag{3.6}$$

where L is a scale length.

The magnetic Reynolds number characterizes the relation between the material particles and magnetic field lines contained in a magnetized fluid flow. When $R_M \gg 1$, as characterizes almost all astrophysical and magnetospheric plasmas, magnetic field is corrected with the material flow and the magnetic field is said to be "frozen in" (see e.g. Parker 1979). When $R_M \simeq 1$, the effects of magnetic diffusion are comparable in magnitude to the convective terms in the equations for the evolution of the magnetic field,

$$\frac{\partial \vec{B}}{\partial t} = \nabla \times (\vec{v} \times \vec{B}) - \nabla \times (\eta \nabla \times \vec{B})$$

$$\tag{3.7}$$

$$= \nabla \times (\vec{v} \times \vec{B}) + \eta \nabla^2 \vec{B}$$

where $\eta = c^2/4\pi\sigma$ is the resistive diffusion coefficient. The second line of (3.7) is

the familiar result obtained when η is constant in space.

Note that while ℓ and L are both scale lengths, they may not be equal; ℓ refers to a scale length in which shielding currents may flow in the conductor, while L is the overall scale of the conducting object. L and ℓ may be different, for example, as for a sphere of a thickness of order ℓ and a radius of order L. We distinguish two scale lengths in this instance of a slightly more complex conductor geometry, and in fact this necessity arises because different physical processes are reflected in the two terms on the right hand side of (3.7). We identify ℓ as a characteristic "fine scale" length over which a magnetic field line must diffuse to become physically tied to the moving conductor. This is a small scale length because diffusion is a local process (controlled by the Laplacian term). This would correspond to the thickness, say, of a conducting shell in which a current system is being resistively dissipated as magnetic field diffuses inwards. We distinguish this from L an overall scale length for the body, which determines a time scale for a magnetic field line to be carried past the body by the external flow, corresponding to the first term in (3.7). The physical situation we are attempting to investigate then is whether a magnetic field line can be "attached" to some small scale feature of the conductor in a time scale over which it is in close proximity to the moving conductor. It should be noted that we are certainly calculating the smallest sensible estimate for the Reynolds number of this flow; magnetic field diffusion effects should be <u>no more</u> important than this simple calculation suggests.

When $R_M \ll 1$, magnetic field can fully diffuse into the conductor in the time in which the objects orbital motion carries it past the magnetic field line. On the other hand, when $R_M \gg 1$ magnetic field exterior to the object does not substantially enter the conducting object, either due to its orbital velocity or high conductivity. In such a situation magnetic field diffuses out of the moving

conductor at the "trailing edge" faster than it diffuses in at the front. Correspondingly, such a moving conductor with large R_M will lose its magnetic field via diffusive processes, even if initially such an field originating in the external plasma permeated the moving conductor. The situation is analogous to that which occurs when the solar wind encounters a conducting ionosphere of a planet or comet in a high magnetic Reynolds number flow (Russel, et al., 1982).

We now consider some characteristic numbers to attempt to characterize the flow regime for magnetized plasma around the plasma contactor experiment. First we shall consider the conducting metal components, independently of the presence of the plasma cloud. Say that the relevant scale length for the thickness of conductors is $\ell \approx$ 1 cm. The resistivity of aluminum is $2.824 \times 10^{-6} \Omega - cm$. This implies a conductivity of 3.54×10^7 mho/m, or 3.19×10^{17} sec^{-1} in cgs units. Calculating the magnetic diffusion time for these parameters yields $\tau = 4.45 \times 10^{-3}$ sec. The magnetic Reynolds number is determined by the length scale of the overall dimensions of the collector, $L \approx$ 15 cm, for the present case. We make take v as the orbital velocity of the Shuttle, i.e. $v \approx$ 8×10^5 cm/sec. These values will yield $R_M \approx$ 237.0, a surprisingly large value, which has significant implications for the collection of current by the plasma contactor when gas flow is turned off. $R_M \gg 1$ implies that the ionospheric field lines passing by the plasma contactor will not significantly penetrate the contactor collecting surface, and so as long as electrons are effectively tied to magnetic field lines, current collection will be very inefficient. In fact, the breakdown of the guiding center approximation, as considered in the calculation above, will be required to obtain any significant current collection.

It is interesting to note that the theories for current collection of conductors in the ionosphere of Parker and Murphy, and other workers, have had their

greatest successes either for geosynchronous satellites, or for sounding rockets launched at high latitudes. These are cases for which velocities transverse to the magnetic field are small and which have correspondingly small values of R_M.

If gas is flowing from the plasma contactor, there will be a sphere of some characteristic size, a, with a characteristic electron number density, n_e, and a characteristic neutral number density, n_o. We need to consider the resistivity of this plasma sphere in order to compute a characteristic magnetic diffusion time and a magnetic Reynolds number.

We will consider two limits, the first in which the ionization of the plasma generated by the plasma contactor cloud is nearly complete, and the second in which the plasma is weakly ionized, either due to the ionization fraction of the plasma produced being low, or due to dilution by ambient ionospheric neutral particles streaming into the plasma contactor cloud.

For the first case which the ionization fraction, $f \approx 1$, the electrical conductivity of the plasma may be expressed in terms of the collision frequency, ν_c and the plasma frequency, ω_p by,

$$\sigma = \omega_p^2 / 4\pi\nu_c \tag{3.8}$$

i.e.

$$\sigma = n_e e^2 / m_e \nu_c \tag{3.9}$$

[Krall and Trivelpiece, 1973]. This may be shown in the weak (electric) field limit to be

$$\sigma = \frac{3m_e}{(16\sqrt{\pi})Ze^2 \ell n\Lambda} \left(\frac{2kT_e}{m_e}\right)^{3/2} \tag{3.10}$$

which is valid when the electric field satisfies

$$E < \frac{n_e e}{\sigma} \sqrt{\frac{kT_e}{m_e}} \tag{3.11}$$

Note that this conductivity is independent of n_e. The number of charge carriers will increase as n_e increases, but the number of scattering centers also increases proportionately, and so the conductivity is unchanged. We will, for purposes of estimation, take $\ell n \Lambda \approx 10$, which is certainly correct within a factor of 2 or better. The plasma produced by the plasma contactor is assumed to be only singly-ionized, and so we take $Z = 1$. The temperature inside the contactor is $T_e \approx 1000$ °K. The temperature inside the plasma cloud will almost certainly be lower due to adiabatic expansion of the plasma as it expands away from the plasma contactor. We note that this implies an upper bound on the plasma conductivity, since $\sigma \propto T_e^{3/2}$. Substituting numerical values into equation (3.10), we find that $\sigma \leq 2.2 \times 10^{11}$ sec^{-1}.

If we attempt to estimate the magnetic diffusion time for the plasma cloud, taking a scale length of 10 meters, we find that $\tau \leq 3.1 \times 10^{-3}$ sec, and that the magnetic Reynolds number is $R_M \leq 2.5$. A magnetic Reynolds number of order unity suggests that the penetration of the magnetic field into the plasma contactor cloud will not be complete and that some reduction of the estimated current collection by the plasma cloud may be in order. However, the sensitive dependence of this result on the value of the electron temperature should be noted. We have used an estimated maximum value for the electron temperature here, and

hence we have almost certainly significantly overestimated the conductivity of the plasma contactor cloud and the magnetic Reynolds number. A modestly reduced value of T_e, owing to adiabatic expansion of the plasma contactor cloud would put the system into a physical regime with $R_M \ll 1$.

Processes which will raise the electron temperature in the plasma contactor cloud must be carefully considered, as they will raise R_M and complicate treatment of mathematical models of current collection. In particular, plasma instabilities or plasma turbulence in the plasma contactor cloud may heat electron significantly. This possibility will require careful consideration.

We shall now consider crudely the conductivity of a plasma contactor cloud when the ionization fraction is small. The conductivity in such a situation is given be equation (3.8), where ν_c is interpreted as an inverse time-scale for momentum exchange between electrons and some other species, in this case neutral atoms emitted by the plasma contactor cloud, as well as ionospheric neutral atoms streaming through the plasma contactor cloud. We take then $\nu_c \sim 10^9$ sec^{-1} and $n_e \sim 10^7$ cm^{-3}, which implies $\sigma = 5.0 \times 10^8$ sec^{-1}. This value is approximately 440 times less than that in the high ionization limit. Accordingly, τ will be less than 7.0×10^{-6} sec and $R_M \leq 5.7 \times 10^{-3}$. In this regime, penetration of ionospheric magnetic field lines into the plasma cloud will be essentially complete.

The implications of these calculations for the development of theoretical descriptions of plasma contactors in the ionosphere are very important. First of all, it is apparent that some metallic conductor geometries may not be efficient charge collectors until the potential on them becomes so great that the guiding center approximation breaks down. Secondly, any theoretical model, either a fluid dynamic model or a plasma kinetic model must be developed assuming significant penetration of geomagnetic field lines into the contactor cloud, if the dimensions

of these clouds are as large as anticipated.

References for Section 3.2 and 3.3

1.   Alfvén, H., 1950.   Cosmical Electrodynamics, Clarendon Press, Oxford.

2.   Krall, N.A. and A.W. Trivelpiece, 1973.   Principles of Plasma Physics. McGraw-Hill.

3.   Parker, L.W. and B.L. Murphy, 1967.   "Potential Buildup on an Electron-Emitting Ionospheric Satellite," Journal of Geophys. Research 72, 1631-1636.

4.   Parker, E.N., 1979.   Cosmical Magnetic Fields: Their Origin and Their Activity, Clarendon Press, Oxford.

5.   Rossi, B. and S. Olbert, 1970.   Introduction to the Physics of Space, McGraw-Hill, New York.

5.   Russel, C.T., J.G. Luhmann, R.C. Elphic and N. Neugebauer, 1982.   "Solar Wind Interaction with Comets: Lessons from Venus." In Comets, Lawel L. Wilkening (ed.), University of Arizona Press, Tucson.

3.4   Fluid-Dynamic Estimation Of Plasma Contactor Characteristic Scales

It is desirable to get a range of realistic estimates of the characteristic size and evolutionary time scales of plasma contactor clouds as a necessary step in planning experiments for testing the efficiency of plasma contactors for exchanging charge between the Shuttle and the ionosphere.

One extreme limit in modeling such a system is to assume the plasma cloud behaves as a fluid medium flowing out of the plasma contactor. This may be justified as long as the mean free path within the cloud is very small. The plasma cloud then exhibits a ram pressure determined by the expansion velocity of the cloud and its density (which is a function of radius from the plasma contactor). The ionosphere is also flowing past the plasma contactor cloud and thus exhibits its own dynamic ram pressure. A characteristic length scale of the plasma contactor cloud, effectively a "stand-off distance," may be obtained by finding the radius at which the dynamic pressure of the plasma contactor cloud is balanced by the dynamic pressure of the ionosphere (as viewed in a reference frame co-moving with the Shuttle).

The similarities of this physical description with the interaction of a comet with the solar wind should be noted. The possibility of the existence of a standing bow shock wave and a contact discontinuity in the flow around the plasma contactor must also be carefully considered. (See Figure 3.1)

Let $\dot{m}$ denote the mass flow rate from the plasma contactor. For the purposes of this crude estimate, assume that the contactor is effectively a point source of adiabatically expanding gas. Sufficiently far from the plasma contactor, the gas flow will be effectively a free expansion, and will thus be characterized by
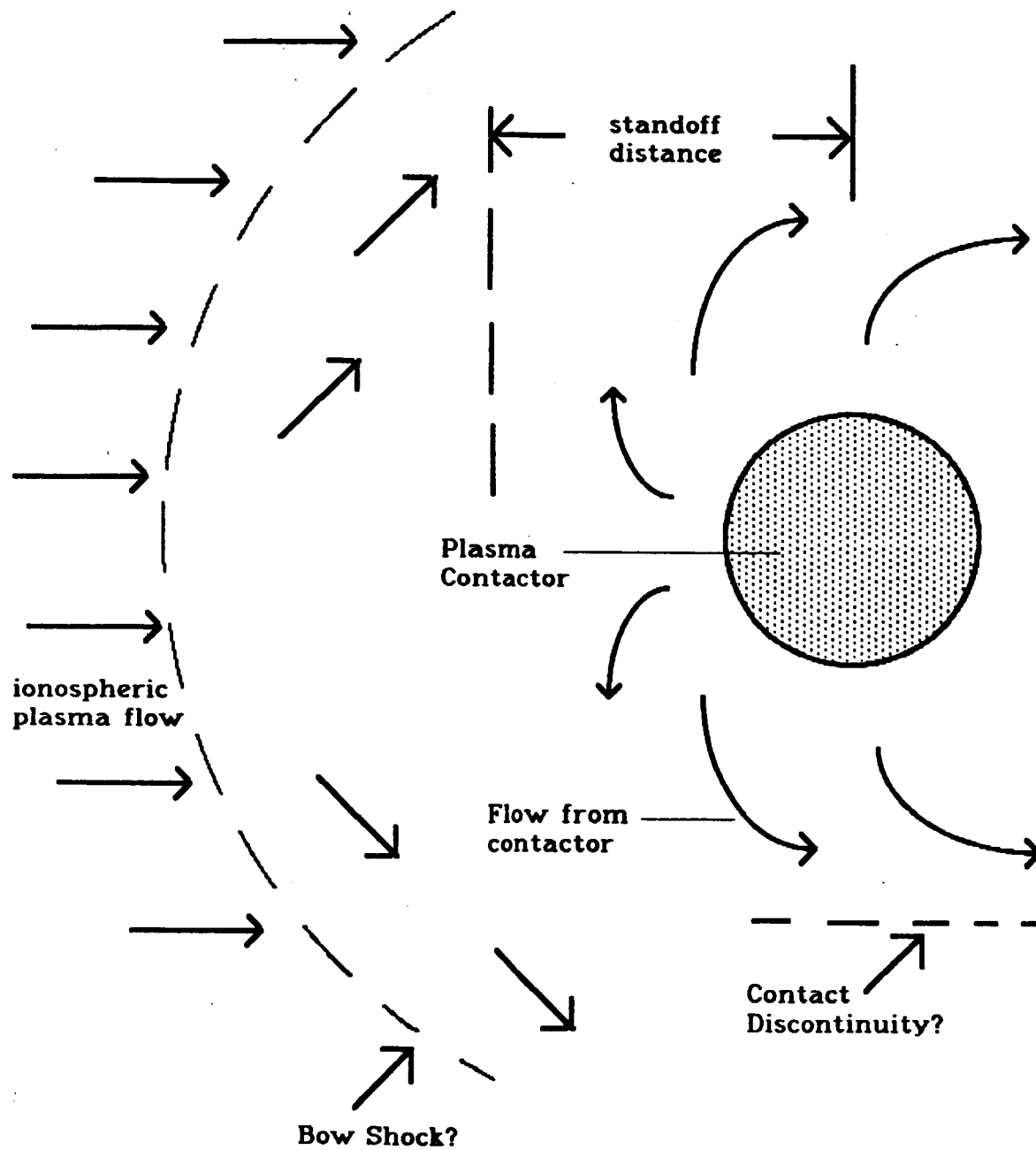
Figure 3.1. Hollow cathode in low-earth orbit.

an expansion velocity,

$$v_{ex} \approx \frac{1}{\sqrt{3}} c_s \approx (kT/m)^{1/2} \qquad (3.12)$$

Here c_s denotes the sound speed, k is Boltzmann's constant, m is the mass of the gas particles (atoms or ions), and T is the temperature at the exit aperture of the plasma contactor. It can be seen that the characteristic expansion velocity of the plasma contactor cloud is determined by the temperature of the gas emitted by the plasma contactor and by the mass of the species released. If T (contactor) $\approx$ 10^3 °K and the gas released is xenon, then $m \approx 2.19 \times 10^{-22}$ gram. This yields $v_{ex} \approx 2.5 \times 10^4$ cm/s = 250 m/s. Now define $\phi(r)$ as the mass flux from the contactor. Then,

$$\dot{m} = 4\pi r^2 \phi(r) \rightarrow \phi(r) = \frac{\dot{m}}{4\pi r^2} \qquad (3.13)$$

We want to determine the mass density as a function of radius in the outflow, $\rho(r)$. Since $\phi(r) = \rho(r) v_{ex}$, then

$$\rho(r) = \frac{\dot{m}}{4\pi r^2 v_{ex}} \qquad (3.14)$$

As the gas is expanding adiabatically, the gas pressure will fall off very rapidly with radius; the contribution from the gas pressure adding to the dynamic pressure of the expanding gas cloud should be insignificant. This may be verified easily. Adiabatic expansion implies that

$$P \propto \rho^\gamma \;\to\; P \propto \left(\dot{m}/4\pi r^2 v_{ez}\right)^\gamma \propto r^{-2\gamma}$$

where P denotes the gas pressure and γ the ratio of specific heats (adiabatic exponent). For inert gases such as xenon and argon, $\gamma = 5/3 \to P \propto r^{-10/3}$. It might be reasonably expected that the expansion factor for the gas might be at least several orders of magnitude (compared to the aperture of the plasma contactor), the gas pressure will drop by at least 10 orders of magnitude from its value at the aperture of the contactor. This of course neglects sources of heat for the the plasma contactor cloud which will certainly be important in the actual experiment, but should not be important for this crude estimate.

We can now balance the pressures and obtain an estimate for the scale size of the plasma contactor cloud. Let v_{orb} be the orbital velocity of the Shuttle, and ρ_{ion}, the mass density of the ionosphere. In the reference frame of the Shuttle, the ram pressure of the plasma contactor cloud is

$$\rho(r)v_{ez}^2 \;=\; \frac{\dot{m}}{4\pi r^2 v_{ez}} \; v_{ez}^2 \;=\; \frac{\dot{m}v_{ez}}{4\pi r^2} \tag{3.15}$$

Now solving for r such that $\rho(r)v_{ez}^2 = \rho_{ion}v_{orb}^2$, we find that

$$r \;=\; \frac{1}{v_{orb}} \; \sqrt{\frac{\dot{m}v_{ez}}{4\pi\rho_{ion}}} \tag{3.16}$$

This then is the desired "stand-off distance" for the flow from the plasma contactor cloud. Experimentally, it is controlled by the release rate of the gas and the expansion velocity (determined by T and $\dot{m}$). There is also a significant

dependence on the ambient plasma density. Substituting appropriate numerical values into equation (3.15), $\rho_{ion} = 2.7 \times 10^{-14}$ gm/cm^3, $\dot{m} = 3.0 \times 10^{-3}$ gm/sec = 1/2 standard cubic centimeter per second, and $v_{orb} = 8.0 \times 10^5$ cm/sec we obtain a value of $r \approx 19$ cm. This value is remarkably small and increases only as the square root of the plasma contactor mass flow rate. Given the assumptions made in the fluid dynamic approximation to the dynamics of the expansion of the plasma contactor cloud, this must be regarded as a lower bound on the size of the cloud. Certainly in the limit of a more collisionless plasma cloud, atoms of the cloud may travel a somewhat larger distance before experiencing collisions with ionospheric particles.

Note that the magnetic field has not been included explicitly in this fluid dynamic treatment. The very small scale size we have obtained indicates that we shall have a very high magnetic Reynolds number for the cloud interaction with the ionosphere, at least within the context of this fluid dynamic model, and the cloud would not be expected to contain a significant geomagnetic field.

This is not to imply that this lower bound accurately reflects the expected size of the plasma contactor cloud, per se, but rather that neglect of internal magnetic fields in this calculation is self-consistent.

We can estimate the range of applicability of the fluid model in the following way. We consider a plasma contactor cloud undergoing simple adiabatic expansion in a steady state (fixed $\dot{m}$).

$$n(r) = n_o \ (r_o/r)^2 \tag{3.17}$$

$$T \propto n^{\gamma-1} \ \rightarrow \ T \propto r^{-(2\gamma-2)} \tag{3.18}$$

$$v_{th} \propto T^{1/2} \ \rightarrow \ v_{th} \propto r^{-(\gamma-1)} \tag{3.19}$$

The thermal velocity considered here is a velocity spread in the mean frame moving with a parcel of gas expanding outward in the plasma contactor cloud flow. This is not to be confused with the expansion velocity of the cloud, which is expected to be nearly constant after the exit aperture of the plasma contactor is left until the flow encounters significant levels of ionospheric material.

$$n(r) \;=\; \frac{\dot{m}/M}{4\pi \; r^2 \; v_{ez}} \qquad (3.20)$$

where M is the mass of an individual plasma contactor cloud particle (atom) the mean free path is given by

$$\lambda_{mfp}(r) \;=\; \frac{1}{n(r)\sigma} \qquad (3.21)$$

Take σ to be a typical gas kinetic cross section of $\sigma \approx 3\times10^{-14}$ cm^2.

Collisional mean free time is

$$\tau_{mfp} \;=\; \lambda_{mfp}/v_{th} \;=\; \frac{1}{n(r)\sigma v_{th}(r)} \qquad (3.22)$$

Take R as the radius of the plasma contactor aperture and T_o the exit temperature

$$T(r) \;=\; T_o \; \left(\frac{R}{r}\right)^{2\gamma-2} \qquad (3.23)$$

$$v_{th}(r) \;=\; v_{th} \; (r=R) \left(\frac{R}{r}\right)^{\gamma-1} \qquad (3.24)$$

where

$$v_{th} \ (r = R) \ = \ \left(\frac{3kT_o}{M}\right)^{1/2}$$

$$v_{th}(r) \ = \ \left(\frac{3kT_o}{M}\right)^{1/2} \left(\frac{R}{r}\right)^{\gamma-1} \ = \ v_{ez} \left(\frac{R}{r}\right)^{\gamma-1} \tag{3.25}$$

$$\tau_{mfp} \ = \ \frac{4\rho r^2 v_{ez}^2 M}{\dot{m}\sigma} \left(\frac{r}{R}\right)^{\gamma-1} \tag{3.26}$$

$$\rightarrow \ \tau_{mfp} \ \propto \ r^{\gamma+1}$$

Since $\gamma = 5/3$ for cases of interest $\tau_{mfp} \propto r^{8/3}$, typically.

A fluid dynamic description of the flow will break down when $\tau_{mfp} > \frac{r}{v_{ex}}$, or equivalently, when $\lambda_{mfp} > r$. We expect this to happen when $\dot{m}$ is small. (Alternatively, we can imagine a value of $\dot{m}$ sufficiently large than the fluid description is valid clear to the standoff distance of the fluid dynamic calculation, but this may not describe a practical regime of plasma contactor operations.)

We have

$$\dot{m} \ = \ 3 \times 10^{-3} \ gm/\sec$$

$$v_{ez} \ = \ 2.5 \times 10^4 \ cm/\sec$$

$$M \ = \ 2.19 \times 10^{-22} \ gm$$

Taking $R = 1$ cm, gives $\tau_{mfp} \ (R) \ = \ 1.9 \times 10^4$ sec and

$$\lambda_{mfp} \ = \ \frac{1}{\sigma} \ \frac{M}{\dot{m}} \ 4\rho r^2 v_{ez}$$

$$= 0.764 \left(\frac{r}{1 \ cm}\right)^2 \ cm$$

We then want r such that

$$\lambda_{mfp} = r$$

$$r = 0.764 \left(\frac{r}{1 \ cm}\right)^2 \ cm \tag{3.27}$$

which gives $r = 1.3$ cm for the radius of fluid model applicability.

One minor correction which must be considered relates to the adiabatic expansion of the plasma contactor cloud from the aperture of the plasma contactor. For the numbers chosen above, the expansion ratio may not be sufficient to drive the gas pressure to very low values. Nonetheless, the basic conclusion of an unexpectedly small contactor cloud can still be expected to hold and should be considered seriously pending the results of a more detailed plasma kinetic calculation.

The characteristic length scales that have been computed here allow us to estimate a characteristic time scale for the establishment and decay of the plasma contactor flow. A rough estimate of the time required to establish the flow field around the contactor is

$$r/v_{ez} \approx \frac{19 \ cm}{2.5 \times 10^4 \ cm/sec} \approx 7.6 \times 10^{-4} \ sec \tag{3.28}$$

i.e. about a millisecond. If it is considered experimentally desirable to measure the electrodynamic behavior of the plasma contactor cloud as the plasma flow is turned on, data rates as high as 10^4 samples/sec. (at least for short periods of time) would be required.

If the flow around the contactor is drawn out into a long "comet tail" as this model calculation permits, we might expect that much of the surface area over which charge transfer with the ionosphere takes place is in this "comet tail." (One possible approach for modeling this system is to consider this plasma stream as a lossy transmission line.) The time scale for the current flow through the contactor to diminish once the mass flow is cut off will be approximately $2r/\nu_e x \approx$ 1.6 $\times$ 10^{-3} sec, at which time a high conductivity path to the tail of the plasma contactor cloud will no longer be available. The possibility exists that the cutoff in the current flow through the plasma contactor cloud may be rather abrupt.

This fluid model calculations gave us a lower limit on the "standoff distance" to which the hollow cathode expands against the atmospheric stream. We note that this quantity varies inversely with the square root of the atmospheric mass density. Increasing the altitude from 220 km up to 300 km (TSS-1 height) results in a ten-fold increase in the fluid model standoff distance to 2 meters, so the altitude in which the experiment takes place can be very significant from the standpoint of ram pressure as well as electron density.

3.5   Kinetic Theory Calculations

In the present analysis we estimate an upper limit to the standoff distance based on the opposite extreme of "weakly interacting" gas particles in the kinetic theory approach sketched below.

Let the plasma contactor rest at the center of the coordinate system. We will work in a reference frame moving with the plasma contactor (see Figure 3.2). We take the Shuttle to be flying in the $+\hat{e}_z$ direction, and so the flow of ionospheric material past the plasma contactor cloud has velocity $-v_{orb}\hat{e}_z$, where v_{orb} is the orbital velocity of the Shuttle (see Figure 3.2).

We begin by writing down the ionospheric distribution function (in the absence of a plasma contactor cloud and the contactor cloud distribution function in the absence of interaction with the ionosphere). Thermal velocity spreads can be neglected for both distribution functions, at least for the initial treatment.

The thermal spread of the ionospheric distribution function may be neglected because the Shuttle motion with respect to ionospheric material is highly supersonic. Consider a typical ionospheric species as represented by oxygen atoms at a temperature of 10^3 °K.

$$m \simeq 16\ m_p = 2.67 \times 10^{-23}\ gm$$

$$v_{th} \simeq \sqrt{3\ kT/m} = \left(\frac{3\left(1.38\times10^{-16}\ erg/°K\right)\left(10^3\ °K\right)}{2.67\times10_o^{-23}\ gm}\right)^{1/2}$$

$$= 1.24 \times 10^5\ cm/\sec = 1.24\ km/\sec$$
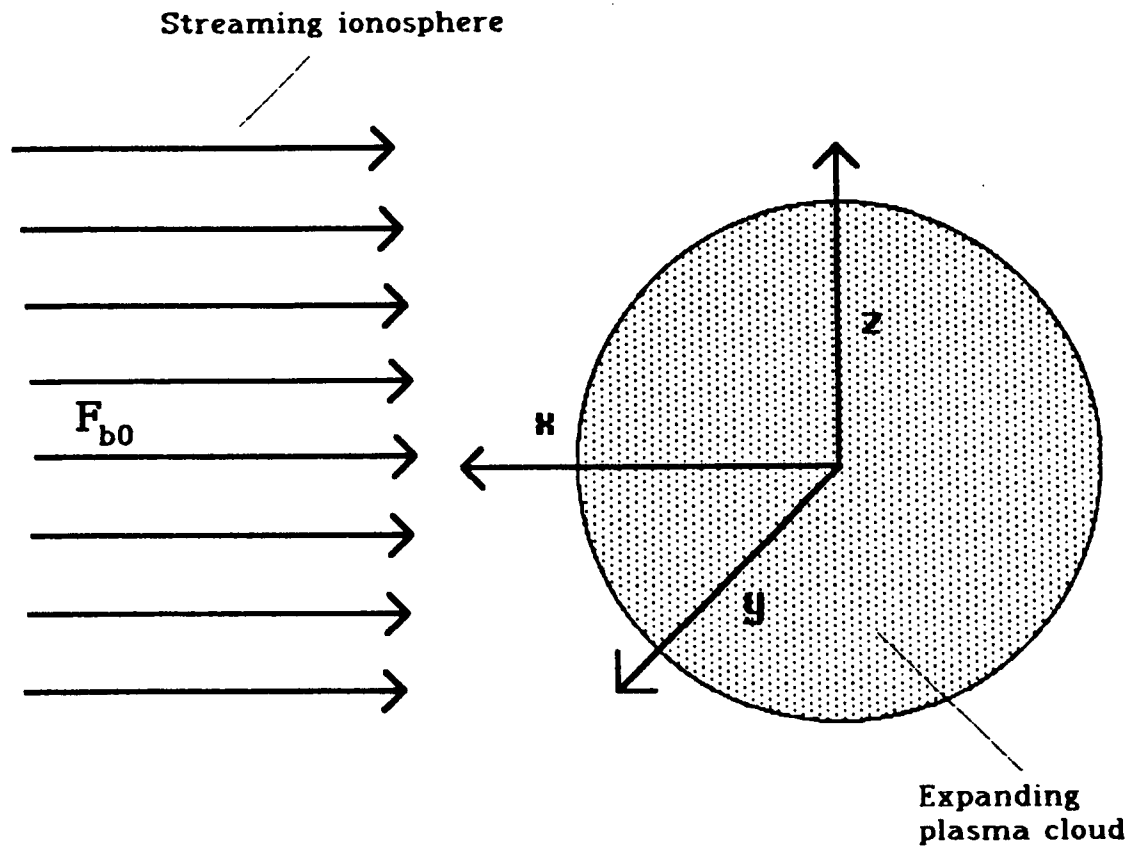
Streaming ionosphere

F_{b0}

z

x

y

Expanding
plasma cloud

Figure 3.2.   The co-ordinate system used in the kinetic theory calculations.

$$\frac{v_{orb}}{v_{th}} \simeq \frac{8 \ km/\sec}{1.24 \ km/\sec} = 6.43$$

Although this is not an enormously large number, it is still probably possible to neglect ionospheric thermal velocities.

The calculations on the adiabatic expansion of the plasma contactor cloud show the contactor cloud to be very cold, furthermore, its expansion velocity

$$v_{exp} \approx 2.5 \times 10^4 \ cm/\sec$$

satisfies

$$\frac{v_{orb}}{v_{ex}} \approx \frac{8 \times 10^5 \ cm/\sec}{2.5 \times 10^4 \ cm/\sec} = 32$$

Therefore, we may to an excellent approximation, neglect the thermal velocities of the plasma contactor cloud and also neglect any velocity dependence of collision cross-sections in treating particles traveling in the $\pm \ \hat{e}_x$ directions.

We begin by adopting a model in which the interaction between the plasma contactor and the ionospheric flow is "weak." In this model calculation wherever a scattering occurs between a contactor cloud particle and an ionospheric particle, the recoil velocities are large compared to any other velocities in the problem except the orbital velocity. The scattered particles are assumed to leave the system "instantaneously" without further scattering. This sort of "weak interaction single-scattering" limit is clearly not realistic throughout the volume of the plasma contactor cloud and will yield an overestimate of the plasma contactor cloud size.

This may be useful, however, as the fluid-dynamic calculation report bounds the size of the plasma cloud from below. It may be possible to obtain a reasonable estimate of the plasma contactor cloud bounded by these two limits.

The distribution function of the ionospheric background, in the absence of interaction with the plasma contactor cloud may be written:

$$F_b\left(\vec{x}, \vec{v}\right) \;=\; N_o\;(\vec{x})\;\;\delta\left(v_x - v_{orb}\right)\;\;\delta\left(v_y\right)\;\;\delta\left(v_z\right) \tag{3.29}$$

It will be assumed that a steady state solution $(\partial/\partial t = 0)$ can be found for the density distribution. Here $N_o(\vec{x})$ = background number density of particles (particles/cm^3), the spatial dependence of $N_o(\vec{x})$ (derivation from $N_o(\vec{x})$ = constant) is determined by scattering with the plasma contactor cloud. For purposes of this calculation it can be assumed that the background is composed of a single neutral atomic species, e.g. atomic oxygen.

We define distribution functions for electrons, ions, and neutral atoms in the plasma contactor cloud as $f_e(\vec{x}, \vec{v})$, $f_i(\vec{x}, \vec{v})$, and $f_n(\vec{x}, \vec{v})$ respectively. However, as ionization and recombination processes may be expected to be negligible outside the plasma contactor itself, we can refer to these generically as $f(\vec{x}, \vec{v})$. Again we are initially concerned only with stationary solutions. The (unperturbed) number density of the plasma contactor cloud particles is proportional to r^{-2}, owing to conservation of particle fluxes, i.e.

$$n(r) \;=\; n_o(r_o)\;\;(r_o/r)^2 \tag{3.30}$$

where n_o and r_o are reference values of number density and radius chosen to avoid

the unphysical singularity at $r = 0$. The values of n_o and r_2 are chosen on the basis of the mass flow rate and other properties of the plasma contactor, as outlined in the calculation reported above. Then the plasma contactor cloud distribution function may be expressed in spherical coordinates as

$$f(\vec{x}, \vec{v}) = n(r) \; \delta(v_r - v_{\exp}) \; v_{\exp}^{-2} \tag{3.31}$$

where v_r is the radial velocity and $v_{\exp}$ the velocity of expansion of the plasma contactor cloud particles. Expressing the distribution function in rectangular coordinates

$$
\begin{aligned}
f(\vec{x}, \vec{v}) &= n(r) \; \delta\Big(v_x^2 \; + \; v_y^2 \; + \; v_z^2 \; - \; v_{\exp}^2 \Big)/v_{\exp} \\
&= n(r) \; \delta\Big(\sqrt{v_x^2 \; + \; v_y^2 \; + \; v_z^2} \; - \; v_{\exp}^2 \Big)/v_{\exp}^2
\end{aligned}
\tag{3.32}
$$

The evolution of the distribution functions $f(\vec{x}, \vec{v})$ and $F_b(\vec{x}, \vec{v})$ are then described by the Boltzmann equations for each distribution function.

$$\frac{\partial f}{\partial t} + \vec{v} \cdot \vec{\nabla} f + \vec{a} \cdot \frac{\partial}{\partial \vec{v}} f = \frac{\delta f}{\delta t}\Big|\, coll \tag{3.33}$$

$$\frac{\partial F_b}{\partial t} + \vec{v} \cdot \vec{\nabla} F_b + \vec{a} \cdot \frac{\partial}{\partial \vec{v}} F_b = \frac{\delta F_b}{\delta t}\Big|\, coll \tag{3.34}$$

In this simple model it is assumed that there are not forces acting on particles except during collisions (i.e. no plasma waves or plasma turbulence) $\rightarrow$ $a = 0$, and we seek a stationary solution $\rightarrow$ $\partial/\partial t = 0$

$$\vec{v} \cdot \vec{\nabla} f = \frac{\delta f}{\delta t}\Big| coll \qquad (3.35)$$

$$\vec{v} \cdot \vec{\nabla} F_b = \frac{\delta F_b}{\delta t}\Big| coll \qquad (3.36)$$

Physical interpretation:

Particles travel along linear phase space trajectories except when removed from their respective distributions by a collision. Each collision removes a particle from the plasma contactor distribution and a particle from the ionospheric distribution

$$\frac{\delta f}{\delta t}\Big| coll = \frac{\delta F_b}{\delta t}\Big| coll \qquad (3.37)$$

(Only binary collisions are considered, and since the species chosen to represent the background distribution is a neutral atom, long-range interactions between particles are ignored.) Both $\frac{\delta f}{\delta t}\Big|_{coll}$ and $\frac{\delta F_b}{\delta t}\Big|_{coll}$ will in general depend on $\vec{x}$ directly and indirectly through the value of the other distribution function. However, the sense in which we should consider the interaction of the distributions is weak is that we shall neglect variations in F_b in calculating $\frac{\partial f}{\partial t}\Big|_{coll}$. We can then use the value of f to calculate a solution for F_b and thus proceed iteratively until we achieve some solution for f and F_b. This iterative process may converge if the interaction of the two populations is sufficiently weak. The full iterative process will doubtless have to be carried out on a computer, but useful analytic results should be obtained by considering the first few iterations. The collisions of

interest for this system are:

1) atom-atom collisions

2) atom-election collisions

3) atom-ion collisions

Since at least one of the particles is neutral in each of these three possibilities and the range of velocities is not very great, we will treat a collision (of whatever type) as being characterized by a collision cross section σ, independent of velocity (approximately) and different for each type of collisions. For the 1st iteration consider the density distribution in the plasma contactor cloud arising from $F_k =$ const. The near free path of the plasma contactor cloud particles is

$$\lambda = 1/N\sigma \tag{3.37}$$

where N is the number density of ionospheric particles.

We can now estimate λ numerically. For standard Shuttle conditions at an altitude of 220 km ($N = 4\times10^{10}$ cm^{-3}) these cross sections should be approximated by a typical gas kinetic cross section: $\sigma \approx 3\times10^{-14}$ cm^2, which gives

$$\lambda = \left(4\times10^{10}\times3\times10^{-14}\right)^{-1} cm = 8.33 \ m$$

which implies that we're going to get a reasonable scale length for the cloud. For the conditions for TSS-1, the height is 300 km $\rightarrow$ $N = 5\times10^8$ cm^{-3} $\rightarrow$

$$\lambda = 667 \ m = 0.667 \ km$$

the plasma contactor density in this limit may be written down by inspection:

$$n(r) = n_o \ (r_o/r)^2 \ e^{-r/\lambda} \tag{3.38}$$

We can calculate a characteristic scale size for the cloud from (8)

$$\left| \frac{1}{n} \frac{dn}{dr} \right|^{-1} = \left| \left\{ \left[n_o^{-1}\left(\frac{r}{r_o}\right)^2 e^{r/\lambda} \right] \left[n_o\left(-2(r_o/r)^2 e^{-r/\lambda} \right) + (r_o/r)^2 \ (-1/\lambda)e^{-r/\lambda} \right] \right\}^{-1} \right|$$

$$= \left| \left(-\frac{2}{r} - \frac{1}{\lambda} \right)^{-1} \right| = \left| \frac{-1}{2/r + 1/\lambda} \right| = \left| \frac{-r\ \lambda}{2\lambda + r} \right| = \frac{r\lambda}{2\lambda + r} \tag{3.39}$$

note that as $r \to \infty$, scale size $\to \lambda$; as $r \to 0$, scale size $\to r/2$. However, it is not surprising that the scale size is a function or r.

We must now take this calculation to one higher iteration to get useful information about deviations from spherical symmetry. Initially consider that any scattering which occurs between plasma contactor cloud particles and ionospheric particles has the effect of subtracting a particle from the ionospheric beam. Let

$F_{bo} \equiv$ unperturbed ionospheric background distribution function

$$F_b\left(x, y, z \right) = F_{bo} \ \exp \left[-\left(\int_{\infty}^{z} \frac{dx'}{\lambda(x', y, z)} \right) \right] \tag{3.40}$$

$\lambda(r) = \dfrac{1}{n(r)\sigma}$ with n(r)=initial iteration of contactor cloud distribution

$$n(r) = n_o\left(r_o/r\right)^2 e^{-r/\Lambda}, \text{ where } \Lambda = 1/N\sigma$$

is the initial mean free path estimated above.

$$r = \sqrt{x^2 + y^2 + z^2}, \; r' = \sqrt{x'^2 + y^2 + z^2}$$

Note that y,z = constant along an integration path. Let $b = \sqrt{y^2 + z^2}$, which has the role of an "impact parameter"

$$F_b\left(x, y, z\right) = F_{bo} \exp\left(-\int_{\infty}^{x} dx' \; n(r')\sigma\right)$$

$$= F_{bo} \exp\left[-n_o r_o^2 \sigma \int_{\infty}^{x} dx' \; \frac{\exp(-1/\Lambda \sqrt{x'^2 + b^2})}{x'^2 + b^2}\right] \qquad (3.41)$$

Begin by considering $b = 0$, i.e. the density distribution along the x axis.

$$F_b(x) = F_{bo} \exp\left[-n_o r_o^2 \sigma \int_{\infty}^{x} dx' \; \frac{\exp(-x'/\Lambda)}{x'^2}\right] \qquad (3.42)$$

From standard integral tables,

$$\int \frac{e^{ax}}{x^m} \, dx = \frac{-1}{m-1} \frac{e^{ax}}{x^{m-1}} + \frac{a}{m-1} \int \frac{e^{ax}}{x^{m-1}} \, dx$$

In this simple-minded model the density of the plasma contactor cloud is infinite at

the origin, and so $F_b(\lambda)$ must go to zero at positive x. We shall assume in what follows that when $b = 0$, $x > 0$.

$$\int_\infty^x dx'\ \frac{\exp(-x'/\Lambda)}{x'^2} = (-1)\ \frac{e^{-x'/\Lambda}}{x'}\ \Big|_\infty^x - \frac{1}{\Lambda}\int_\infty^x \frac{e^{-x'/\Lambda}}{x'}\ dx$$

$$= -\frac{1}{x}\ e^{-x/\Lambda} + \left(\frac{1}{\Lambda}\right)\int_{x/\Lambda}^\infty \frac{1}{t}\ e^{-t}\ dt$$

$$= -\frac{1}{x}\ e^{-x/\Lambda} + \frac{1}{\Lambda}\ E_1(x/\Lambda)$$

(See Abramowitz and Stegun, Chapter 5, pp. 227ff.)

$E_1(x)$ has a series expansion:

$$E_1(x) = -\gamma - \ln x - \sum_{n=1}^\infty \frac{(-)^n x^n}{n\ n!}$$

as

$$x \to 0 \qquad E_1(x) \to \infty$$

as

$$x \to \infty \qquad E_1(x) \to 0$$

Which guarantees proper limiting behavior for $F_b(x)$

$$F_b(x) = F_{bo}\ \exp\left\{n_o^2 r_o^2 \sigma\left[\frac{1}{\Lambda}E_1(x/\Lambda) - \frac{1}{x}e^{-x/\Lambda}\right]\right\} \qquad (3.43)$$

Note that (13) gives us $F_b(x) < F_{bo}$ for all $x < \infty$, $(x > 0)$ as we would expect
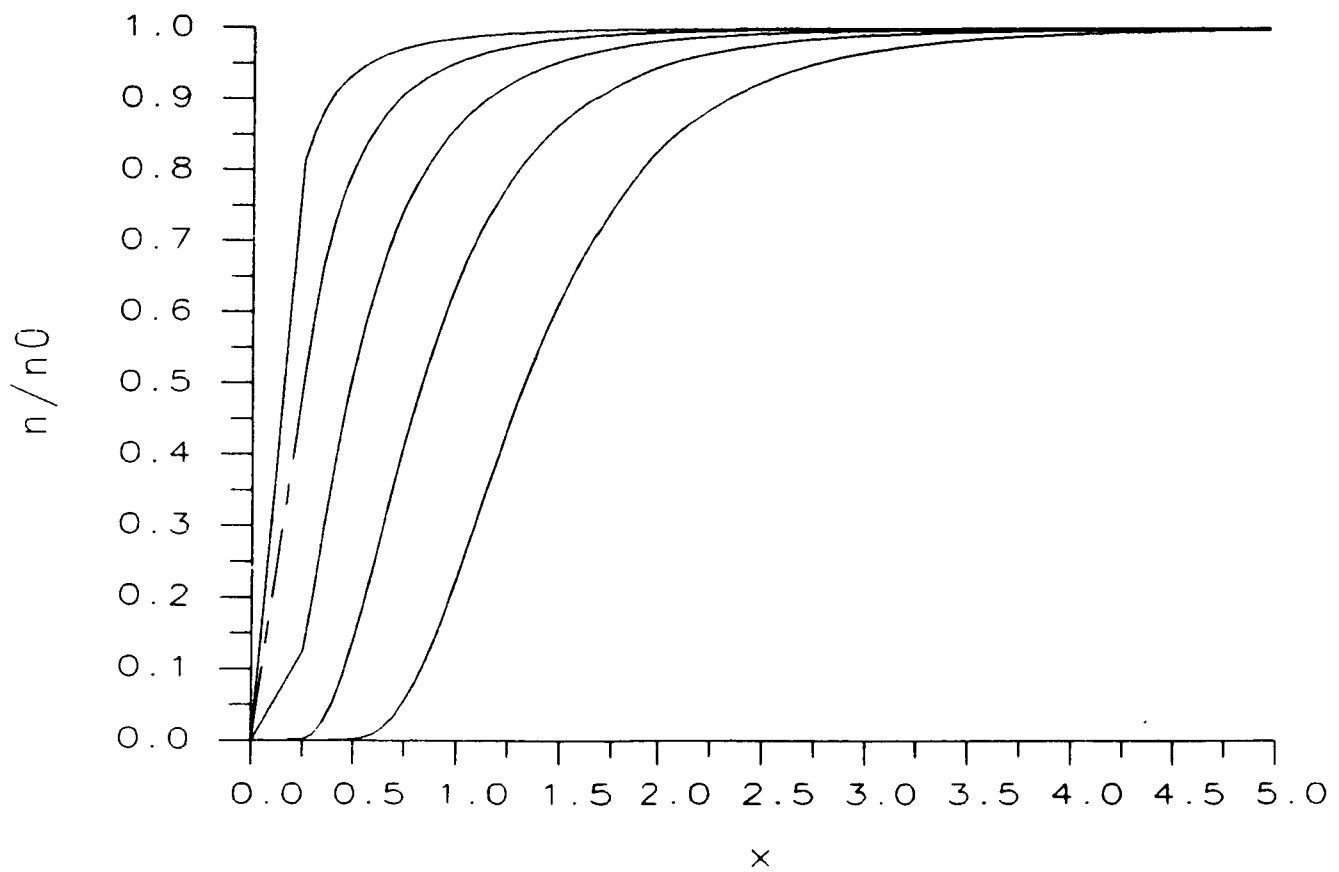
Figure 3.3.   Ionospheric particle density (on-axis) for different values of a vs. upstream distance measured in units of $\Lambda = \dfrac{1}{N\sigma}$.

on physical grounds.

Figure 3.3 displays the results of some calculations using the expressions derived above. The ionospheric particle density along the line of flight ahead of the plasma contactor (x measured in units of Λ) is shown for five different values of $a \equiv n_o{}^2 r_o{}^2 \sigma / \Lambda$: a=10, 3, 1, 1/3, and 1/10. The curves for large a values lie below the curves for small a values as would be expected, since large a values correspond to larger values of the mass flux from the plasma contactor.

We now want to examine the behavior of the solution off the $b = 0$ axis. First we expand in b as a small parameter

$$\int_{\infty}^{x} dx' \; \frac{exp\left(-\sqrt{x'^2+b^2}\,/\Lambda\right)}{x'^2+b^2}$$

$$= \int_{\infty}^{x} dx' \; \frac{\left\{ e^{-x'/\Lambda} \; \exp\left[-\frac{1}{2}\,\frac{b^2}{x'\Lambda}\right] \cdots \right\}}{x'^2} \left(1 - \frac{b^2}{x'^2} + \cdots\right)$$

Now

$$\exp\left(-\frac{1}{2}\,\frac{b^2}{x'\Lambda}\right) \approx 1 - \frac{1}{2}\,\frac{b^2}{x'\Lambda} \quad ,$$

so to $0(b^2)$:

$$\int_{\infty}^{x} dx' \; \frac{exp\left(-\sqrt{x'^2+b^2}\,/\Lambda\right)}{x'^2+b^2}$$

$$= \int_\infty^z \frac{\exp\left(-x'/\Lambda\right)}{x'^2} \, dx' \; - \; \frac{b^2}{2\Lambda} \int_\infty^z dx' \; \frac{e^{-x'/\Lambda}}{x'^3} \; - b^2 \int_\infty^z dx' \; \frac{e^{-x'/\Lambda}}{x'^4} \; + \; O(b^4)$$

Now

$$\int_\infty^z \frac{e^{-x'/\Lambda}}{x'^4} \, dx' \; = \; \frac{1}{3} \left[-\, \frac{e^{-x/\Lambda}}{x^3} \; - \; \frac{1}{\Lambda} \int_\infty^z \frac{e^{-x'/\Lambda}}{x'^3} \, dx' \right]$$

$$= \; \frac{1}{3} \left[-\, \frac{e^{-x/\Lambda}}{x^3} \; - \; \frac{1}{\Lambda} \int_\infty^z \frac{e^{-x'/\Lambda}}{x'^3} \, dx' \right]$$

and

$$\int_\infty^z \frac{e^{-x'/\Lambda}}{x'^3} \, dx' \; = \; \left(\frac{1}{2\Lambda x} \; - \; \frac{1}{2x^2} \right) e^{-x/\Lambda} \; - \; \frac{1}{2\Lambda^2} \; E_1(x/\Lambda)$$

Therefore

$$\int_\infty^z \frac{e^{-x'/\Lambda}}{x'^4} \, dx' \; = \; -\frac{1}{3} \; \frac{e^{-x/\Lambda}}{x^3} \; - \frac{1}{3\Lambda} \left[\left(\frac{1}{2\Lambda x} - \frac{1}{2x^2} \right) e^{-x/\Lambda} \; - \; \frac{1}{2\Lambda^2} \; E_1(x/\Lambda) \right]$$

Finally,

$$\int_{\infty}^{z} dx' \, \frac{\exp\left[-1/\Lambda \sqrt{x'^2 + b^2}\right]}{x'^2 + b^2} = \left(-\frac{1}{x} - \frac{1}{12}\frac{b^2}{\Lambda^2 x} + \frac{1}{12}\frac{b^2}{\Lambda x^2} + \frac{b^2}{3x^3}\right)e^{-z/\Lambda} +$$

$$+\left(\frac{1}{\Lambda} + \frac{1}{12}\frac{b^2}{\Lambda^3}\right) E_1(x/\Lambda) + O(b^4) \qquad (3.44)$$

And so the ionospheric background for small b is

$$F_b(x, b) \simeq F_{bo}\exp\left\{ n_o^2 \, r_o^2 \sigma\left[\left(\frac{1}{\Lambda} + \frac{1}{12}\frac{b^2}{\Lambda^3}\right) E_1(x/\Lambda) + \right.\right.$$

$$\left.\left.\left(-\frac{1}{x} - \frac{1}{12}\frac{b^2}{\Lambda^2 x} + \frac{1}{12}\frac{b^2}{\Lambda x^2} + \frac{b^2}{3x^3}\right) e^{-z/\Lambda}\right]\right\} \qquad (3.45)$$

Results for a selection of b values are shown for different values of a in Figures 3.4(a)-(e). The steep increases in ionospheric density for small upstream distances merely indicate the point at which the approximation breaks down.
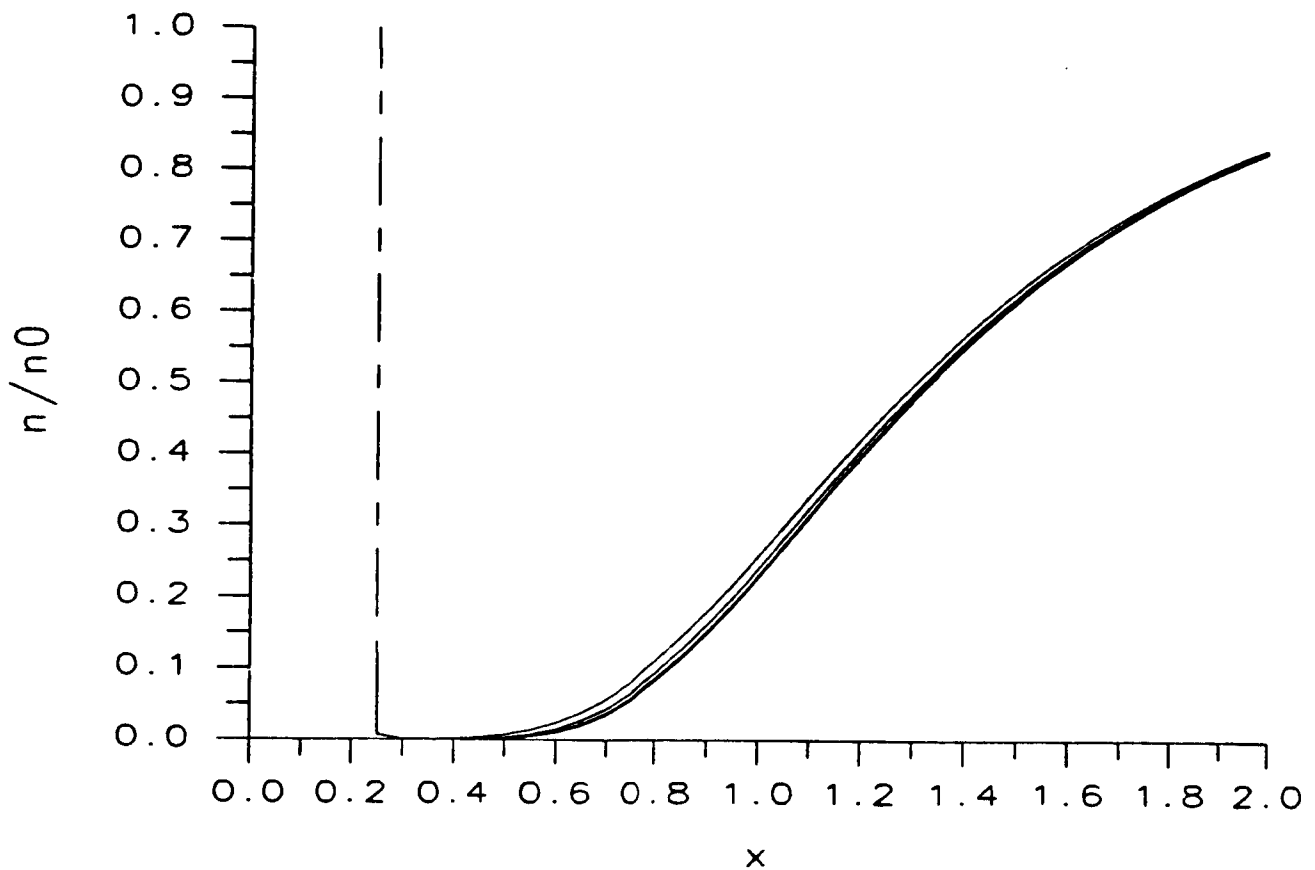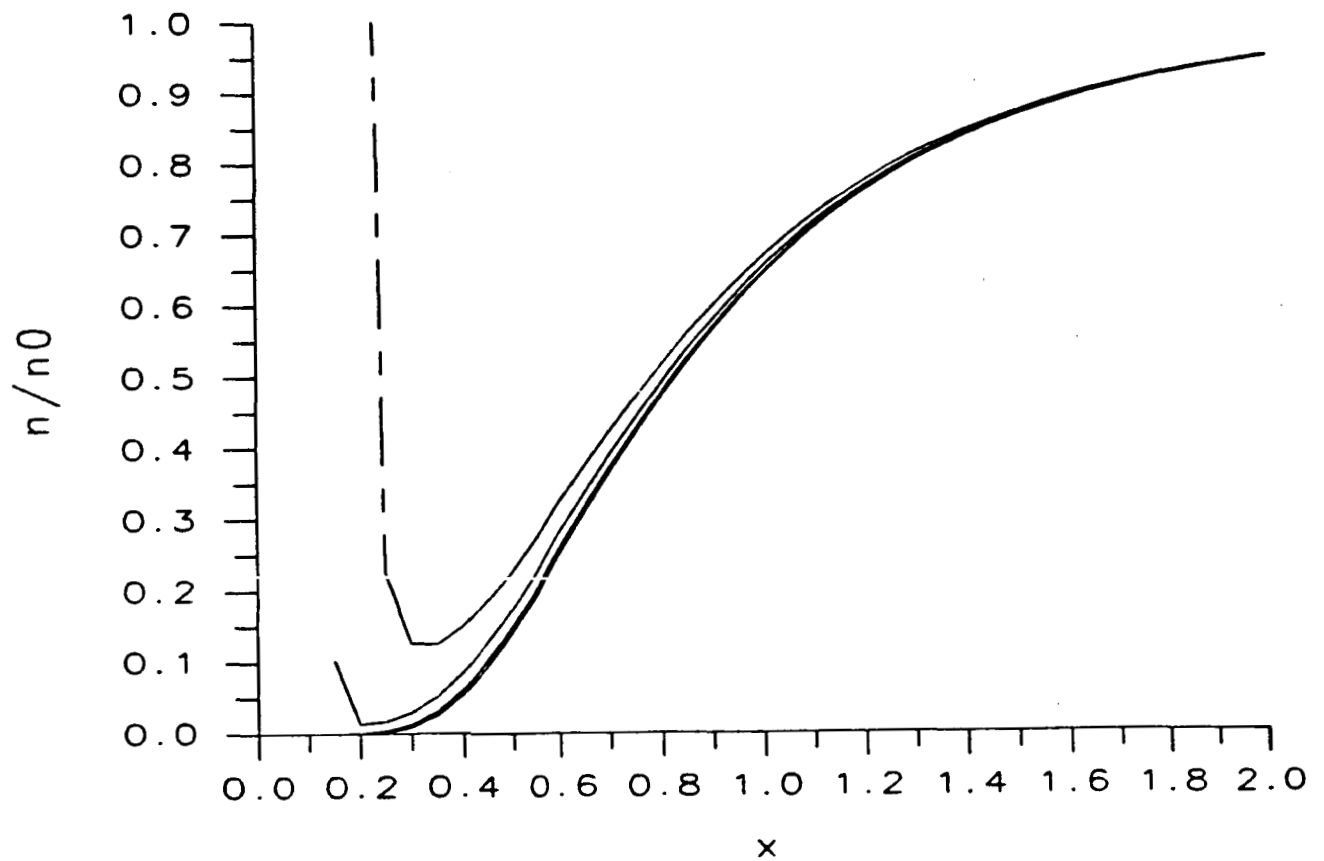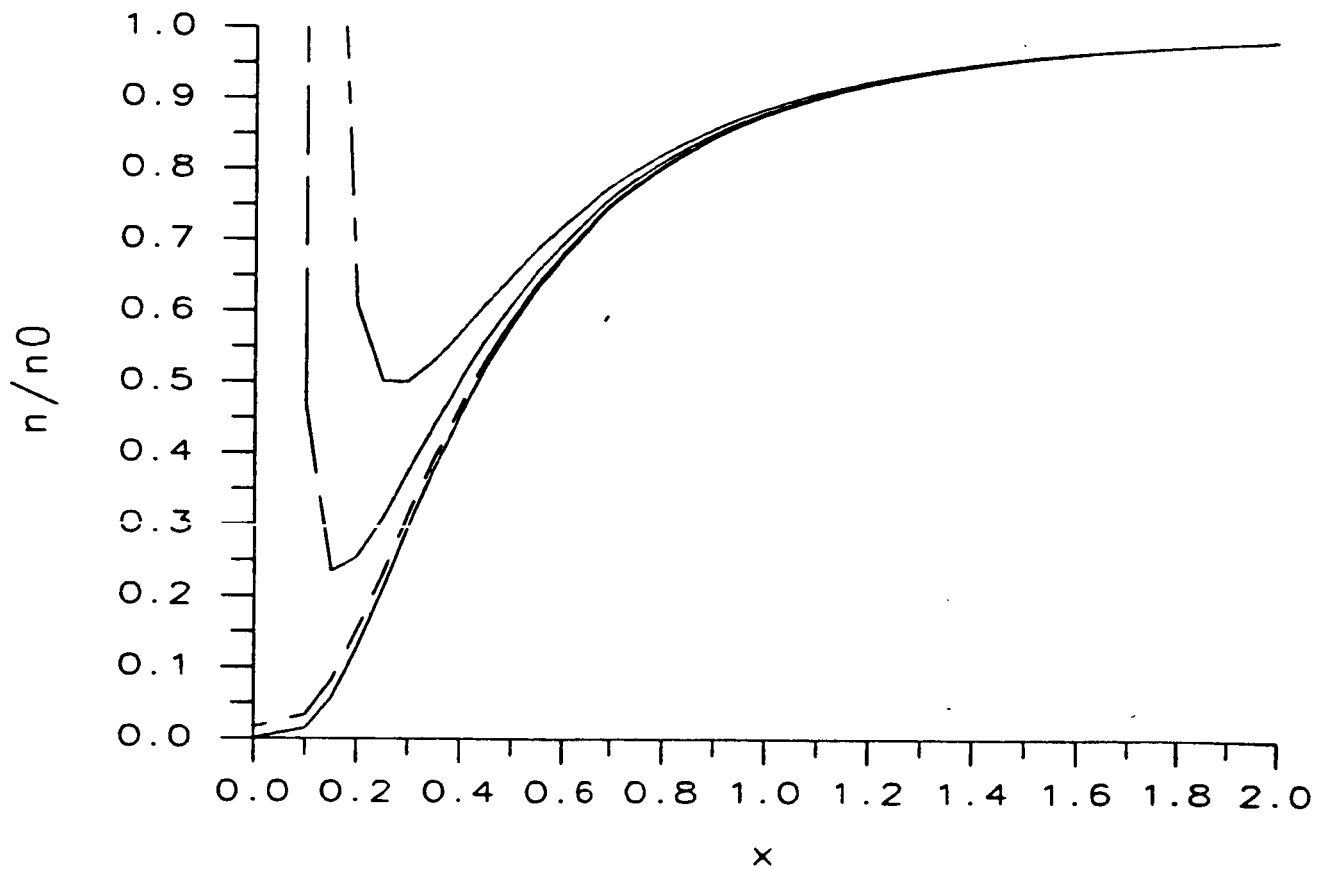
Ionospheric Particle Density

Figure 3.4(a).   Ionospheric particle density off axis for different values of the "impact parameter" b plotted versus upstream distance for $a \equiv n_o^2 r_o^2 \sigma = 10.0$. $b = 0, 0.1, 0.2$, and 0.3, with curves for higher b values lying above those for lower values.   All distances measured in units of Λ.
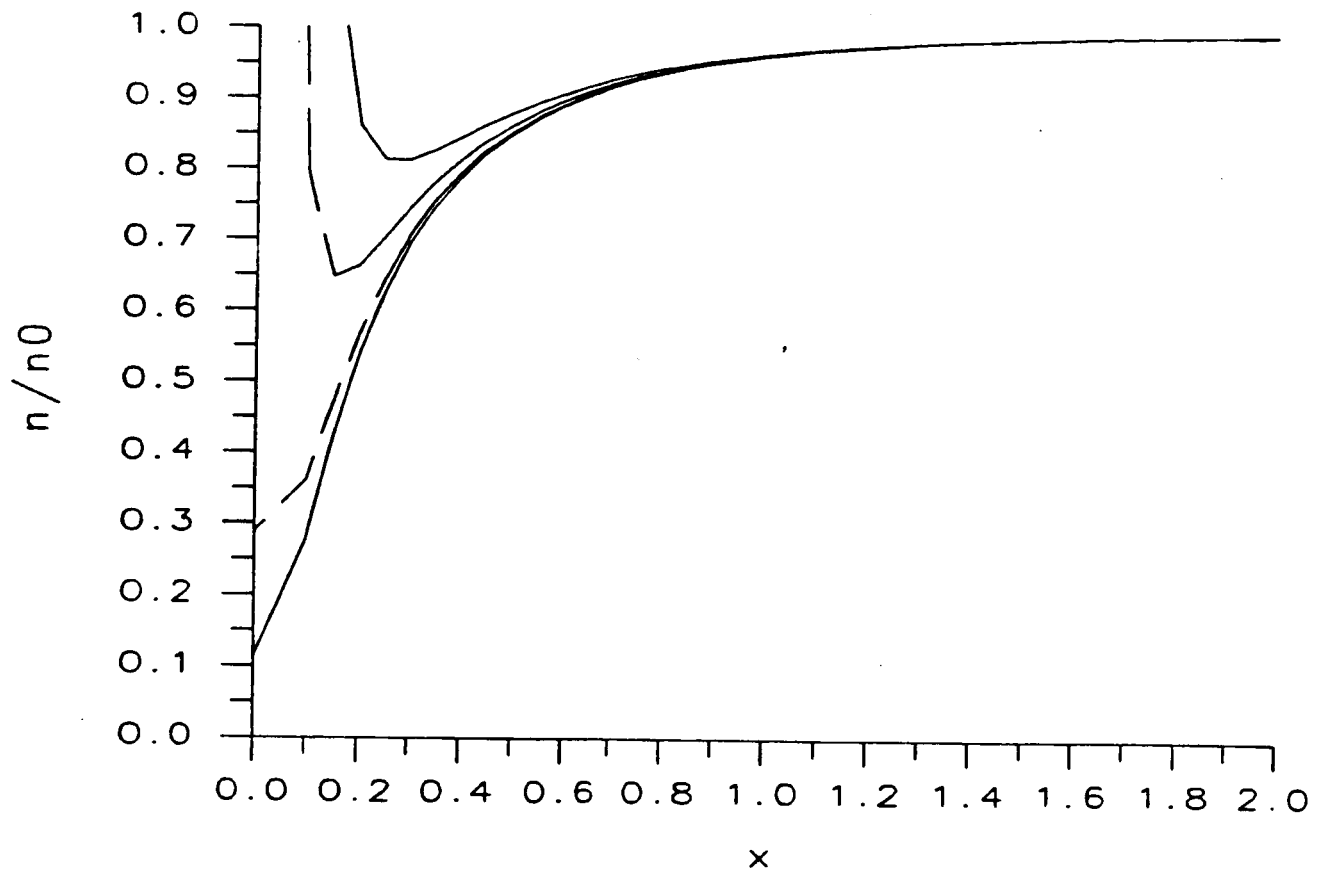
Ionospheric Particle Density

Figure 3.4(b). Ionospheric particle density off axis for different values of the "impact parameter" b plotted versus upstream distance for $a \equiv n_o^2 r_o^2 \sigma = 3.0$. $b = 0, 0.1, 0.2$, and 0.3, with curves for higher b values lying above those for lower values. All distances measured in units of Λ.

Ionospheric Particle Density

Figure 3.4(c). Ionospheric particle density off axis for different values of the "impact parameter" b plotted versus upstream distance for $a \equiv n_o^2 r_o^2 \sigma = 1.0$. $b = 0$, 0.1, 0.2, and 0.3, with curves for higher b values lying above those for lower values. All distances measured in units of Λ.
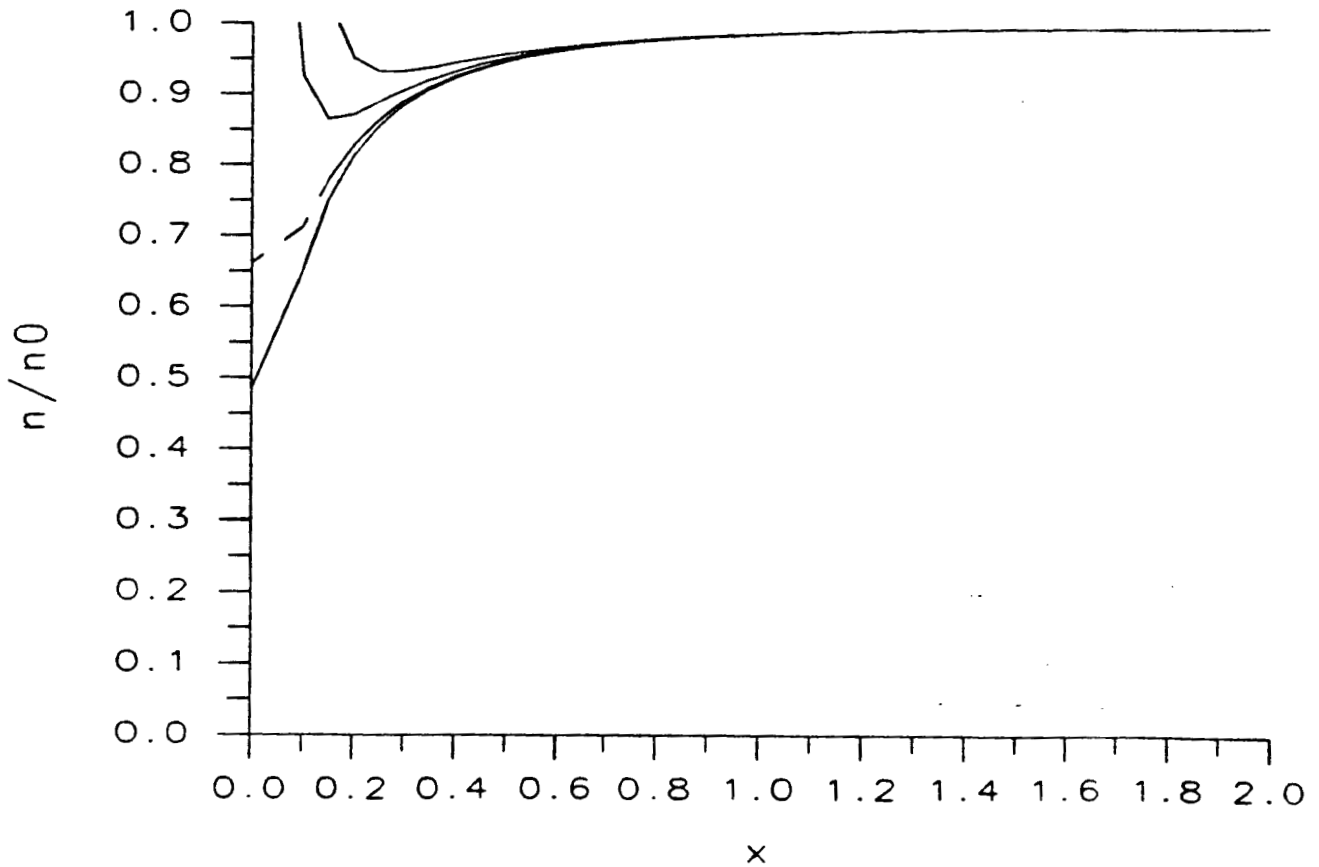
Ionospheric Particle Density

Figure 3.4(d).   Ionospheric particle density off axis for different values of the "impact parameter" b plotted versus upstream distance for $a \equiv n_o^2 r_o^2 \sigma = .3$. $b = 0, 0.1, 0.2$, and 0.3, with curves for higher values lying above those for lower values.   All distances measured in units of Λ.

Ionospheric Particle Density

Figure 3.4(e).   Ionospheric particle density off axis for different values of the "impact parameter" b plotted versus upstream distance for $a \equiv n_o^2 r_o^2 \sigma = .1$. $b = 0$, 0.1, 0.2, and 0.3, with curves for higher b values lying above those for lower values.   All distances measured in units of Λ.

4.0   COMPUTER SIMULATION OF A PLASMA CONTACTOR CLOUD

A simulation of an expanding cloud of conducting plasma has been developed by Prof. Hohlfeld and some of his coworkers. This simulation was developed originally to model the dynamics of a chemical release cloud in the earth's magnetosphere. Modifications to this program allow modeling of plasma contactor clouds, at least for times early in the expansion of the cloud.

The principal limitation of this program at present is that no account is taken of the dynamical effects of the relative motion of the plasma contactor cloud and the ambient medium. Therefore, this program is presently applicable, say, to a plasma contactor experiment conducted at the the apogee of a sounding rocket trajectory or in geosynchronous orbit. It is also applicable to experiments conducted in laboratory plasma chambers. Modifications of this simulation program under development will allow inclusion of the effects of relative motion of the plasma contactor cloud and the ambient medium.

The most important novel feature of this simulation program is its treatment of the magnetic boundary value problem. An expansion in spherical harmonics of the magnetic field surrounding the plasma contactor (see Hohlfeld, Fang, and Vonick, in preparation for submission to JGR) allows the treatment of a very general geometry of the magnetic perturbation caused by the expanding plasma contactor cloud. The magnetic pressure acting to retard the expansion of the plasma contactor cloud is anisotropic, maximal in the direction transverse to the unperturbed magnetic field, and falling to zero along the direction of the unperturbed magnetic field. The full Maxwell stress tensor is computed to evaluate this magnetic pressure. Contributions to the pressure tensor retarding

the expansion due to an isotropic particle distribution and a gyrotropic (i.e. due to particles executing Larmor orbits about magnetic field lines) is also included in the description of forces opposing the expansion of the chemical release cloud.

One example of the output of this simulation program is shown in Figures 4.1 and 4.2. In Figure 4.1 we plot the radius along (θ = 0 degrees) and perpendicular (θ = 90 degrees) to the magnetic field during the first 20 milliseconds of the plasma contactor cloud expansion. The expansion velocity of the plasma leaving the contactor is 250 m/s, 1/2 standard cubic centimeter per second of gas is being released, and the ambient magnetic field is 1/3 gauss. No background particle pressure is included in this particular simulation run. At a time of approximately 15 milliseconds the size of the cloud transverse to the magnetic field is reaching its maximum size, though the volume of the cloud is still increasing owing to the expansion along the magnetic field. Magnetic diffusion effects, currently being included in the program, will begin to be important at these times, and so the simulation is terminated at this point. The first few nonzero spherical harmonic expansion coefficients are plotted over this time interval in Figure 4.2 and show the progressive deviation of the cloud from a spherical form.

Broadly speaking, the results of this computer simulation are consistent with the theoretical expectations developed as a result of this research. Measurements must be taken over millisecond time scales to properly monitor the development (and presumably the dissolution) of a plasma contactor cloud. Characteristic scale lengths of a few meters appear realistically obtainable for plasma contactor clouds, but large mass flow rates may be required to achieve plasma contactor cloud sizes much in excess of 10 meters. The orientation of the ambient magnetic field emerges as a significant variable and its orientation must be carefully considered for experiments involving two plasma contactors.
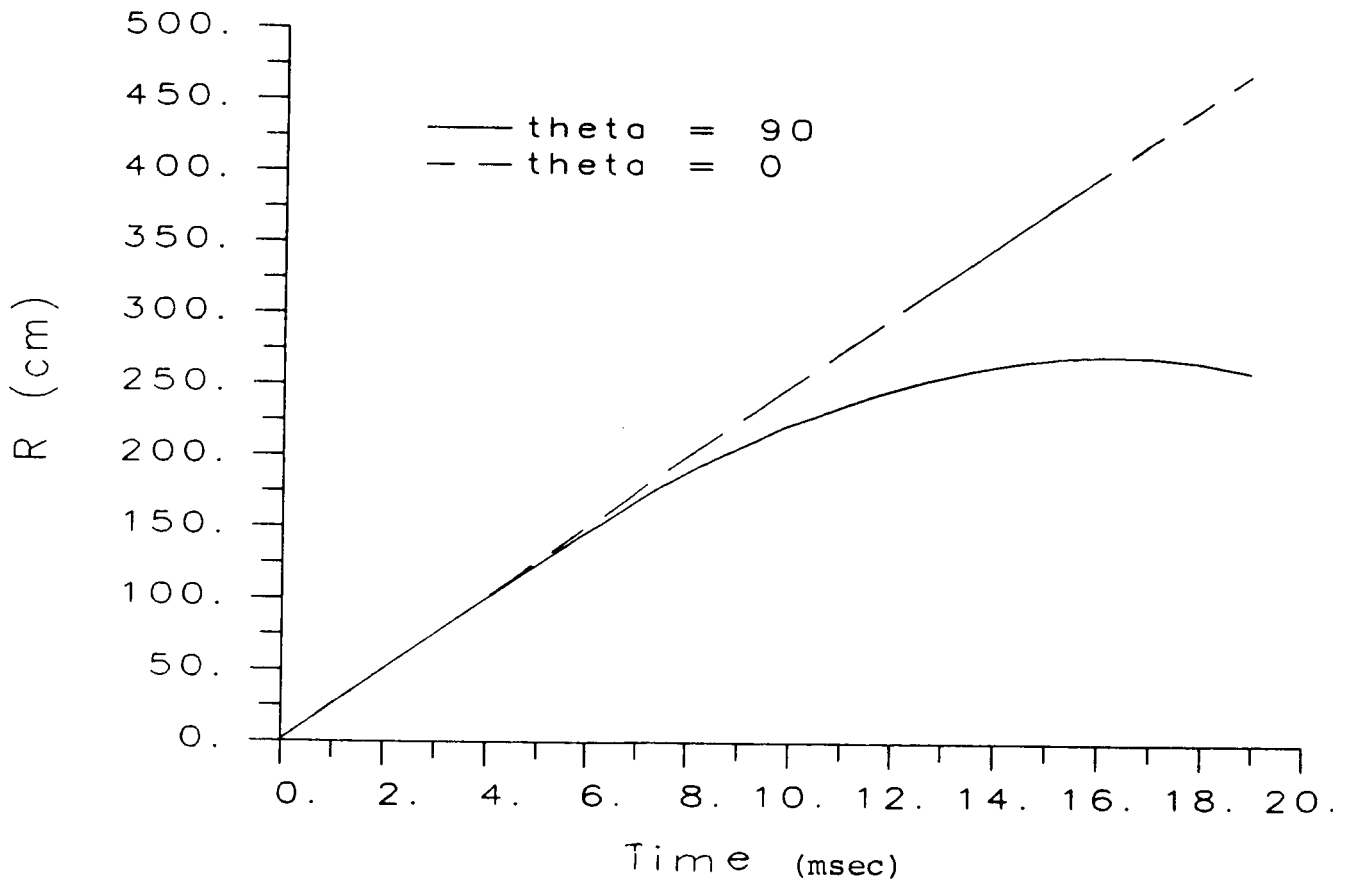
Radius vs. Time

Figure 4.1. Cloud size versus time for axes aligned with and perpendicular to the magnetic field.
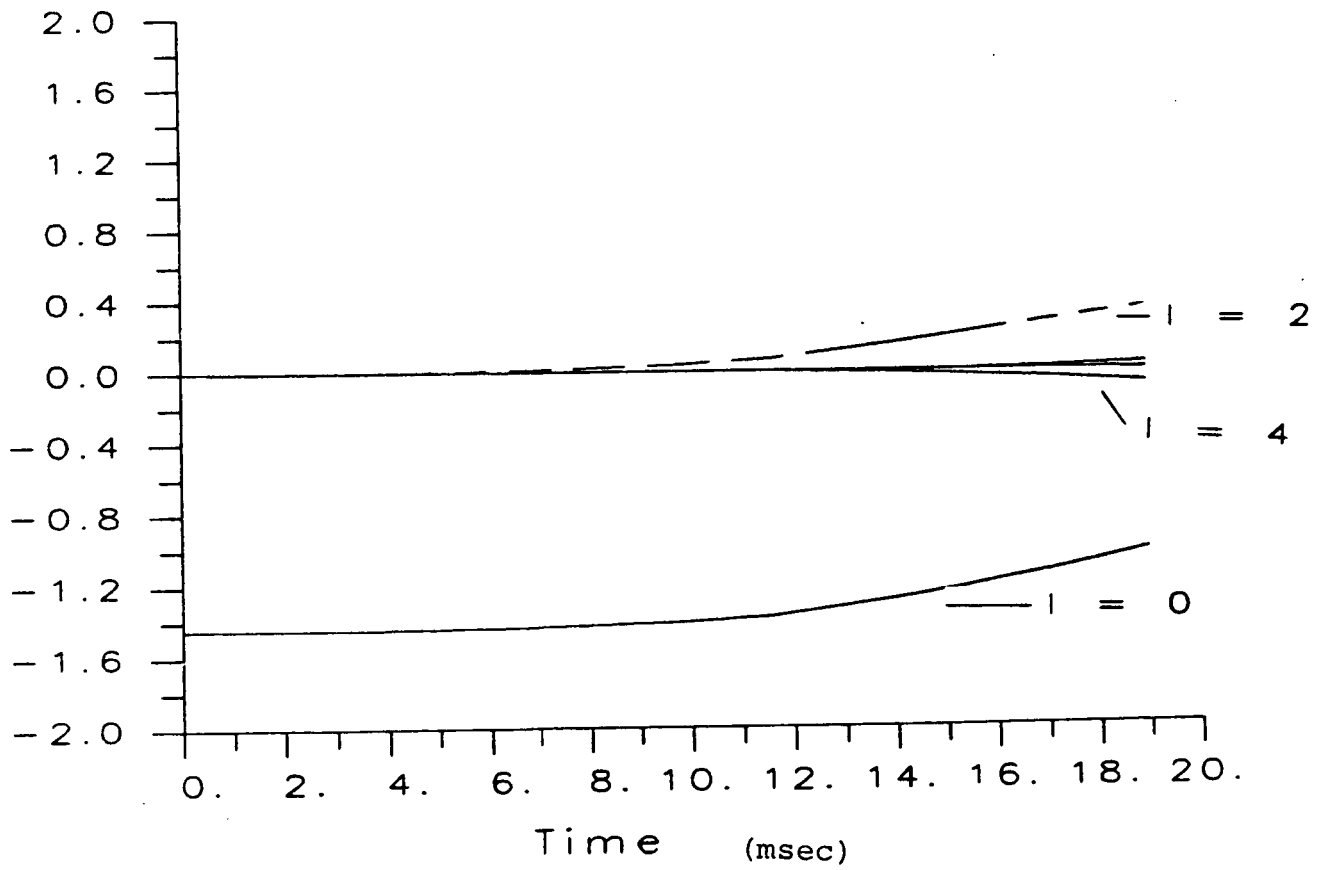
Harmonic coeffs. vs. Time

Figure 4.2. Harmonic coefficients of magnetic field versus time.

5.0 IONOSPHERIC CIRCUIT CLOSURE

Up until now, the problems generically referred to as "circuit closure" issues in the analysis of electrodynamic tethered satellite systems have been approached from two separate viewpoints, which we might call the global and the local.

By global we mean the approach that considers the complete system of ionosphere plus tethered system from the standpoint of the waves and currents established in the ionospheric magnetoplasma by the operation of the orbiting electrodynamic system, i.e. those phenomena that depend upon the ionosphere as a wave medium and are observable at large distances from the system. There have been a number of studies dealing with the waves excited in the ionosphere by a tethered satellite in recent years (Barnett and Olbert, 1986; Dobrowolny and Veltri, 1986; Drell et al., 1965; Rasmussen et al., 1985). These studies have in common the assumption that the tether current has been established at a constant value and that a steady state has been achieved in which charge-exchange takes place at a constant rate between the ionosphere and the system at the ends of the system. No attempt is made to analyze the region in which the charge-exchange actually takes place. The charge-exchange is just a moving local disturbance that drives the current-carrying waves observed at long distances. Although a number of over-simplifications have been made in these studies—they either use straight magnetohydrodynamic theory or assume an "ice-cold" plasma—the geomagnetic field and the motion of the tethered satellite system are taken into account. Indeed, the wave phenomena described depend entirely on these two factors. On the contrary, however, analyses of the local interaction of the system with the ionospheric plasma have tended to ignore these factors since e they

complicate the analysis significantly. The local interaction analyses are forced to deal with other complications ignored in the global approach, however, since the local interaction depends upon collision frequencies and upon nonlinear processes such as sheath formation, for example. Clearly a synthesis of the two approaches is desirable. This will be a difficult task. In the meantime we can see how results obtained from the two approaches relate to the proposed short tether experiments.

Both the local and the global interactions have relevance for the proposed experiments presently under discussion. The importance of the local interactions is obvious. It is in the region immediately surrounding the system that the hollow cathode devices will do their work. That the global effects can be important is perhaps not so immediately apparent. It is necessary to keep in mind that even a steady exchange between the system and the ionosphere appears as a time-varying phenomenon to the ionospheric plasma as it streams by. The time-varying charge densities that the streaming plasma encounters give rise to time-varying fields which generate plasma waves. These waves not only carry electromagnetic energy away from the system, they also carry the net charge injected into the plasma at each end of the tethered system. In effect, the ionosphere acts as a transmission line to carry away this charge. If the ionosphere did not cooperate, it could create a bottleneck to tether current flow. Thus it becomes important to estimate the wave impedance.

This task was made imperative during the course of this study when Barnett and Olbert of MIT published a paper in which they claimed that the wave impedances for an electrodynamic tethered satellite system were as high as 10,000-100,000 ohms, due to a hitherto ignored frequency band lying between the lower hybrid and electron cyclotron frequencies. If this were true, it would clearly be impossible to draw any significant currents through even a very long, high voltage
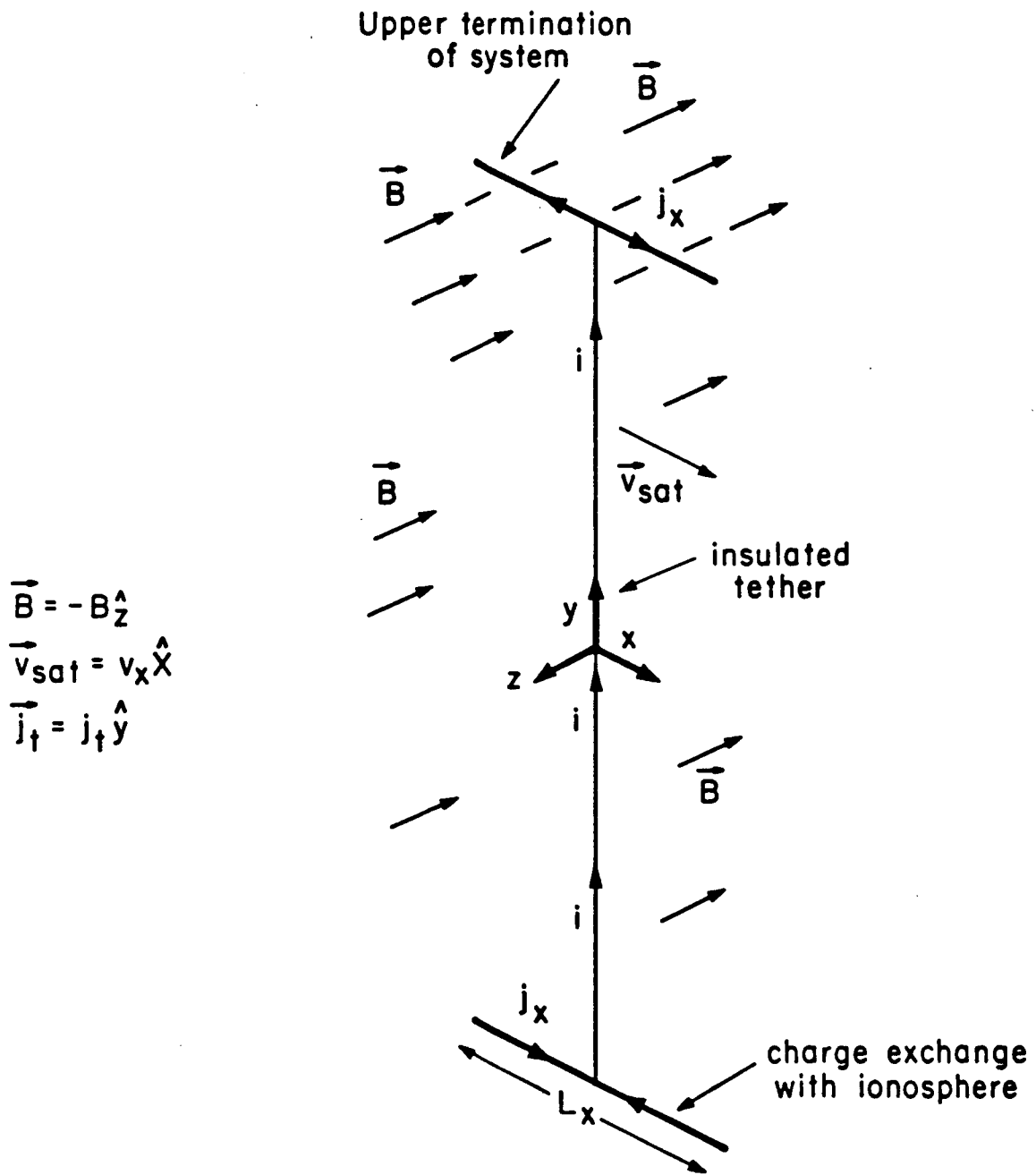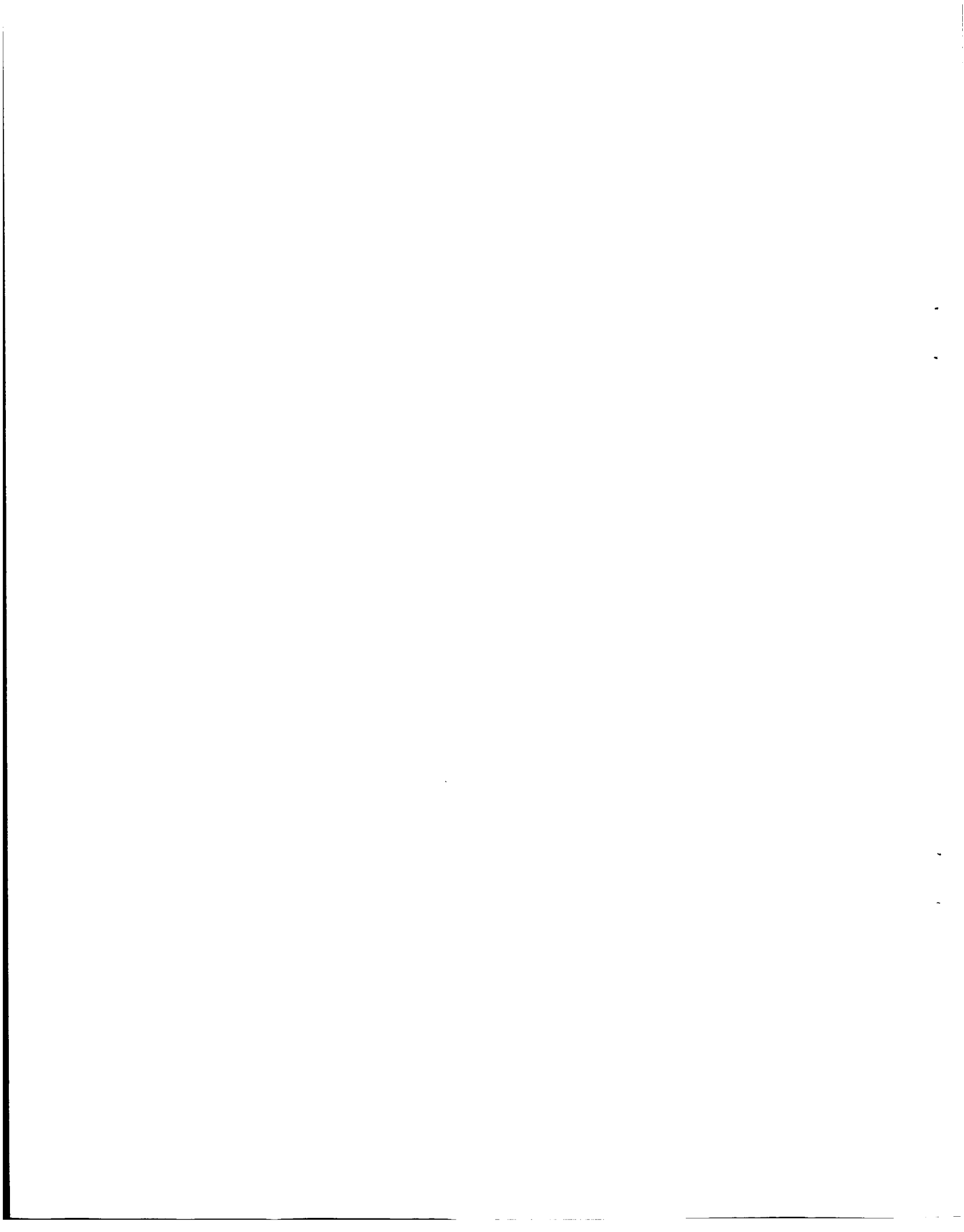
Figure 5.1. The electrodynamic tethered system current model used in the Alfvén wing calculations.

electrodynamic tethered satellite system, let alone the short, low voltage system we are talking about for the initial experiments. Part of our effort was thus directed to an examination of this challenge to the feasibility of electrodynamic tethered satellite systems. This was done in conjunction with work already in progress on the excitation of electromagnetic waves by tethered systems in the ionosphere. A full report of this analysis can be found in a paper by R. Estes to be published in the Journal of Geophysical Research. Since the physics of ionospheric wave excitation is fundamental to all electrodynamic tethered satellite experiments, and since it has been a source of some controversy, we present the outlines of our analysis here along with some results for the wave impedance of a short tether not previously reported.

Previous analyses of wave excitation by an electrodynamic tethered satellite system, including the one by Barnett and Olbert, failed to take into account the peculiar "dumbbell" shape of the system, which consists of a long, thin wire terminated by charge-exchange structures (the hollow cathode clouds in our case) with dimensions much larger than the tether diameter. It turned out to be easy to do this in first approximation by assuming a current distribution for the system that consists of a current filament along the tether length with other lines of current along the line-of-flight at the ends of the system. The current distribution at the ends of the system drops off linearly in the forward and backward directions, going to zero at the limits, thus modeling constant charge-exchange along the interface between the system and the ionosphere. This amounts to contracting the hollow cathode cloud to a line segment, as shown in Figure 5.1. Using this current distribution as the source current, we then apply Maxwell's equations in a plasma to the system and utilize Fourier integral methods to obtain the fields and currents excited in the ionospheric plasma.
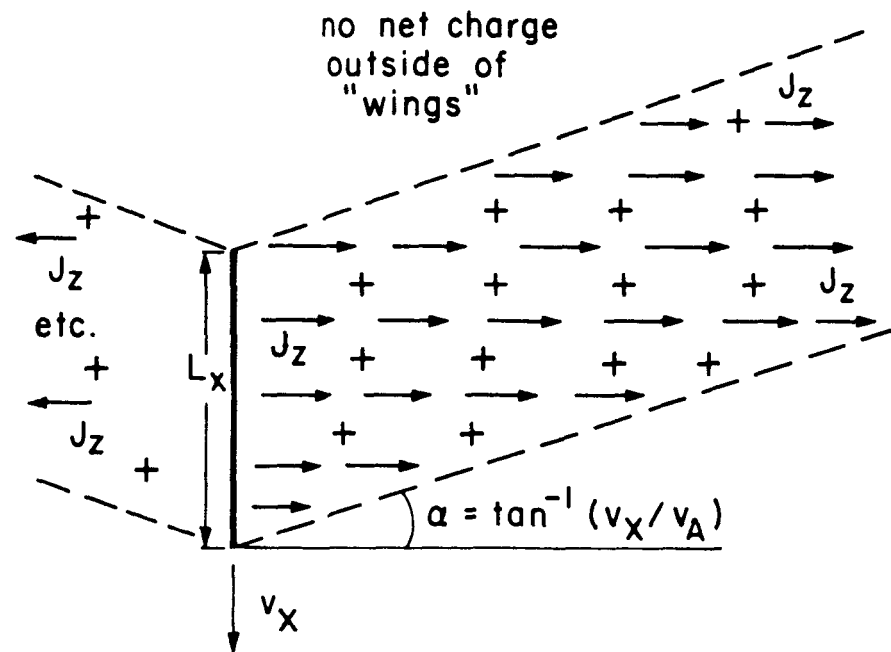
Figure 5.2. Electrodynamic tethered system viewed from above, showing upper Alfvén wings in the case where $L_x \gg V_z/\Omega_{ci}$ (infinite L_z, strictly peaking, for the "perfect" wings shown in the figure).

The "Alfvén wings" of current sheets at the ends of the system emerge naturally in this analysis. They are seen to be charge-carrying wave packets made up of components with non-vanishing divergence of the electric field, i.e., with electric field components that lie along the direction of the phase front. The group velocity of the dominant Alfvén wave components lies along the geomagnetic field lines however, so that the energy and charge flows down the field lines as the wing structure moves along parallel to the direction of the satellite system's motion.

Although the problem of electromagnetic wave excitation by a constant current tethered satellite system is sometimes approached as a classical antenna problem, the basic source of electromagnetic energy transfer is different in the two cases. In the case of an ordinary antenna, electromagnetic waves arise from the oscillation of the electrons in the antenna. In the case of an electrodynamic tethered satellite system that draws a constant current this source of radiation is absent. To an observer in the tethered satellite system, things appear to be constant in time for this ideal case. Nonetheless, the plasma that streams by sees time-varying fields due to the regions of net electrical charge it encounters at the ends of the system, where the charge-exchange is taking place between the tethered satellite system and the ionospheric plasma. The frequency of this time-variation is determined by the time it takes for the plasma to flow past this disturbed region. Thus it is the dimensions of the terminating, charge-exchanging parts of the tethered system that are crucial for wave-generation.

Barnett and Olbert, in their analysis, failed to draw the physical consequences of the mathematical formulas they derived, which showed the wave fields to be determined by the divergence of the tether current. They modeled the system as a long, orbiting wire, insulated along its length and with a diameter measured in millimeters. By using this model they in effect reduced the charge-

exchange region to the cross-section of the wire, which in turn increased the frequencies of the field variations seen by the ionosphere by several orders of magnitude. This unphysical modeling of the problem is the source of the high wave impedances they obtained, which were due to a frequency band above the lower hybrid frequency. We found that applying their expressions to a system with charge-exchange dimensions of only a few meters led to a reduction of the wave energy in this frequency band to levels that were completely negligible compared to that for frequencies below the ion cyclotron frequency.

The expression we found for the wave impedance is

$$Z_A = -\int_{-L/2}^{L/2} E_y(x' = 0, y, z = 0) \; dy \, / I$$

$$= \frac{4v_A}{\bar{L}_x c^2} \int_0^1 dk(1 - e^{-k\bar{L}}) \frac{\sin\left(k\bar{L}_x/2\right)\sqrt{1-k^2}}{k^2}$$

(5.1)

where v_A is the Alfvén speed, c the speed of light, and $\bar{L}$ and $\bar{L}_x$ are the tether length and charge-exchange dimension (in units of the satellite velocity divided by the ion cyclotron frequency), respectively. When we apply this result to the parameters of the short-tether, hollow cathode experiments we obtain the curve shown in Figure 5.3. The most noteworthy fact is the very low values of the wave impedance throughout the experiment. According to these results, then, the wave impedance should be a negligible factor in these experiments. As we have already pointed out, however, these calculations depend on a number of approximations that are difficult to justify accept as a starting point for
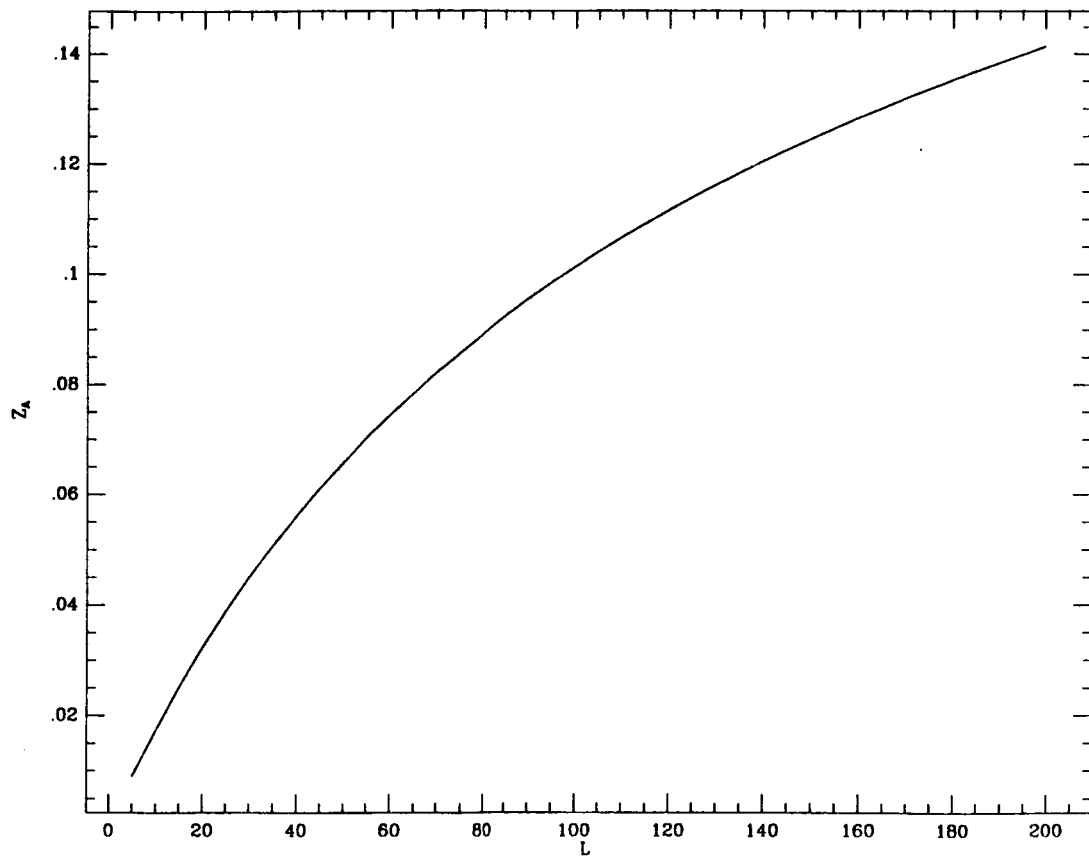
Figure 5.3. Wave impedance (ohms) versus tether length (meters) for end dimension 5 meters. F-region maximum $(v_A = 10^{-3}c)$ assumed: Z_A scales with v_A the Alfvén speed; curve virtually unchanged for end dimension = 50 meters.

comparison with other analyses.

Having dealt with the challenge raised by the MIT results, we now consider some of the details of the analysis beyond the wave impedance calculation. One of the striking results (which, along with other results, may be subject to change once a more realistic model that includes warm plasma effects is utilized) is that the region of net space charge extends beyond the system in both directions along the line-of-flight. This is just a consequence of the exclusion of waves with $\omega_{ci} < \omega < \omega_{LH}$, which places a lower limit on wavelengths for $\partial I_t / \partial t = 0$). The current-carrying "Alfvén wings" are wider than the dimensions of the system, once a steady state has been reached. The dimensions of the system in our case would be the effective charge-exchange dimensions of the plasma cloud emitted by the hollow cathodes. If these dimensions along the line-of-flight are not large compared with the system's orbital velocity divided by Ω_{ci}, the ion cyclotron frequency of the ionosphere (around 25m at 300 km altitude), then plasma wave phenomena will produce regions with both net charge and net field line currents well beyond the cloud dimensions. It would be very interesting to measure the currents in the neighborhood of the system to see if this phenomenon really exists, but that is beyond the capabilities of the first short tether experiments. This phenomenon is shown in Figure 5.4b. Figure 5.4a shows that the "boxcar function" perfect Alfvén wing current distribution corresponding to Figure 5.2 is a good approximation for very large L_z.

The theoretical calculations of Barnett and Olbert were not the only challenge to the feasibility of electrodynamic tethers that arose during the course of our investigation. Stenzel and Urrutia (see references 5 and 6 below) of UCLA presented experimental results which, according to them, indicated that electrody-
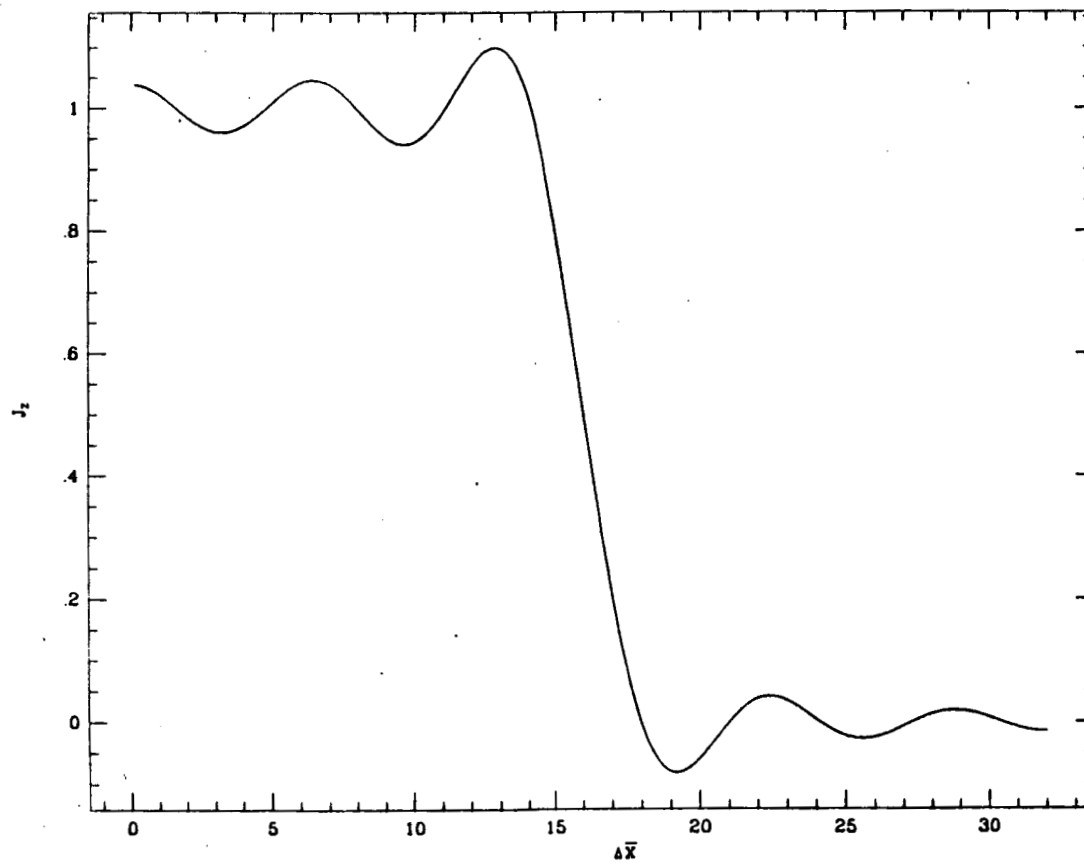
Figure 5.4(a).   Alfvén wing sheet current (in units of $I_t/2L_z$) near the system end plotted versus distance along line-of-flight. All distances in units of v_{sat}/Ω_{ci} (25 m at F-maximum). $\bar{L}_z = 32$. ($L_z = 800$ m at F-maximum).
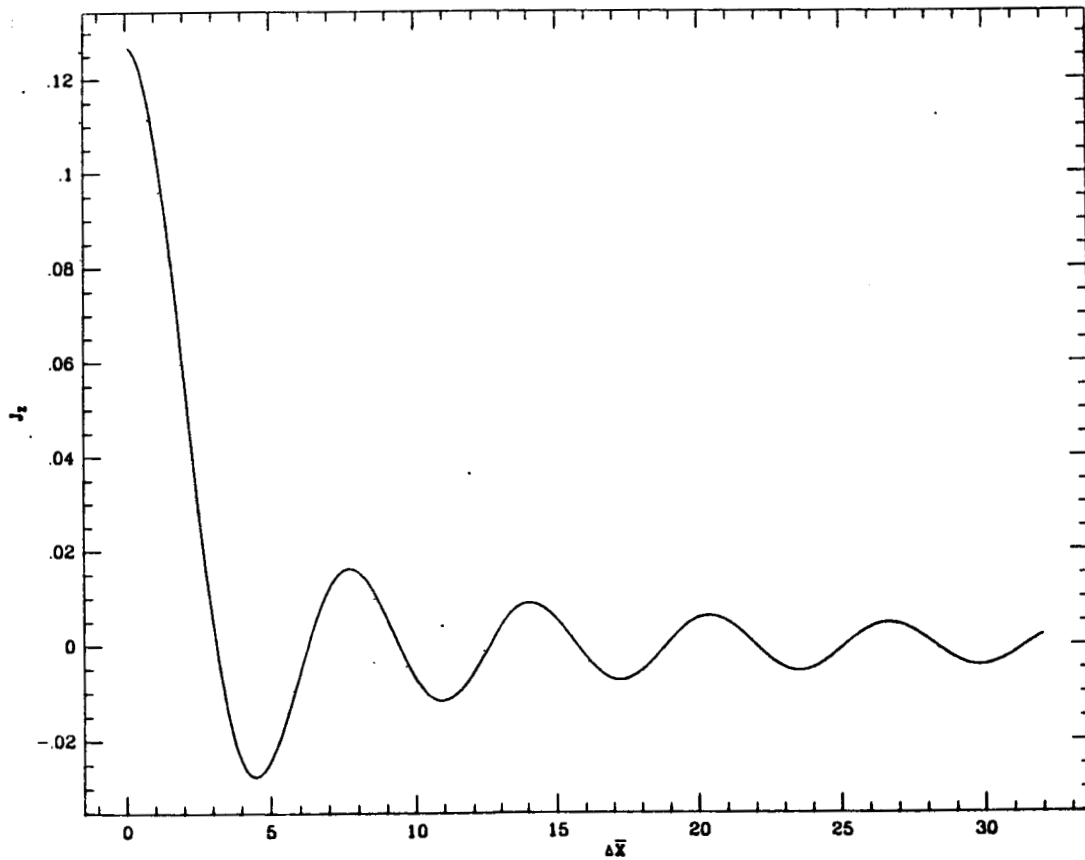
Figure 5.4(b).   Alfvén wing sheet current (in units of $I_t/2L_z$) near the system
end plotted versus distance along line-of-flight. All distances in
units of v_{sat}/Ω_{ci} (25 m at F-maximum). $\bar{L}_z = .4$ ($L_z = 10m$ at
F-maximum).

namic tethers would be able to draw only a fraction of the current calculated from probe theory and that this current would be periodically interrupted by plasma instabilities. They further claimed that the results indicated circuit closure would be local and not at great distances via currents confined to magnetic field lines. Thus they claimed their experiments had a bearing on both local and global system/plasma interactions. After careful consideration of their experiments, we have concluded that no conclusions about tethered satellite performance can be drawn from them due to a number of significant deviations in their experimental conditions from those that will prevail for a tethered system in low earth orbit.

The experimental results and a more complete description of the experimental setup can be found in the references listed at the end of this section, but we shall sketch them here. There are two different experiments. They have in common that they were performed in a quiescent afterglow plasma inside a plasma chamber with a length of 2m and diameter 1.5m. A uniform dc axial magnetic field of 30G was applied. The plasma density was $2 \times 10^{11}/cm^3$.

In one experiment, current collection by a single electrode, positively biased by a pulsed voltage of 80V with a rise time of 200 nsec, was observed. In the other experiment, which is supposed to represent a tethered system, there were two electrodes immersed in the plasma with a pulsed bias potential of 250V applied between them. The heated, oxide-coated cathode had a diameter of 2.5cm in the tether simulation. The cathode emits an electron beam, so it resembles an electron gun more than a passive device such as a hollow cathode. No information is given about the beam density, but the report of an earlier experiment (Whelan and Stenzel, 1985), which appears to have used the same or a similar cathode, states that the beam density is controlled by the cathode temperature. The electrode currents are monitored during the experiment. In addition, a magnetic probe is used to measure plasma currents throughout the

vessel.

In each experiment the electron current collected by the positive electrode quickly $(t = 2\mu\sec)$ rose to ten times the random electron current, then fell to a much lower value. Then a series of current pulses were observed at intervals of around 5μsec with peak values an order of magnitude lower than the original peak. The authors explain this as being due to "anomalous cross-field currents" (initially) "caused by current-driven instabilities" followed by ion expulsion from the "current channel" and current collapse. In the dual-electrode experiment significant crossfield currents were observed, so that circuit closure in the plasma was local.

Our first criticism of the experiments is directed at the use of the pulsed voltage. Given that the lifetime of the plasma is reported to be 120 μsec, there would seem to be no necessity for a voltage ramp time of 200 nsec. The authors explicitly state that the initial large currents are "possible only when the electrode bias is rapidly switched above the plasma potential." Since the only <u>known</u> time variation in a dc tether is due to the motion of the system—with frequencies therefore determined by the orbital velocity divided by the satellite dimension—a plasma chamber simulation should try to minimize impulsive phenomena. The pulsing may be necessary for the cathode to generate a beam, but that would not apply to the single electrode experiment, nor should an electron beam be necessary to model an electrodynamic tether. In any case, the authors make it clear that the pulsing is meant to be a critical part of the tethered satellite simulation. In a sense then, they have made a mistake in their experiments equivalent to the theoretical mistake of Barnett and Olbert.

More fundamentally, however, the difference is that in the case of an orbiting system part of the plasma is seeing an increasing electric field while another part sees a decreasing field. This basic feature of tethered satellite physics

is impossible to duplicate for an electrode at rest with respect to the surrounding plasma.

In the case of the dual electrode experiment, the edge-to-edge separation of the electrodes is only 5cm, or roughly 30 electron gyroradii. In terms of electron gyroradii, this would correspond to a tether length in the ionosphere of less than half a meter. Furthermore, the 250V applied across this short distance, corresponds to an electric field of of 5000V/m as opposed to the 0.2V/m maximum due to orbital motion. No explanation is given for the more than three-fold increase in the voltage over that used in the single electrode experiment. The impulsive application of a voltage this high between two closely placed electrodes immersed in a plasma almost certainly puts us in a regime in which the approximations of linear plasma theory are invalid. Nonetheless, the frequency determined by the inverse of the voltage ramp time is considerably larger than all the classical collision frequencies and the electron cyclotron frequency, though less than the electron plasma frequency, so that the linear dielectric tensor one obtains is diagonal, with all diagonal components about the same magnitude. Thus plasma currents along the components of the electric field perpendicular to the magnetic field are not surprising.

The difficulties of simulating a tethered satellite system in a plasma chamber have been enumerated elsewhere in this report. A more realistic experiment, using much of the same equipment as the original UCLA experiments, could be made using a much lower voltage, slower ramp time, and a wider electrode separation. It would be interesting to see if the observed phenomena persisted. At this point we cannot take the experiments seriously as models of an electrodynamic tethered satellite system, even one with a short tether.

Prof. Stenzel, in an oral report of his experiments to the NASA Ionospheric Circuit Closure Workshop in April of 1987, made passing reference to some new

results that would seem to be of more interest to us. He discovered that when the background neutral density was increased from 10^{-4} to 10^{-3} Torr, the behavior of the system was altered remarkably. The initial sharp rise in the current to a value ten times the probe theory estimate still occurred, but the high current level persisted instead of dropping off to a low value. He tentatively attributed this to the ionization of neutrals, which created, in effect, a plasma contactor.

References to Section 5.

1. Barnett, A. and S. Olbert, 1986. "Radiation of Plasma Waves by a Conducting Body Moving Through a Magnetized Plasma." Journal Geophys. Research 91, 10117.

2. Dobrowolny, M. and P. Veltri, 1986. "MHD Power Radiated by a Large Conductor in Motion Through a Magnetoplasma." Nuovo Cimento 9C, 27.

3. Drell, S.P., H.M. Foley and M.A. Ruderman, 1965. "Drag and Propulsion of Large Satellites in the Ionosphere: An Alfvén Engine in Space." Journal Geophys. Research 70, 3131.

4. Rasmussen, C.E., P.M. Banks and K.J. Harker, 1985. "The Excitation of Plasma Waves by a Current Source Moving in a Magnetized Plasma: The MHD Approximation." Journal Geophys. Research 90, 505.

5. Stenzel, R.L. and J.M. Urrutia, 1986. "Laboratory Model of a Tethered Balloon — Electron Beam Current System." Geophys. Research Letters, 13, 1977.

6. Urrutia, J.M. and R.L. Stenzel, 1986. "Anomalous Currents to an Electrode in a Magnetoplasma." Physical Review Letters, 57, 713.

7. Whelan, D.A. and R.L. Stenzel, 1985. "Electromagnetic Radiation and Nonlinear Energy Flow in an Electron Beam-Plasma System." Phys. Fluids 28, 958.

6.0   VARIATIONS IN THE ENVIRONMENT ALONG THE ORBIT

The operation of an electrodynamic tethered satellite system depends upon there being a $\vec{v} \times \vec{B}$ force to drive the current and sufficient charge in the ionospheric plasma to feed the tether current across the charge-exchanging interfaces of the system with the ionosphere. Just what plasma density is sufficient depends on how well the hollow cathode devices (or other charge-exchange mechanisms) are able to fulfill their role as plasma contactors as a function of ionospheric plasma density and on what tether current is desired. Clearly, if a certain minimum current were required at all times, then the hollow cathode system would have to be designed to attain that level under the least favorable conditions encountered in its orbit.

In the present context of preparing for a "one-shot," short-duration experiment, our task is rather to plan the experiment so that it takes place in an ambient plasma density likely to give both a demonstration of the system's ability to draw a substantial current and to maximize the scientific return.

Understanding of hollow cathode devices is insufficient at present for us to be able to describe hollow cathode performance as a function of ionospheric plasma density. All indications are that it is desirable to maximize the plasma density. This is crucial for us to know how the ionospheric plasma density encountered by the system varies. It is not widely appreciated how much the electron density encountered by an orbiting system can vary in a single revolution around the earth. One of the purposes of this section is to make this point, so that adequate planning can be made.

The $\vec{v} \times \vec{B}$ force experienced by the system also varies along the orbital path. Since the vertical component of this force drives the tether current

Page 96

$(\vec{v} \times \vec{B} \cdot \vec{L}$ is the equivalent voltage across the tether, where L is the vector parallel to the tether with magnitude L, the tether length), it is the quantity whose variation needs to be determined.

The variations in plasma density and induced voltage have been examined in the following way. The SKYHOOK computer program previously developed at SAO to study tethered satellite system dynamics already included a model of the terrestrial magnetic field and ionospheric plasma. Since the tether dynamics were not of primary interest at this point, we modified the SKYHOOK code to advance the system in its orbit by an analytical formula, while obtaining values of the induced tether voltage and ionospheric plasma density at points along the orbital path.

The ionospheric model included in SKYHOOK was the Jones-Stewart [1970] model. This model is based on a trigonometric expansion fit to a large number of measurements made worldwide during the month of November in 1966 (a year of moderate solar activity). The obvious weakness of the model is that its strict applicability is limited to that month or other periods with similar solar activity levels, etc. It may, however, be a better picture of such periods than what can be obtained by a model that attempts to model the physical processes that cause the variations in ionospheric parameters.

SAO has obtained the International Reference Ionosphere computer code from the World Data Center in Boulder. This model, however, is least accurate for lower latitudes, the very region we are most interested in at present. Comparisons with SLIM [Anderson, 1985], the ionospheric model soon to be incorporated into IRI for low latitudes, showed that the Jones-Stewart model, with its large variations in plasma density encountered in a circular orbit, probably gives a more believable picture of the range of plasma densities encountered, although this range will depend upon the season and the solar activity level.

We consider a 300 km orbital height circular orbit. The first two plots (Figures 6.1 and 6.2) show the latitude and longitude versus elapsed time. These can be used to get an idea of the geographical co-ordinates that correspond to the features seen in the other plots of quantities versus time. Since the orbit shown has an inclination of 28°, the latitude varies between ±28°. The local time is plotted versus elapsed time in Figure 6.3.

The electron density (in units of electrons/m^3) is plotted versus elapsed time in Figure 6.4. This plot shows some well-known features of the electron density distribution. The most obvious of these is the big decrease in electron density at night due to recombination in the absence of ionizing solar radiation. These are the deep troughs that occur in each orbit (of which roughly 11½ are displayed). A sharp spike is seen to emerge from each of these nighttime troughs, in some cases rising above the peak daytime value encountered. The daytime values encountered shown in some revolutions (most prominently in the last three) two peaks on the left side (morning side) of the daytime distribution. The trough between these peaks is the Appleton anomaly or equatorial trough.

The electron density is translated into random electron current collected by a sphere with radius two meters in Figure 6.5 which displays the current versus local time. A sphere with radius 20 meters would collect 100 times as much current, and so on. For a 20 m radius the current collected would vary all the way from 60A (at the maximum peak in electron density encountered, where $n_e >$ $2\times10^{12}/m^3$) down to less than 0.3A. This obviously is relevant to the experiments we are considering, even if the dependence of current collected on plasma density is not linear. The deep troughs in electron density are seen to occur between 1800 and 2000 local time. The Appleton anomaly occurs between 0900 and 1200 local time. Other low values of electron density are seen just before sunrise. The nighttime peaks occur between 2000 and 2200 local time.

The tether voltage due to the $\vec{v} \times \vec{B}$ force is plotted in Figure 5.6 for a 200 m tether. Since the voltage is linear in the tether length, obtaining results for other lengths is simple. The variation in the voltage encountered in the first few revolutions is relatively small, but in one of the later revolutions the voltage is seen to vary all the way from 17.5V to 45.0V.

A choice of late morning to early afternoon local time near the maximum excursion in latitude would maximize both electron density and motional emf, by avoiding low nighttime electron densities and the equatorial trough, while having the orbital velocity vector nearly perpendicular to the geomagnetic field. The simulations indicate that the variations from one revolution to another are greater for the motional emf encountered than for the peak in electron density. This is due to local deviations from the dipole field. Magnetic field considerations might outweigh electron density considerations, so experiment planning should take this into account.

References to Section 6

1. Anderson, D.N., M. Mendillo and B. Herniter, 1985. "A Semi-Empirical, Low-Latitude Ionospheric Model," Air Force Geophysics Laboratory Report AFGL-TR-85-0254.

2. Jones, W.B. and F.G. Stewart, 1970. "A Numerical Method for Global Mapping of Plasma Frequency," Radio Science 5, 773.
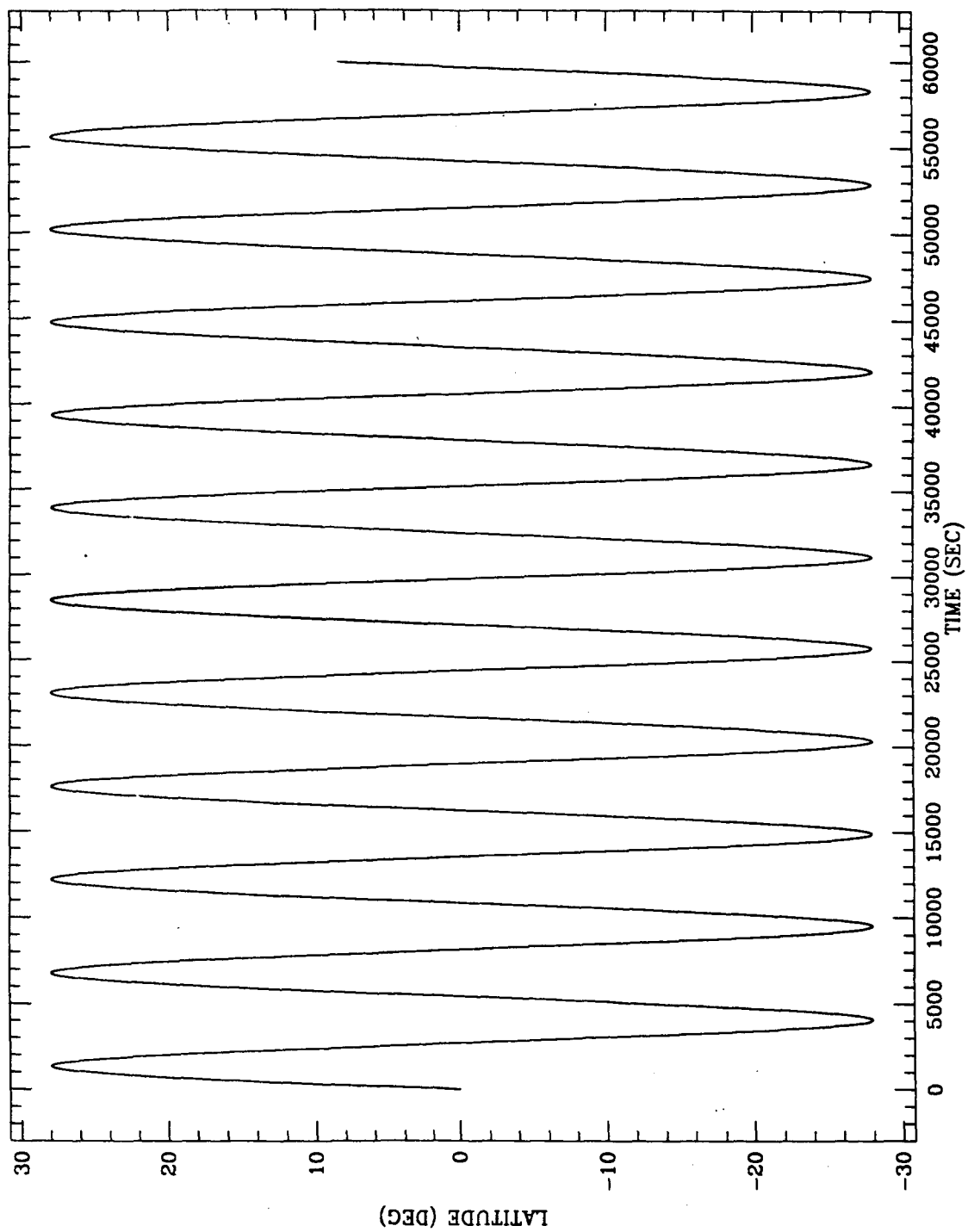
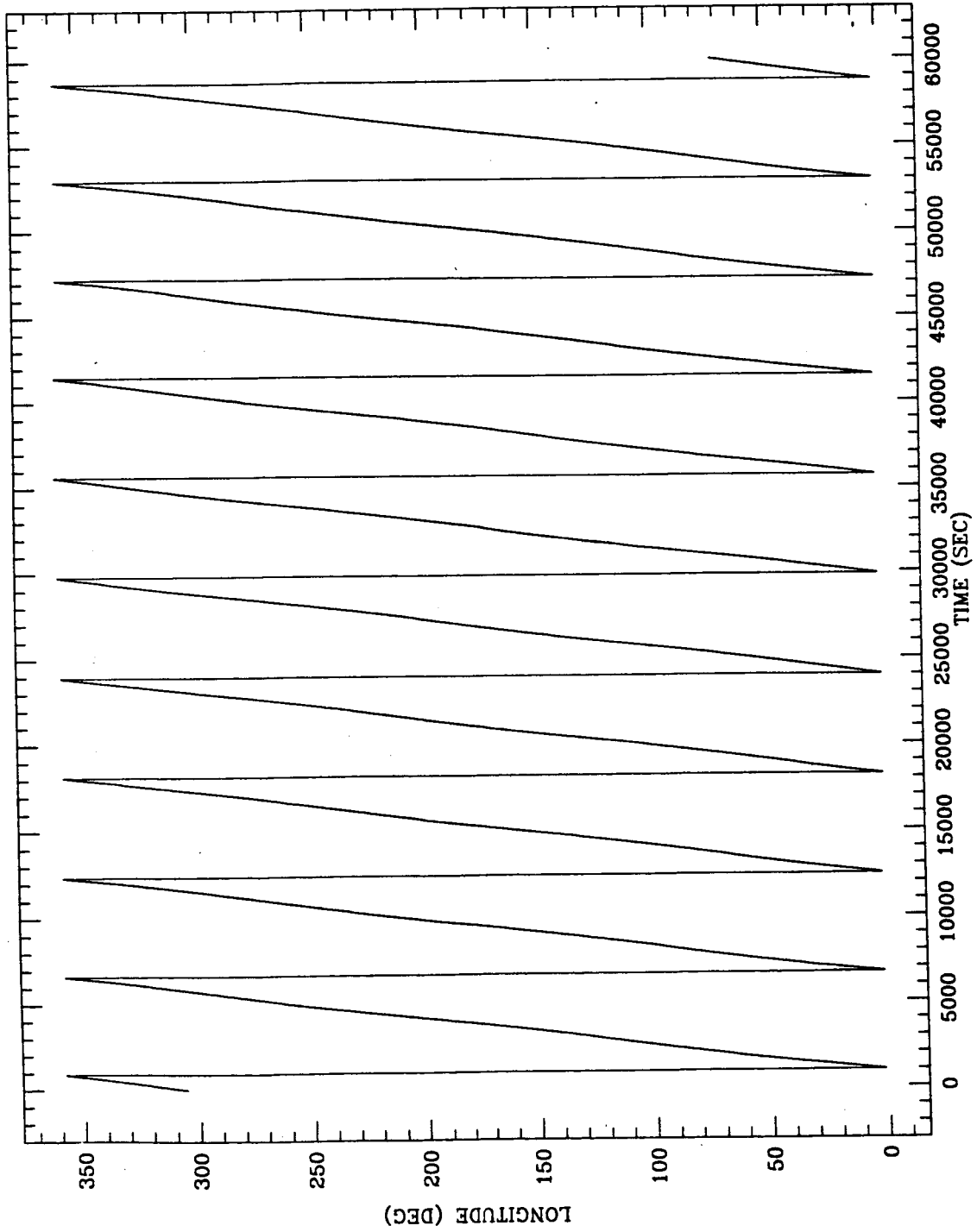Figure 6.1. Latitude versus elapsed time.
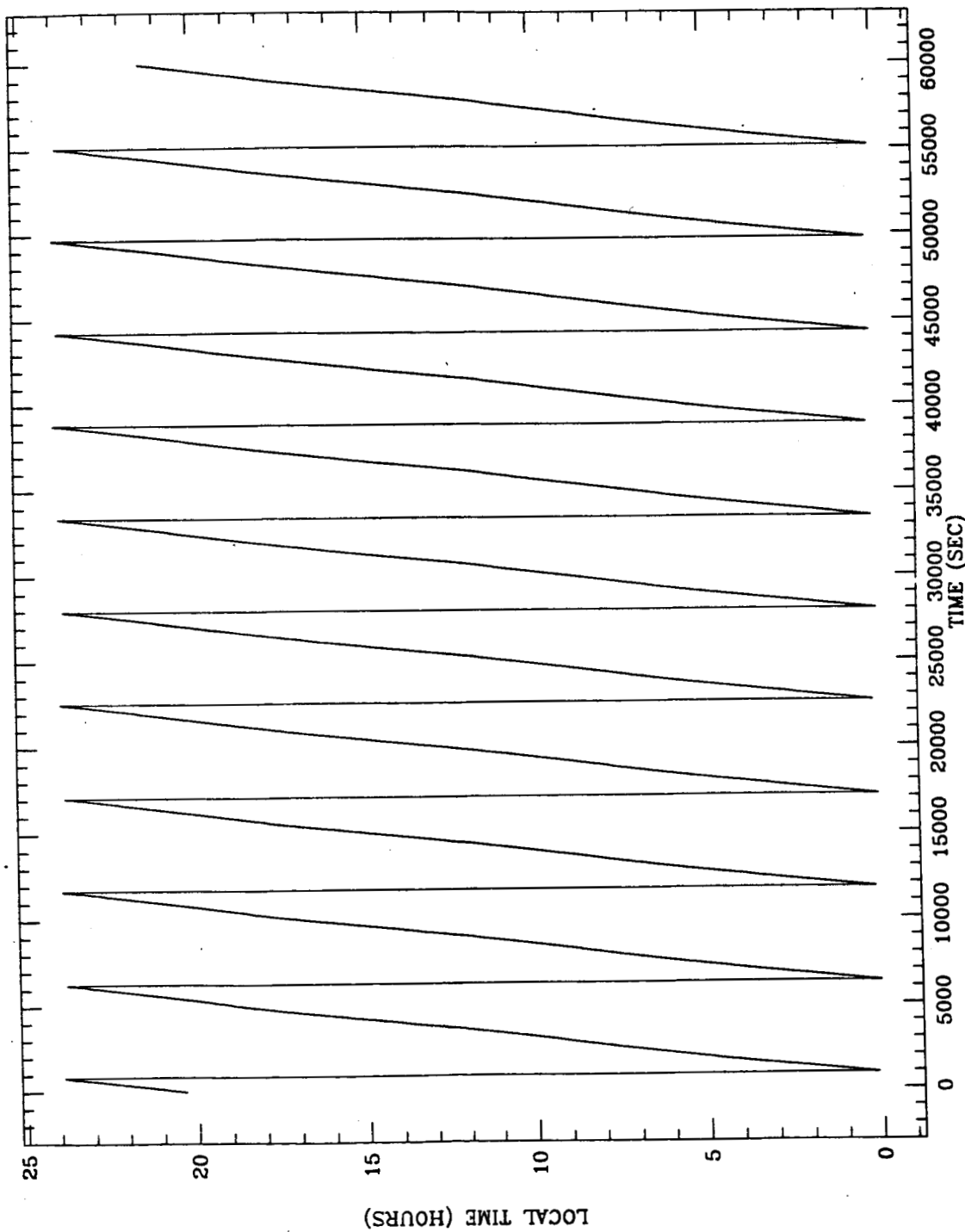
Figure 6.2.   Longitude versus elapsed time.

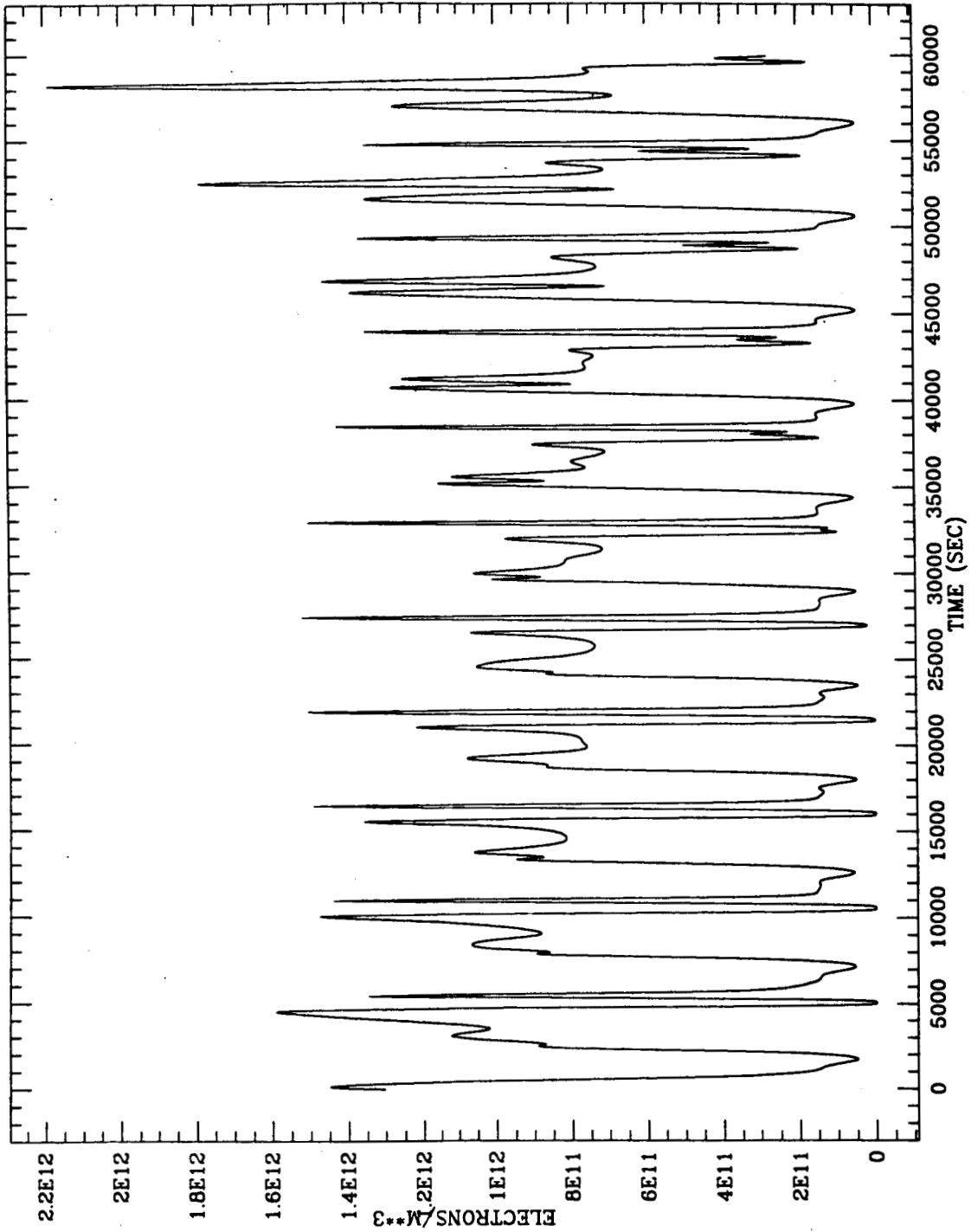Figure 6.3. Local time versus elapsed time.

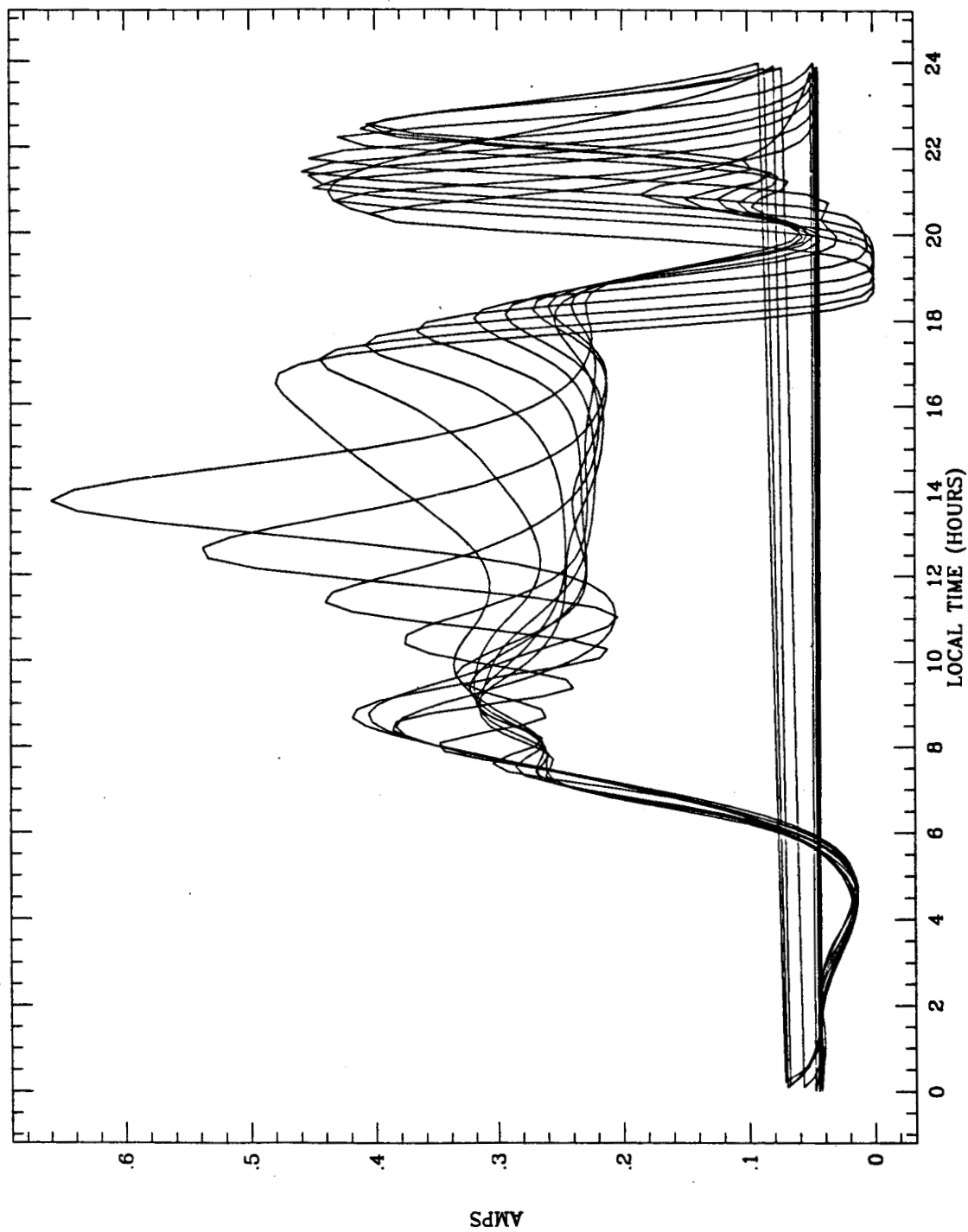Figure 6.4. Electron density encountered versus elapsed time.

Figure 6.5. Random electron current collected by a sphere with
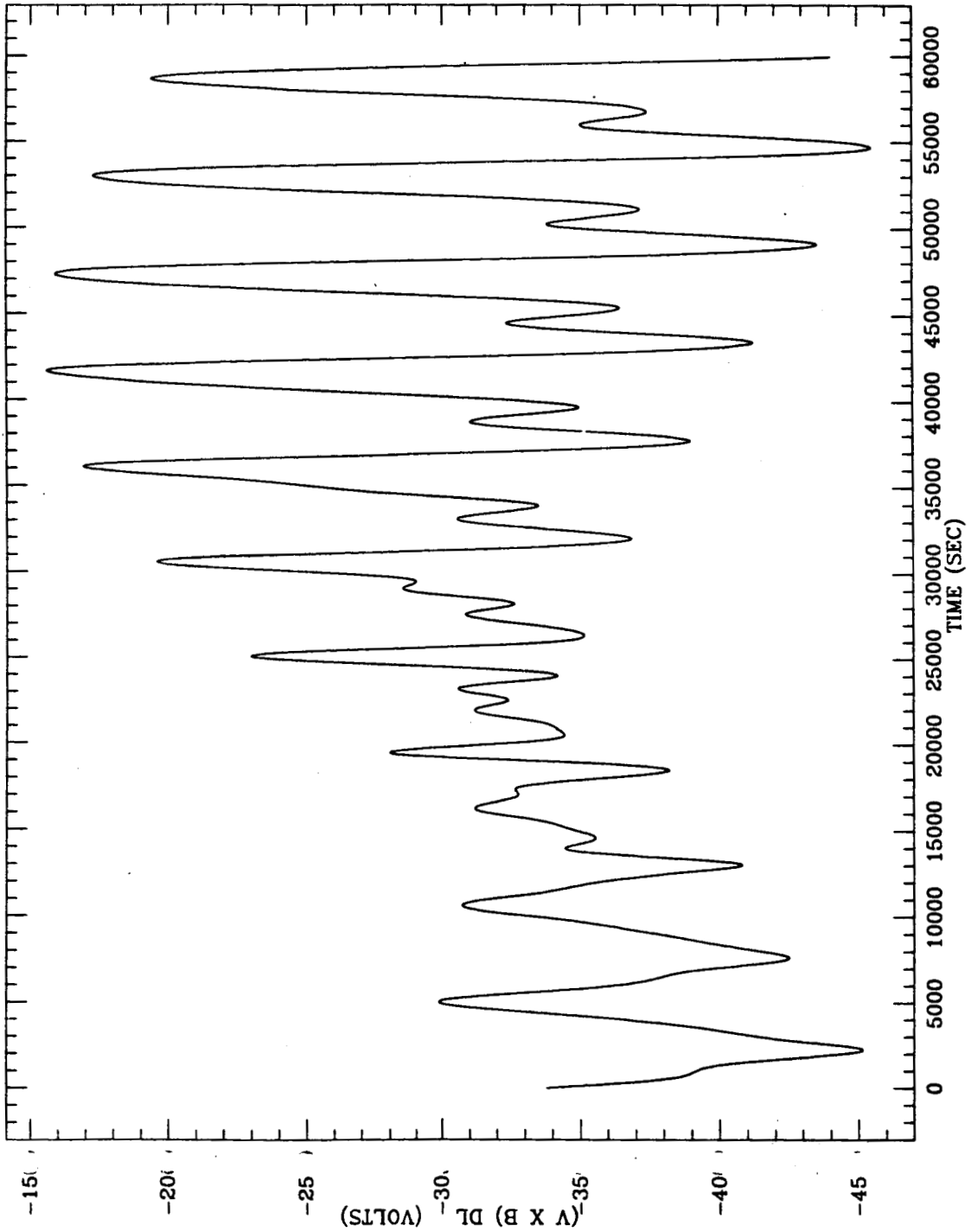2 meter radius versus local time.

Figure 6.6. Induced voltage in a 200 m tether versus elasped time.

7.0   CONCLUSIONS

The proposed Shuttle-based short tether experiments with hollow cathodes have the potential for providing important data that will not be obtained in long tether experiments such as TSS-1 or in sounding rocket experiments. They have the advantage of being conducted in conditions that correspond to those of electrodynamic tether operation, while providing measurements of the tether current over a continuous range of tether lengths, running from the very short on out to 200 meters. A critical property for hollow cathode effectiveness as a plasma contactor is the cross-magnetic-field conductivity of the emitted plasma cloud. The varying tether length, combined with the option of inserting batteries into the tether circuit will, at the very least, make it possible to observe the hollow cathode separation at which cross-cloud currents effectively end for different voltages. This will provide a measure of the effective hollow cathode plasma cloud size.

We have emphasized the different effects of hollow cathode cloud overlap in the cases of motion-driven and battery-driven operation. This difference lies at the heart of the electrodynamic tether concept. In the wholly motion-driven mode for which there are no batteries in the circuit and the entire emf is due to the motion of the system across the geomagnetic field lines, the combined tether/plasma system acts as a conducting path between the ionospheric layers at the upper and lower ends of the system when there is substantial overlap of the hollow cathode plasma clouds. In this case, the plasma column acts as an alternative electrical path to the tether. When the dominant emf in the circuit is supplied by a battery, the overlapping plasma clouds serve as a local circuit closure path in competition with the ionospheric transmission line. This is because the plasma clouds experience the applied voltage only through their contact with the

tether, while they are immersed in the motional electric field and experience it directly. Thus, inserting a battery with the polarity chosen to add to the motional emf would reverse the direction of the plasma current flowing across the overlapping hollow cathode clouds, for a sufficiently high applied voltage. We have used simplified but instructive circuit diagrams to illustrate this difference.

The calculations presented on the size and shape of the hollow cathode cloud improve our qualitative picture of hollow cathodes in low earth orbit and provide estimates of the time constants for establishing the fully-expanded cloud. Time constants for cloud expansion are in the tens of milliseconds range, which indicates that the currently planned data acquisition rate of 10/sec will not be high enough to observe transients. The magnetic boundary value problem calculations indicate the way in which the magnetic field will affect the shape of the cloud by resisting expansion in the direction perpendicular to the field.

The large-scale interactions of the system have also been considered. We have argued that they are important since the net charge density is carried away from the region of charge-exchange between the ionosphere and the system by ionospheric electromagnetic wave packets—the "Alfvén wings." We have pointed out a flaw in the analysis of investigators that published values of the wave impedance that were so high as to preclude the attainment of any significant currents in electrodynamic tethered systems. Our calculations show the wave impedance to be less than an Ohm and thus of negligible importance in the experiments. We also conclude that recent plasma chamber experiments by Stenzel and Urrutia do not model an electrodynamic tether well enough to apply the results to tethered system behavior.

Simulations of orbital revolutions at 300 km altitude and 28 degrees inclination indicate that a good deal of thought and planning should go into choosing the timing (and hence location) of the experiments in order to combine

high electron densities with high motional emf. If it is feasible to do so, it would be better to leave the decision of when to commence the experiment to the last minute, since a slight delay in launch could throw the timing of passage through the most desirable conditions off enough to make a significant difference.

Up until now there has been no completely satisfactory analysis of a hollow cathode operating in the conditions of low earth orbit. Nor have there been plasma chamber experiments that model all the conditions. Adding an external electric field and streaming background plasma to a plasma chamber will be difficult. Since the interactions are so complex and the factors so manifold, this would seem to be a problem to which the methods of computer simulation could usefully be applied. We recommend that a program of carefully thought out simulations be carried out. The first step would be to attempt to duplicate plasma chamber results in order to verify that the model is working or to refine it until it is. Then the additional effects of orbital motion and the geomagnetic field would be added. Simulation results could be useful in the planning and interpretation of both plasma chamber and space experiments.

Orbiting short tether experiments on hollow cathodes will provide critical information on hollow cathode performance and the underlying physics that cannot be obtained any other way. They should be conducted as soon as funding and a suitable space vehicle are available.